REPORT DOCUMENTATION PAGE

Form Approved OMB NO. 0704-0188

1. REPORT DATE (DD-MM-YYYY)	2. REPORT TYPE	3. DATES COVERED (From - To)
01-08-2017	Final Report	1-Apr-2014 - 31-Mar-2017

4. TITLE AND SUBTITLE	5a. CONTRACT NUMBER
Final Report: Propagating Molecular Recognition Events through Highly Integrated Sense-Response Chemical Systems	W911NF-14-1-0169
	5b. GRANT NUMBER
	5c. PROGRAM ELEMENT NUMBER
	611102

6. AUTHORS	5d. PROJECT NUMBER
	5e. TASK NUMBER
	5f. WORK UNIT NUMBER

7. PERFORMING ORGANIZATION NAMES AND ADDRESSES	8. PERFORMING ORGANIZATION REPORT NUMBER
University of California - San Diego Office of Contract & Grant Adm 9500 Gilman drive, MC 0934 La Jolla, CA 92093 -0934	

9. SPONSORING/MONITORING AGENCY NAME(S) AND ADDRESS (ES)	10. SPONSOR/MONITOR'S ACRONYM(S)
U.S. Army Research Office P.O. Box 12211 Research Triangle Park, NC 27709-2211	ARO
	11. SPONSOR/MONITOR'S REPORT NUMBER(S)
	65293-CH.8

12. DISTRIBUTION AVAILIBILITY STATEMENT

Approved for public release; distribution is unlimited.

13. SUPPLEMENTARY NOTES
The views, opinions and/or findings contained in this report are those of the author(s) and should not contrued as an official Department of the Army position, policy or decision, unless so designated by other documentation.

14. ABSTRACT

15. SUBJECT TERMS

16. SECURITY CLASSIFICATION OF:			17. LIMITATION OF ABSTRACT	15. NUMBER OF PAGES	19a. NAME OF RESPONSIBLE PERSON
a. REPORT	b. ABSTRACT	c. THIS PAGE			Nathan Gianneschi
UU	UU	UU	UU		19b. TELEPHONE NUMBER
					858-246-0857

Agency Code:

Proposal Number: 65293CH
Agreement Number: W911NF-14-1-0169
INVESTIGATOR(S):

Name: Nathan C. Gianneschi
Email: ngianneschi@ucsd.edu
Phone Number: 8582460857
Principal: Y

Organization: **University of California - San Diego**
Address: Office of Contract & Grant Adm, La Jolla, CA 920930934
Country: USA
DUNS Number: 804355790
EIN: 956006144
Report Date: 31-Dec-2015
Date Received: 01-Aug-2017
Final Report for Period Beginning 01-Apr-2014 and Ending 31-Mar-2017
Title: Propagating Molecular Recognition Events through Highly Integrated Sense-Response Chemical Systems
Begin Performance Period: 01-Apr-2014
End Performance Period: 31-Mar-2017
Report Term: 0-Other
Submitted By: Nathan Gianneschi
Email: ngianneschi@ucsd.edu
Phone: (858) 246-0857
Distribution Statement: 1-Approved for public release; distribution is unlimited.

STEM Degrees: 3   **STEM Participants:**

Major Goals: General strategies that permit amplification and transduction of molecular recognition events over multiple length scales are of tremendous interest for a range of applications, including advanced sensor design and responsive, smart materials. Liquid crystals (LCs) provide an exciting opportunity in this regard as the supramolecular organization of mesogens within LC phases can be dynamically coupled to nanoscopic and molecular-scale interfacial events such that the response of the LC results in a detectable optical signal on the micrometer length scale. For example, biological recognition events, including enzymatic reactions, occurring at the aqueous interfaces of thermotropic LCs show promise as the basis of biomolecular triggers of LC reorganization that can be conveniently, transduced using optical methods. While several examples of LCs triggered by biomolecular events do exist, general design strategies that can be applied broadly to interfacial assemblies and transformations of biomolecules are yet to be establish. Such principles, if identified, would significantly advance and expand the potential utility of LCs as the basis of triggerable supramolecular materials.

The goals of this project involved both the development of triggerable polymeric elements, and their implementation in liquid crystal sensing arrays.

1) To develop novel brush polymer and copolymer architectures as biomolecule-responsive synthons for reactive nanomaterials. A particular focus of this work will be on novel peptide- and peptide nucleic acid (PNA)-based brush polymer systems.

2) To develop low molecular weight polymers capable of undergoing enzyme-induced assembly into larger, more complex nanostructures. A key expected outcome is an approach for transducing an enzyme-peptide interaction into a nanoscale self-assembly process.

3) To utilize peptide and nucleic acid brush copolymers as surfactants at a variety of interfaces including air-water and water-liquid crystal. A key expected outcome is the development of systems capable of converting molecular scale recognition events into microscale responses and beyond.

Accomplishments: See "Upload" section for PDF in response to this field.

Training Opportunities: Over the course of this funding period, the proposal supported an active collaboration with Prof. Nick Abbott's group at Wisconsin. This involved supporting the training of a graduate student in the Gianneschi group at UC San Diego, who has since graduated with her PhD. The training included travel to Wisconsin to work together with Prof. Abbott's team to develop formulations of our polymers with liquid crystal micro droplets. Systems that were subsequently published, and form the basis of multiple manuscripts now in final stages of preparation, and/or in review at the time of writing this report.

Results Dissemination: Lisa Adamiak, in her role with SWIGS (Society for Women in Graduate Studies) at UC San Diego, has participated in numerous outreach activities. In this capacity, she has engaged in discussions of this and related work.

Honors and Awards: STUDENT:

Lisa Adamiak:

Teddy Traylor Award for Exceptional Graduate Studies

Graduate Diversity and Outreach Award

PI:

Nathan Gianneschi:

2015 Outstanding Young Scientist Award, ACS Applied Materials & Interfaces, PAT 2015

2016 Fellow of the Royal Society of Chemistry

2016 Tianfu Distinguished Lecturer in Polymer Science and Engineering, Sichuan University

2017 Blavatnik Young Scientist Award Finalist

Protocol Activity Status:

Technology Transfer: Nothing to Report

 PARTICIPANTS:

 Participant Type: PD/PI
 Participant: Nathan Gianneschi
 Person Months Worked: 1.00   **Funding Support:**
 Project Contribution:
 International Collaboration:
 International Travel:
 National Academy Member: N
 Other Collaborators:

 Participant Type: Graduate Student (research assistant)
 Participant: Lisa Adamiak
 Person Months Worked: 6.00   **Funding Support:**
 Project Contribution:
 International Collaboration:
 International Travel:
 National Academy Member: N
 Other Collaborators:

RPPR Final Report
as of 12-Oct-2017

ARTICLES:

Article Title: Poly(oligonucleotide)
Authors:
Abstract: Here we report the preparation of poly- (oligonucleotide) brush polymers and amphiphilic brush copolymers from nucleic acid monomers via graft-through polymerization. We describe the polymerization of PNA-norbornyl monomers to yield poly-PNA (poly(peptide nucleic acid)) via ring-opening metathesis polymerization (ROMP) with the initiator, (IMesH2)- (C5H5N)2(Cl)2RuCHPh.1 In addition, we present the preparation of poly-PNA nanoparticles from amphiphilic block copolymers and describe their hybridization to a complementary single-stranded DNA (ssDNA) oligonu- cleotide.

Article Title: Polymer-Stabilized Perfluorobutane Nanodroplets for Ultrasound Imaging Agents
Authors: Yuran Huang, Alexander M. Vezeridis, James Wang, Zhao Wang, Matthew Thompson, Robert F. Mattre
Abstract: In this paper, we describe a method for the stabilization of low-boiling point (low-bp) perfluorocar- bons (PFCs) at physiological temperatures by an amphiphilic triblock copolymer which can emulsify PFCs and be cross-linked. After UV-induced thiol?ene cross- linking, the core of the PFC emulsion remains in liquid form even at temperatures exceeding their boiling points. Critically, the formulation permits vaporization at rarefac- tional pressures relevant for clinical ultrasound.

FINAL REPORT

Subject: Statement to Dr. Jennifer J. Becker
Contract/Grant Title: Propagating Molecular Recognition Events Through Highly Integrated Sense-Response Chemical Systems
Contract/Grant #: W911NF-14-1-0169
Reporting Period: 04/01/2014 – 03/31/2017

Summary of Accomplishments:
Our research has focused on brush polymer systems for controlling liquid crystal interfaces and other phases including ultrasound responsive perflourocarbons. This work involves extensive efforts to establish design rules for propagating responses over multiple length scales.

Archival Publications (published) during funding period:

1)   James, C. R.; Rush, A. M.; Insley, T.; Vukovic, L.; Kral, P.; **Gianneschi, N. C.** "Poly(oligonucleotide)" *J. Am. Chem. Soc.* **2014**, *136*, 11216-11219. PMID: 25077676; PMCID: PMC4140503.

2)   Bell, N. C.; Doyle, S. J; Battistelli, G.; LeGuyader, C. L. M.; Thompson, M. P.; Poe, A. M; Rheingold, A.; Moore, C.; Montalti, M.; Thayumanavan, S.; Tauber, M. J; **Gianneschi, N. C.** "Dye Encapsulation in Polynorbornene Micelles" *Langmuir* **2015**, *31*, 9707-9717

3)   Blum, A.P.; Kammeyer, J.K.; Rush, A.M.; Callmann, C.E.; Hahn, M.E.; **Gianneschi N. C.** Stimuli-Responsive Nanomaterials for Biomedical Applications. *J. Am. Chem. Soc.* **2014**, *137*, 2140-2154

4)   Blum, A. P.; Kammeyer, J. K.; Yin, J.; Crystal, D. T.; Rush, A. M.; Gilson, M. K. **Gianneschi, N. C.** "Peptides Displayed as High Density Brush Polymers Resist Proteolysis and Retain Bioactivity" *J Am. Chem. Soc.* **2014**, *136*, 15422-15437.

5)   Ma, C. D.; Adamiak, L.; Miller, D. S.; Wang, X.; **Gianneschi, N. C**.*; Abbott, N. L.* "Liquid Crystal Interfaces Programmed with Enzyme-Responsive Polymers and Surfactants" *Small* **2015**, 11, 5747-5751. (*co-correspinding authors

6)   Carlini, A. S.; Adamiak, L.; **Gianneschi, N. C.** "Biosynthetic Polymers as Functional Materials" *Macromolecules* **2016**, *49*, 4379-4394.

7)   Huang, Y.; Vezeridis, A.; Wang, J.; Wang, Z.; Thompson, M.; Mattrey, R.; Gianneschi, N. C. Polymer-Stabilized Perfluorobutane Nanodroplets for Ultrasound Imaging Agents. *J. Am. Chem. Soc.* **2017**, *139*, 15-18.

Changes in research objectives: None

Change in ARO program manager: None

Extensions granted or milestones slipped: None

Patent Disclosures in this reporting period: None

<u>Detailed Description of Accomplishments</u>

Abstract

Over the course of this grant, our group has looked at developing the basic polymer chemistry of responsive, biopolymer/polymer hybrid materials. This began with us generating a nobornyl-PNA (peptide nucleic acid) monomer and polymerizing it to generate homopolymers and block copolymers of PNA. This work was reported in an article published in the *Journal of the American Chemical Society* and is the first example of a polymerized nucleic acid. This has led to several follow up studies utilizing these materials and related systems in biomedical applications. In addition to nucleic acid based brush polymer systems, we have also developed peptide based systems. This work has resulted in a key publication, again in *JACS*, and ongoing work to understand the basic physical parameters governing their behavior. This knowledge has then been used to develop multi-stimuli responsive systems in collaboration with the laboratory of Prof. Nick Abbott to explore the use of these molecules as surfactants combined with liquid crystals, and in more recent work using them as surfactants for perfluorocarbons. This work has also resulted in two patents related to these subjects.

In addition, we have investigated fundamental encapsulation capabilities of polymeric micelles and have published one article on this subject.

We have continued work on developing fundamental synthetic approaches to incorporating bioactive sidechains into complex brush polymers. The focus of this work over the past 12 months has been on developing design rules for interfacing these systems with liquid crystals with manuscripts in preparation at the time of writing this report. This type of work will be described in the pages that follow.

Stated Objectives for 3 year period

1)   To develop novel brush polymer and copolymer architectures as biomolecule-responsive synthons for reactive nanomaterials. A particular focus of this work will be on novel peptide- and peptide nucleic acid (PNA)-based brush polymer systems.

2)   To develop low molecular weight polymers capable of undergoing enzyme-induced assembly into larger, more complex nanostructures. A key expected outcome is an approach for transducing an enzyme-peptide interaction into a nanoscale self-assembly process.

3)   To utilize peptide and nucleic acid brush copolymers as surfactants at a variety of interfaces including air-water and water-liquid crystal. A key expected outcome is the development of systems capable of converting molecular scale recognition events into micronscale responses and beyond.

Key Findings

SECTION 1: Programming Liquid Crystal Interfaces with Enzyme-Responsive Polymers and Surfactants

Introduction

General strategies that permit amplification and transduction of molecular recognition events over multiple length scales are of tremendous interest for a range of applications, including advanced sensor design and responsive, smart materials.[1–3] Liquid crystals (LCs) provide an exciting opportunity in this regard as the supramolecular organization of mesogens within LC phases can be dynamically coupled to nanoscopic and molecular-scale interfacial events such that the response of the LC results in a detectable optical signal on the micrometer length scale. For example, biological recognition events, including enzymatic reactions, occurring at the aqueous interfaces of thermotropic LCs show promise as the basis of biomolecular triggers of LC reorganization that can be conveniently, transduced using optical methods.[4] While several examples of LCs triggered by biomolecular events do exist,[5–9] general design strategies that can be applied broadly to interfacial assemblies and transformations of biomolecules are yet to be establish. Such principles, if identified, would significantly advance and expand the potential utility of LCs as the basis of triggerable supramolecular materials.

In this report, we describe the design and synthesis of biologically active peptide-polymer amphiphiles (PPA) that mediate enzymatically triggered optical responses in thermotropic liquid crystal (LC) microdroplets. The PPAs were designed with biphenyl side-chains to promote co-assembly at the aqueous interfaces of LC microdroplets and with peptidic moieties for enzymatic processing. We show that enzymatic cleavage of the PPAs triggers changes in PPA-surfactant complexes formed at the interface of the LC, thus giving rise to an easily observable optical response to the enzymatic reaction. The combined use of PPAs and surfactants represents a simple and modular strategy for targeting and triggering biomolecular events at LC microdroplet interfaces.

Strategy for triggering liquid crystal ordering transitions using peptide polymer amphiphiles and surfactants

The strategy described herein for the design of biomolecular triggers of LC ordering transitions is based on the synthesis of biologically active peptide-polymer amphiphiles (PPAs)[10,11] that form interfacial complexes with synthetic surfactants and thus regulate the ordering of LC microdroplets. The design incorporates PPAs with (i) biphenyl side-chains that promote co-assembly of the PPAs at the aqueous interfaces of LCs, and (ii) peptidic side-chains that can be enzymatically processed at the LC interface (Figure 1). A surfactant is selected to differentially interact with the PPA before and after enzymatic processing to change the ordering of the LC. The approach builds from past studies demonstrating that interfacial assemblies formed by polymer and surfactants depend sensitively on the chemical functionality and architecture of both species,[12–18] and that the mesoscale reordering of LCs can be triggered by subtle changes in the organization of interfacial molecular assemblies.[6,19–23][1-6] The LC used in the current study is a nematic phase of 4-cyano-4'-pentylbiphenyl (5CB) formulated as micrometer-sized droplets dispersed in aqueous phosphate buffered saline (PBS) (Figure 1).

We used LC microdroplets because (i) in contrast to micrometer-thick films of LCs, the use of microdroplets eliminates the need for a chemically functionalized solid to support the LC,[24] (ii) microdroplets can be rapidly screened (10,000 microdroplets in less than one minute) using the light scattering mode of a flow cytometer,[25] and (iii) elastic strain of the LC within the droplet geometry can trigger ordering transitions at low concentrations of analytes.[26]
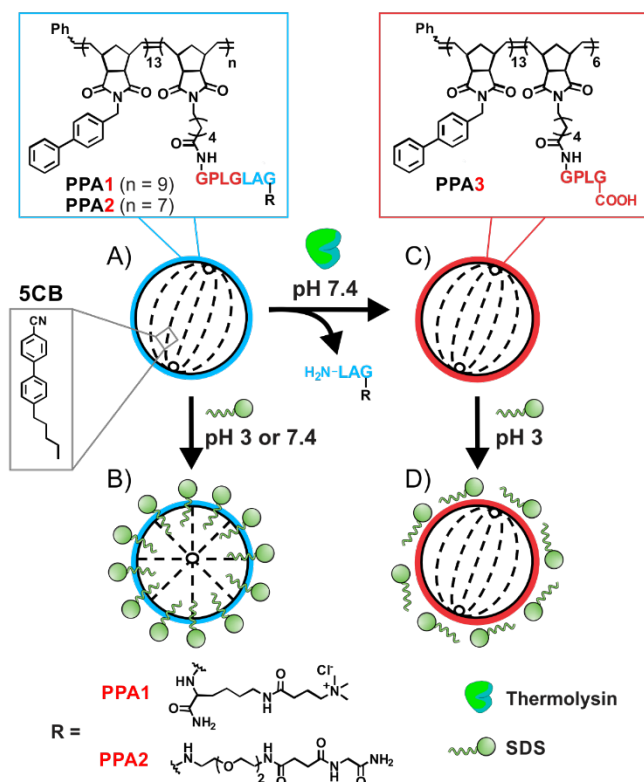
Figure 1 Response of PPA-programmed LC microdroplet to enzymatic reactions at their aqueous interface. (A) PPA-decorated 5CB microdroplet in bipolar configuration. (B) PPA-decorated 5CB microdroplet in radial configuration after exposure to SDS at either pH 3 or pH 7.4. (C) PPA-decorated 5CB microdroplet in bipolar configuration after *in situ* enzyme treatment at pH 7.4. (D) Enzyme processed PPA-decorated 5CB microdroplet in bipolar configuration after exposure to SDS at pH 3.

PPAs were synthesized via ring-opening metathesis polymerization (ROMP)[27–29] using norbornene-based monomers containing either biphenyl moieties or peptidic moieties (GPLGLAGK for PPA1, GPLGLAG for PPA2) to form hydrophobic and hydrophilic blocks, respectively (resulting ring-opened products as polymers are shown in Figure 2).[10,11,30] The biphenyl group was used as the hydrophobic block to promote the co-assembly of the PPA at the interface of the biphenyl-based LC. The amino acid sequence of the peptidic moieties incorporated into the PPAs was selected to be enzymatically processable by Thermolysin.[31] We prepared PPA3 to serve as an analogue of the enzymatic product of PPA1 and 2 (Figure 2).
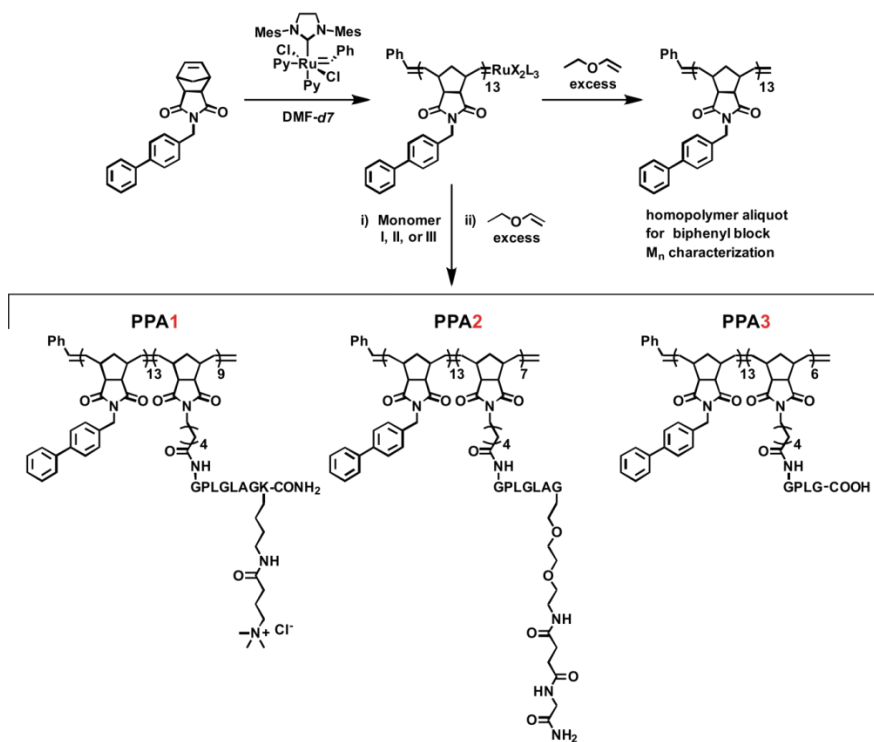
Figure 2 Block copolymer synthesis of PPA 1, 2, and 3 *via* ROMP.

Surface activities of PPA-decorated LC microdroplets

Prior to assembly of PPAs at the interfaces of LC microdroplets and to our exploration of the influence of PPA-surfactant complexes on LC ordering, we characterized the surface activity of the PPAs by measuring their surface pressure-area (Π-A) isotherms at the aqueous/air interface at physiological pH 7.4 (Figure 3).

Inspection of Figure 3A reveals that PPAs form stable monolayers at the surface of PBS solutions and that the Π-A isotherms are dependent on the structure of the PPAs. By rescaling the Π-A isotherms to the interfacial concentration of peptidic moieties presented by each PPA, we found that PPA1 and PPA2 were similar to each other but significantly different from PPA3 (Figure 3B). This result indicates that the peptidic moieties of PPA1 and PPA2 play a central role in determining the interfacial properties of the PPAs, and that enzymatic cleavage of the peptide side-chain, which generates structures analogous to PPA3, should lead to substantial changes in interfacial properties.
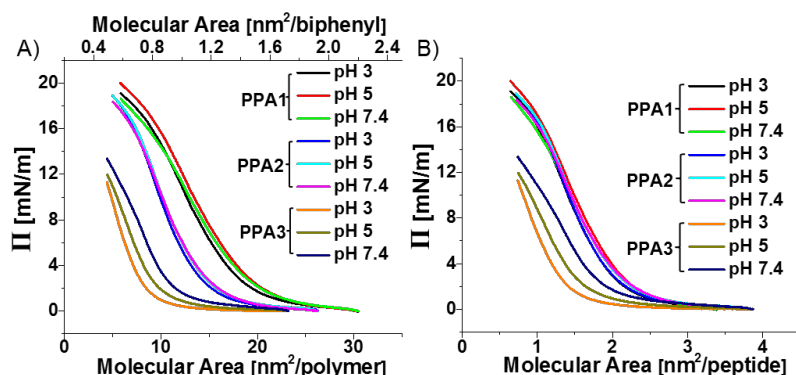
Figure 3 Surface pressure (Π) –area isotherms of the PPAs measured on aqueous PBS solutions at 25 °C with varying pH. Molecular area was scaled to the number of (A) polymer molecules along with the number of (A) biphenyl and (B) peptide groups within the PPA.

In addition, we note that PPA3 differs from PPA1 and PPA2 by the presence of a C-terminal carboxylic acid (Figure 1). Based on this difference in chemical functionality, we predicted that the Π-A isotherms of PPA3 but not PPA1 nor PPA2 would change with acidification of the PBS. The pH-dependent change in the Π-A isotherm of PPA3 confirms this prediction (Figure 3) and is consistent with protonation of carboxylate groups and reduction in the electrostatic contribution to the surface pressure. In the section that follows, we return to the pH-dependent rearrangement of PPA3 in the context of tuning the interactions of surfactants with PPA-decorated interfaces of LCs.

Next, we formed LC-in-PBS emulsions at pH 7.4 with PPAs dissolved in the 5CB microdroplets at concentrations of 1 to 100 mg PPA/mL 5CB. Electrophoretic mobility measurements revealed microdroplets of pure 5CB in PBS to possess a negative ζ-potential of -28 ± 3 mV, similar to previous studies showing that hydrophobic surfaces acquire excess negative surface charge density in aqueous solutions.[32–34] By contrast, 5CB microdroplets doped with 10 mg/ml PPA1, PPA2 or PPA3 exhibited either positive (30 ± 3 mV), neutral (-5 ± 1 mV) or negative (-55 ± 4 mV) values of ζ-potentials, respectively (Table 1).

Table 1 ζ-potentials (mV) of PPA-laden 5CB droplets at various PPA concentrations, measured in PBS at pH 7.4.

	1 mg PPA/ mL 5CB	10 mg PPA/ mL 5CB	100 mg PPA/ mL 5CB
PPA 1	1 ± 3	30 ± 3	28 ± 2
PPA	-10 ± 2	-5 ± 1	-5 ± 1

	2		
PPA	·48 ± 3	·55 ± 4	·55 ± 3
3			

The PPA-dependent ζ-potentials are consistent with the influence of quaternary ammonium, amide and carboxylic acid groups of PPA1, PPA2 and PPA3, respectively, on the interfacial charging of the LC microdroplets (Figure 3), and thus provide evidence that the PPAs added to the 5CB spontaneously assemble at the aqueous interface of the LC droplets. Furthermore, for all PPAs, the ζ-potential changed significantly when PPA concentration increased from 1 to 10 mg PPA/mL 5CB but remained constant when the PPA concentration increased from 10 to 100 mg PPA/mL 5CB. These results indicate that 10 mg PPA/mL in 5CB corresponds to saturation coverage. We also calculated the ζ-potentials for PPA1 and PPA3-coated 5CB droplets (with 10 mg PPA/mL 5CB, Table 1) to correspond to surface charge densities of 0.18 e/nm2 and -0.38 e/nm2, respectively (see methods). The corresponding molecular areas of PPA1 and PPA3 obtained from Figure 3B are ~2.4 and ~2 nm2/peptide, respectively, consistent with each peptide group at the interface bringing approximately one charge to the interface. Finally, we note that acidification had the largest effect on the ζ-potentials of the LC droplets decorated with PPA3 as compared to PPA1 and PPA2 (Table 2), consistent with our measurements of Π-A isotherms as a function of pH (Figure 3).

Table 2 ζ-potentials (mV) of bare and PPA-laden 5CB droplets doped at 10 mg PPA/mL 5CB, measured in PBS at pH 3 or 7.4, with or without 1mM SDS.

	pH 7.4	pH 7.4 w/ SDS	pH 3	pH 3 w/ SDS
5CB	·28 ± 3	·70 ± 5	·7 ± 2	·73 ± 5
PPA 1	·30 ± 3	·48 ± 2	·28 ± 2	·47 ± 2
PPA 2	·5 ± 1	·35 ± 2	·5 ± 1	·32 ± 2
PPA 3	·55 ± 4	·50 ± 4	·6 ± 2	·38 ± 2

Past studies have shown that the charge status of polymers can regulate the organization of interfacial polymer-surfactant assemblies.[12,19,21,22] Therefore, we hypothesized that the transformation of PPA1 or PPA2 to generate structures analogous to PPA3 could lead to changes in polymer-surfactant complexation at the interface of the LCs and thus changes in the ordering of the LCs.

Characterization of liquid crystal microdroplets in the presence of surfactants by polarized light microscopy

To characterize the influence of interfacial PPAs and PPA-surfactant complexes on the internal ordering of the LC microdroplets (containing 10 mg PPA/mL 5CB), we used polarized light microscopy (Figure 4). We measured the PPA-decorated LC microdroplets to exhibit optical signatures characteristic of a so-called bipolar configuration of the LC, which results from LC anchored parallel to the PPA-decorated droplet interface (Figure 4C).[35,36]
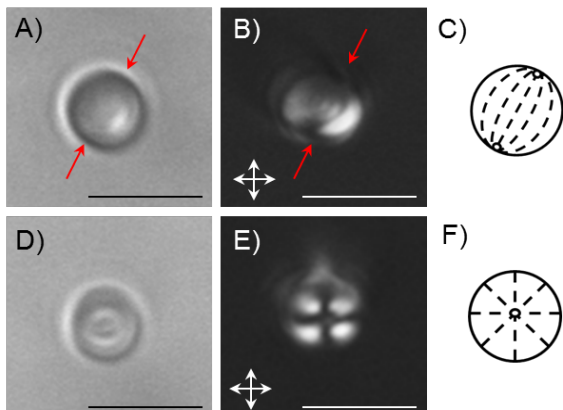
Figure 4 Representative optical micrographs of PPA3-decorated LC microdroplets in the presence of SDS at (A-B) pH 3 and (D-E) 7.4. A and D are bright field images whereas B and E were obtained using crossed-polars. C and F are schematic illustrations of the ordering of the LC within the microdroplets. Red arrows indicate boojums at the LC microdroplet/aqueous interface. Scale bars are 5 μm.

However, in contrast to the PPAs, past studies have shown that a range of surfactants with linear aliphatic tails, such as sodium dodecylsulfate (SDS) and dodecyltrimethylammonium bromide (DTAB), cause perpendicular orientations of LCs at aqueous interfaces due to interdigitation of the surfactant tails into the LC.[37–39] For LC microdroplets, the perpendicular orientation of the LC leads to a so-called radial configuration (Figure 4F).[35,36] However, surfactants with branched tails, such as Triton X-100, do not perturb LC microdroplets from bipolar configurations (Figure 4C).[37,39] To explore the influence of interfacial PPA-surfactant complexes on LC ordering transitions, we next screened PPA-decorated LC microdroplets against solutions of surfactants (Triton X-100, DTAB and SDS), by adding 1 mM surfactant to the aqueous phase after formation of the PPA-laden 5CB droplets. At pH 7.4, we observed all three types PPA-coated 5CB droplets with or without Triton X-100 to exhibit bipolar configurations. In contrast, exposure to DTAB at pH 7.4 caused radial configurations for bare LC droplets and bipolar configurations when DTAB complexed with PPA interfacial assemblies, indicating that the PPAs changed

the interaction between DTAB and the 5CB. SDS at pH 7.4 triggered formation of radial droplets for bare and PPA-laden 5CB droplets (Figure 4D-F), indicating that SDS can complex with the interfacial PPA layer such that interdigitation with 5CB is preserved.

Because the Π-A isotherms and ζ-potential measurements reported above revealed that PPA3 but not PPA1 nor PPA2 exhibit pH-dependent interfacial activity (Figure 3, Table 2), we also explored the effect of changes in pH on the PPA-mediated interactions of SDS with the LC microdroplets. Significantly, at pH 3, radial configurations were observed for 5CB droplets decorated with PPA1 and PPA2 while bipolar droplets were found for PPA3-laden 5CB droplets (Figure 4A-C). We note that the carboxylic acid groups of PPA3 are expected to have a pK_a between 2 (pK_a of glycine carboxylic acid) and 5 (pK_a of acetic acid), leading us to conclude that protonation of the carboxylates of PPA3 at pH 3 leads to an interfacial PPA3-SDS complex that prevents the interdigitation of SDS with 5CB.

The results above demonstrate that PPA1 and PPA2 modulate the interaction of SDS with the LC microdroplets at pH 3 in a manner that is distinct from PPA3. To provide insight into this observation, we sought to determine if the differential effect of PPA3 relative to PPA1 and PPA2 occurred via differences in either (i) the extent of adsorption of SDS with the PPA-decorated microdroplet or (ii) the organization of co-assemblies formed by PPA and SDS at the LC interface. Accordingly, we performed electrophoretic mobility measurements at pH 3 and 7.4 using PPA-decorated LC microdroplets with and without SDS (Table 2). Significantly, at pH 3, the ζ-potentials of all PPA-decorated 5CB droplets became more negative upon exposure to SDS (Table 2), consistent with SDS adsorption onto the microdroplet interface. This result thus supports our hypothesis that the PPAs mediate the surfactant-triggered response of the LCs not through changes in the extent of adsorption but rather through changes in the organization of PPA interfacial assemblies and SDS at the interface.

In situ detection of proteolytic degradation of peptide polymer amphiphile-coated liquid crystal microdroplets

A key result, described above, is identification of experimental conditions under which SDS can be used to develop a differential LC response to PPA3 (the analogue of an enzymatically cleaved PPA1 or PPA2) relative to PPA1 and PPA2. To further evaluate this finding as the basis of a modular and general strategy for triggering LC ordering transitions using biomolecular events, we next characterized the response of LC microdroplets to *in situ* enzymatic treatment of PPA1 and PPA2 decorated 5CB droplets. We formed PPA-containing 5CB aqueous emulsions at pH 7.4 and then incubated the LC droplets against Thermolysin. After incubation, the response of the emulsion was "developed" using acidified SDS aqueous solutions (Figure 1). Initially, LC

droplets decorated with PPA1 and PPA2 exhibited radial configurations after acidified SDS development (0 hr, Figure 5). However, upon incubation with Thermolysin, the fraction of LC droplets exhibiting radial configurations decreased with increasing time of Thermolysin incubation. Specifically, we observed the optical response of the LC microdroplets to correlate closely with the extent of conversion of the PPA as determined by HPLC (Figure 6).
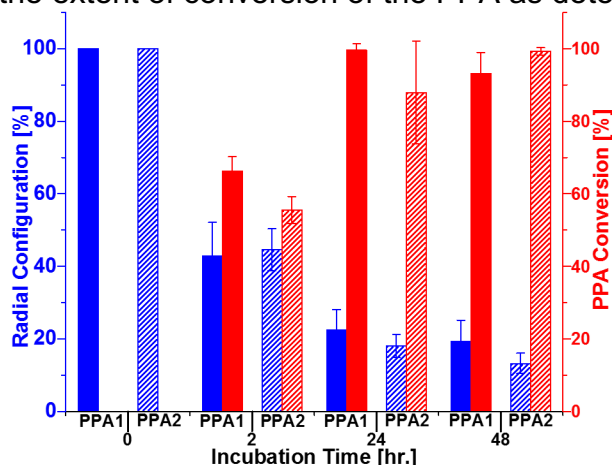

Figure 5 Optical response of LC microdroplets triggered by enzymatic processing of either PPA1 or PPA2, as a function of time of incubation against Thermolysin (left axis, blue bars). Extent of PPA conversion, as determined by HPLC (right axis, red bars). Error bars represent triplicates with > 400 droplets analyzed.

We note that the presence of Thermolysin alone does not induce LC ordering transitions in PPA-free LC droplets and Thermolysin alone also does not prevent SDS interdigitation with LC mesogens at the interface of PPA-free LC droplets (see methods section). In summary, these results demonstrate that SDS can "develop" the optical response of the LC microdroplets to enzymatically triggered processing of PPAs.

Conclusion and future outlook

In conclusion, we have demonstrated the design of biologically active PPAs with oligopeptide and biphenyl side-chains that spontaneously assemble at the aqueous interface of LC microdroplets. PPAs can be enzymatically processed to regulate the formation of PPA-surfactant complexes at the LC microdroplet aqueous interface, thus triggering changes in the optical properties of the microdroplets. A significant merit of the approach is that the design of the system is modular, involving specification of (i) the LC-directing functional side-chain of the PPA, (ii) the biologically active oligopeptide of the PPA, and (iii) the synthetic surfactant that differentially interacts with the PPA before and after enzymatic processing. This modularity offers the promise of a generalizable approach that makes possible the triggering of changes in LC

microdroplet optical properties by a wide range of biomolecular transformations. When combined with recently developed high throughput (10,000 droplets per second) flow-based methods of optically transducing LC microdroplets,[7] such a capability would form the basis of a new and broadly useful class of stimuli-responsive supramolecular systems, such as programmable emulsions, droplet-based microreactors or microanalytical systems.

This work is a summary of published work: C. Derek Ma, Lisa Adamiak, Daniel S. Miller, Xiaoguang Wang, Nathan C. Gianneschi, and Nicholas L. Abbott. "Liquid Crystal Interfaces Programmed with Enzyme-Responsive Polymers and Surfactants." Small, 2015, 11, 5747-5751. Copyright 2015 Wiley.

Methods

General methods

All reagents were purchased from commercial sources and used without further purification. A Malvern Zetasizer Nano ZSP was used to obtain ζ-potentials of emulsions. Sealed ampules of DMF-d_7 (Cambridge Isotopes) were used without further modification. Amino acids were purchased from AAPPTEC and Novabiochem. Peptides were either synthesized by hand or using an APPTTEC Focus XC automated synthesizer. Monomer *N*-(hexanoic acid)-*cis*-5-norbornene-*exo*-dicarboximide was prepared as previously described.[40] Grubbs' initiator (IMesH$_2$)(Cl)$_2$(C$_5$H$_5$N)$_2$Ru=CHPh [IMesH2 = 1,3-dimesityl-4,5-dihydroimidazol-2-ylidene] was prepared according to methods described by Sanford.[28] Flash column chromatography of *N*-(4-phenylbenzyl)-*cis*-5-norbornene-*exo*-dicarboximide was performed using silica gel 60 (230 - 400 mesh). All polymerizations were conducted in J Young NMR tubes (5 mm diameter) in a glove box under dinitrogen atmosphere at room temperature using DMF-d_7 from sealed ampules. Polymer dispersities and molecular weights were determined by size-exclusion chromatography (Phenomenex Phenogel 5u 10, 1K-75K, 300 x 7.80 mm in series with a Phenomex Phenogel 5u 10, 10K-1000K, 300 x 7.80 mm (0.05 M LiBr in DMF)) using a Shimadzu LC-AT-VP pump equipped with a multi-angle light scattering detector (DAWN-HELIOS: Wyatt Technology), a refractive index detector (Hitachi L-2490) and a UV-Vis detector (Shimadzu SPD-10AVP) normalized to a 30,000 MW polystyrene standard (Flow rate: 0.75 mL/min). The dn/dc value used for each polymer was 0.179. ^{1}H NMR (400 MHz) and ^{13}C NMR (100 MHz) spectra were recorded on Varian Mercury Plus spectrometers. All NMR spectra were recorded in DMF-d_7 or CDCl$_3$ and referenced to the residual protons. RP-HPLC analyses were performed on a Jupiter Proteo90A phenomenex column (150 x 4.60 mm) using a Hitachi-Elite LaChrom L-2130 pump equipped with a UV-Vis detector (Hitachi-Elite LaChrome L-2420) using a binary gradient

(Buffer A: 0.1% TFA in water; Buffer B: 0.1% TFA in acetonitrile; Flow rate: 1 mL/min). Peptides were purified using a Jupiter Proteo90A Phenomenex column (2050 x 25.0 mm) on a Waters DeltaPrep 300 system using a binary gradient (Buffers A and B; Flow rate: 22 mL/min). Mass spectra were obtained at the UCSD Chemistry and Biochemistry Molecular Mass Spectrometry Facility.

Estimation of charge densities

The surface charge density (σ) of a colloid can be estimated from its ζ-potential (ζ) using:[41]

$$\sigma = \frac{2\varepsilon_r \varepsilon_0 k_B T}{ve\lambda_D} \sinh\left(\frac{ve\zeta}{2k_B T}\right) \left[1 + \frac{\lambda_D}{r} \frac{1}{\cosh^2(ve\zeta/4k_B T)}\right] \qquad [1]$$

where ε_r and ε_0 are the permittivity of water at room temperature ($\varepsilon_r = 78.54$ $C^2 J^{-1} m^{-1}$) and vacuum ($\varepsilon_0 = 8.85 \times 10^{-12}$ $C^2 J^{-1} m^{-1}$), respectively, k_B is the Boltzmann constant, T is the temperature, v is the valence number ($v = 1$), e is the electron charge ($e = 1.6 \times 10^{-19}$ C), r is the radius of the LC microdroplet (r ~2 μm), and λ_D is the Debye screening length:[42]

$$\lambda_D = \left(\frac{\varepsilon_r \varepsilon_0 k_B T}{e^2 \sum_i z_i^2 M_i}\right)^{\frac{1}{2}} \qquad [2]$$

where z_i is the ionic charge and M_i is the molar concentration of the salt in bulk solution. From equation 2, we estimate λ_D to be 0.74 nm for 10 mM PBS.

Response of LC microdroplets to Thermolysin

Bare 5CB droplets were incubated in the presence of Thermolysin under the same conditions as described for the PPA-laden 5CB microdroplets in section 3.5. The presence of Thermolysin resulted in bipolar LC microdroplets for all conditions tested. For bare 5CB droplets incubated against Thermolysin, the addition of SDS triggered a LC ordering transition from a bipolar to a radial configuration (for all incubation times reported in Figure 4.5). Furthermore, the addition of SDS at pH 7.4 to Thermolysin-treated, PPA-laden 5CB droplets triggered LC ordering transitions from bipolar to radial configurations (for all incubation times reported in Figure 4.5). We thus conclude that the adsorption of Thermolysin onto the LC/PBS interface does not induce LC ordering transitions and that its presence does not interfere with SDS induced LC ordering transitions.

Peptide synthesis and purification

Peptide monomers were synthesized *via* standard FMOC-based solid phase synthesis using Rink Amide MBHA resin (AAPPTEC) for the preparation of a C-terminal amide or FMOC-Gly-Wang resin (Novabiochem) for the preparation a C-terminal carboxylate. In brief, FMOC deprotection was performed using 20% 4-methylpiperidine in DMF. Amino acid couplings were carried out using HBTU and DIPEA (resin/amino acid/HBTU/DIPEA 1:3:2.9:6). FMOC-Peg$_2$-

Suc-OH (Anaspec) was coupled in the same way as other amino acids. To ensure complete loading, the initial amino acid was double coupled (i.e. loaded onto the resin for 45 min followed by a rinse cycle with DMF and a second application of fresh amino acid/coupling reagent for another 45 min). *N*-(hexanoic acid)-*cis*-5-norbornene-exo-dicarboximide was double coupled to the N-terminus of the peptide (2.5 equiv). Side chain deprotection of Lys(Mtt) groups was afforded by shaking with DCM/TIPS/TFA 92:5:3 for five cycles (6 min each). Between each deprotection cycle, the resin was rinsed twice with DCM. (3-Carboxypropyl)trimethylammonium chloride (Sigma-Aldrich) was double-coupled to the Lys residue following deprotection (2.5 equiv). The resin was rinsed several times with DCM prior to cleavage of the final peptide. The final peptide monomers were cleaved from the resin using a mixture of trifluoroacetic acid (TFA), water, and triisopropylsilane (TIPS) (TFA/H$_2$O/TIPS 95:2.5:2.5) for 1 hr. The desired peptide was precipitated with cold ether followed by centrifugation at 3000 rpm for 7 min. The ether was decanted and the remaining pellet was dissolved in buffer A with minimal amounts of buffer B. Peptides were analyzed using RP-HPLC and purified using preparative RP-HPLC. Peptide identity and purities were confirmed using ESI-MS and RP-HPLC monitoring at I$_{Abs}$ = 214 nm.
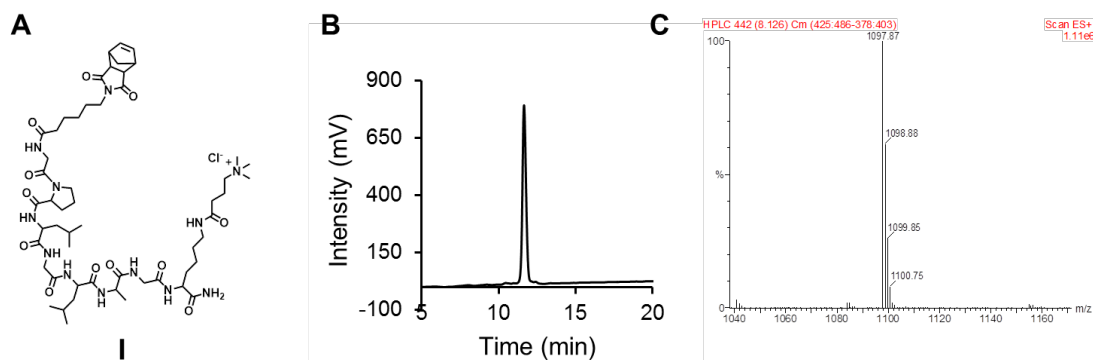
Figure 6 Purification of peptide monomer (I), (A) N-(Hexanamide-Gly-Pro-Leu-Gly-Leu-Ala-Gly-Lys(4-trimethylammonium butyramide))-cis-5-norbornene-exo-dicarboximide. (B) RP-HPLC analysis post-purification (20-60 % buffer B, retention time = 12.5 min). (C) ESI-MS: Mass calcd: 1097.67; Mass obs: [M]+ 1097.87.
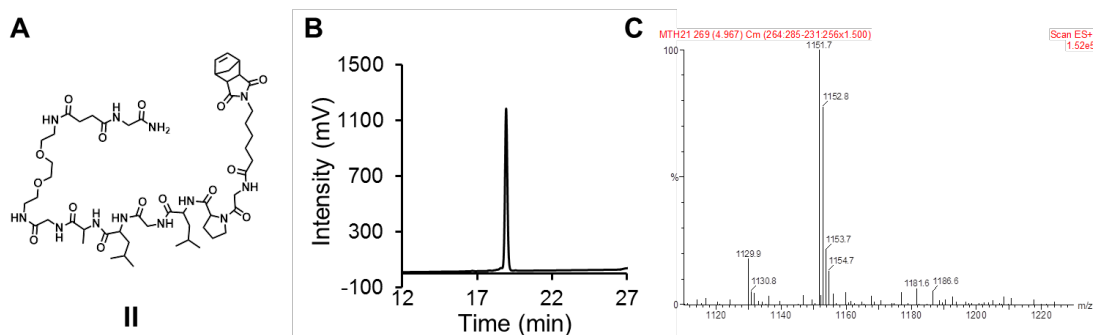
Figure 7 Purification of peptide monomer (II), (A) N-(Hexanamide-Gly-Pro-Leu-Gly-Leu-Ala-Gly-Peg-Succ-Gly)-cis-5-norbornene-exo-dicarboximide. (B) RP-HPLC analysis post-purification (20-60 % buffer B, retention time = 18.5 min). (C) ESI-MS: Mass calcd: 1128.62; Mass obs: [M+H]+ 1129.9, [M+Na]+ 1151.7.
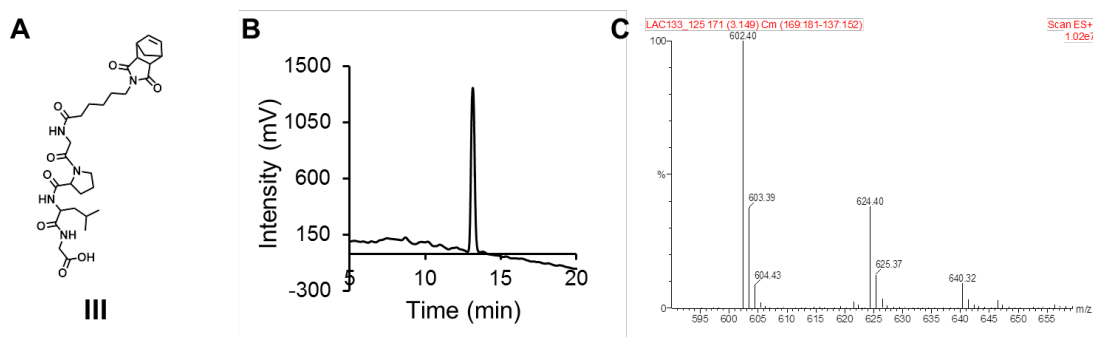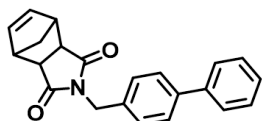

Figure 8 Purification of peptide monomer (III), (A) *N*-(Hexanamide-Gly-Pro-Leu-Gly)-*cis*-5-norbornene-*exo*-dicarboximide. (B) RP-HPLC analysis post-purification (20-60 % buffer B, retention time = 13 min). (C) ESI-MS: Mass calcd: 601.31; Mass obs: [M+H]+ 602.40, [M+Na]+ 624.40, [M+K]+ 640.32.

Synthesis of biphenyl monomer

***N*-(4-phenylbenzyl)-*cis*-5-norbornene-*exo*-dicarboximide** (Nor-biphenyl). A round-bottom flask was charged with *cis*-5-norbornene-*exo*-2,3-dicarboxylic anhydride (2.5 g, 15.2 mmol) and 4-phenylbenzylamine (2.9 g, 15.8 mmol). To the solid mixture was added toluene (40 mL), followed by sonication for several minutes. Et$_3$N (212 μL, 1.52 mmol) was added. The flask was heated to reflux for 12 h. The mixture was then allowed to cool to room temperature and concentrated. The reaction mixture was diluted with CH$_2$Cl$_2$ (40 mL) and washed with 1 M aqueous HCl (2 × 20 mL). The organic layer was washed

with saturated aqueous NaCl (20 mL), dried Na_2SO_4), filtered, and concentrated under reduced pressure. Purification by flash chromatography (4:1, hexanes:EtOAc) gave the desired product (3.0 g, 60%) as a white solid: ^{1}H-NMR (400 MHz, $CDCl_3$) δ 7.32 - 7.58 (m, 9H), 6.28 (t, 2H, J = 1.8 Hz), 4.67 (s, H), 3.27 (m, 2H), 2.69 (d, 2H, J = 1.3 Hz), 1.42 - 1.44 (m, 1H), 1.10 - 1.13 (m, 1H); ^{13}C NMR (100 MHz, $CDCl_3$) δ 177.7, 140.8, 140.6, 137.9, 134.9, 129.4, 128.8, 127.41, 127.38, 127.1, 47.9, 45.3, 42.7, 42.1; HRMS expected: 329.14 [M + H]$^+$, found: 352.13 [M + Na]$^+$
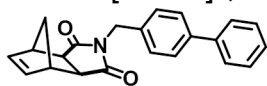
(400 MHz, $CDCl_3$)
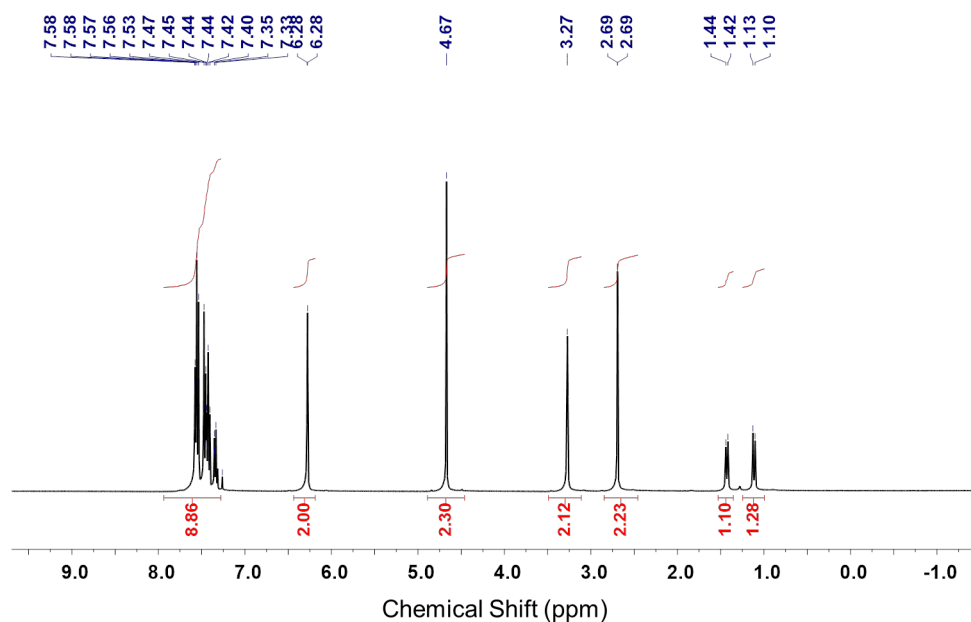
Figure 1 ^{1}H NMR spectrum of Nor-biphenyl.

(100 MHz, CDCl₃)
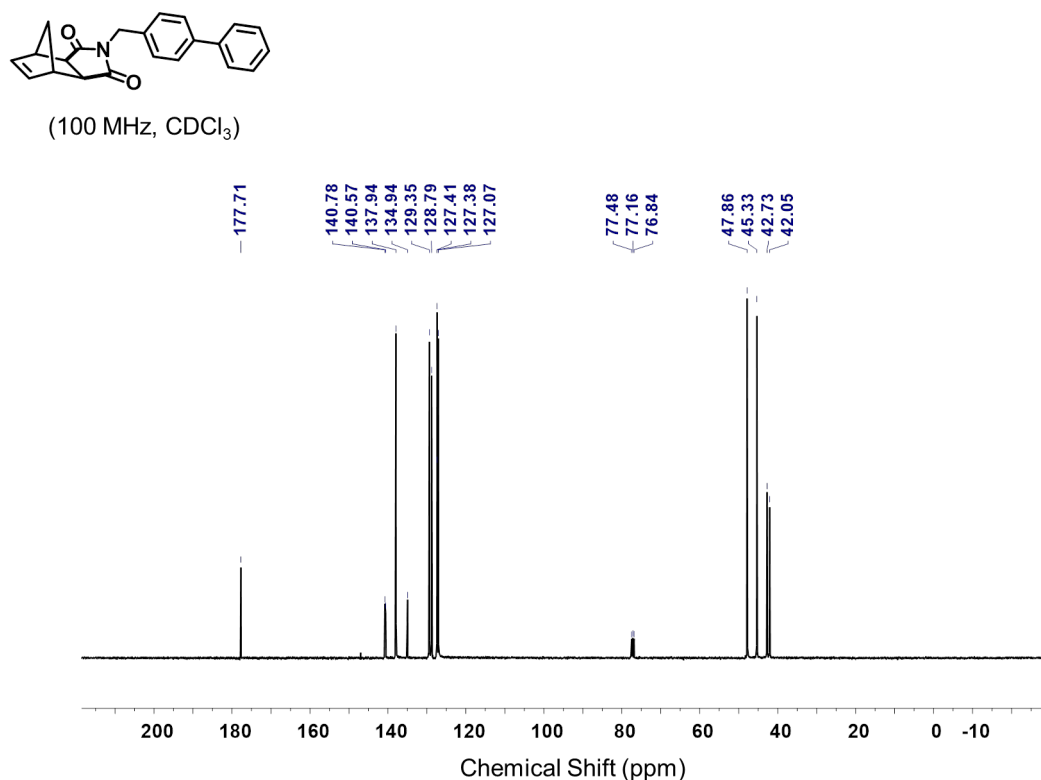
Figure 2 ¹³C NMR spectrum of Nor-biphenyl.

Polymer synthesis and purification

All polymerization reactions were accomplished in a glove box under dinitrogen atmosphere with anhydrous solvents. Grubbs' modified second generation catalyst (IMesH₂)(Cl)₂(C₅H₅N)₂Ru=CHPh (1 equiv) was dissolved in DMF-d_7 and added to the Nor-biphenyl monomer (15 equiv) in DMF-d_7 to a final volume of 450 µL in a J Young NMR tube. The tube was inverted several times to ensure mixing. A ¹H NMR spectrum was recorded to confirm complete monomer consumption at 30 min. An aliquot (20 µL) of the homopolymer was removed from the glove box and terminated with 20 µL ethyl vinyl ether. The homopolymer solution was split into three portions and the respective peptides in DMF-d_7 were added (0.1 mL, 15 equiv). The copolymer solutions were then transferred to three J Young NMR tubes. ¹H NMR spectra were recorded to confirm the complete consumption of the peptide monomers at 1.5 hr. The copolymer solutions were transferred to vials and each polymerization reaction was terminated with excess ethyl vinyl ether (50 µL). Characterization of polymer molecular weights and dispersities was afforded via SEC-MALS. All polymers were triturated with DMF and cold ether and centrifuged at 3000 rpm for 7 min. The ether was decanted and the process was repeated 3 times. The remaining pellet was dissolved in water with a minimal amount of acetonitrile and lyophilized to afford a white powder.
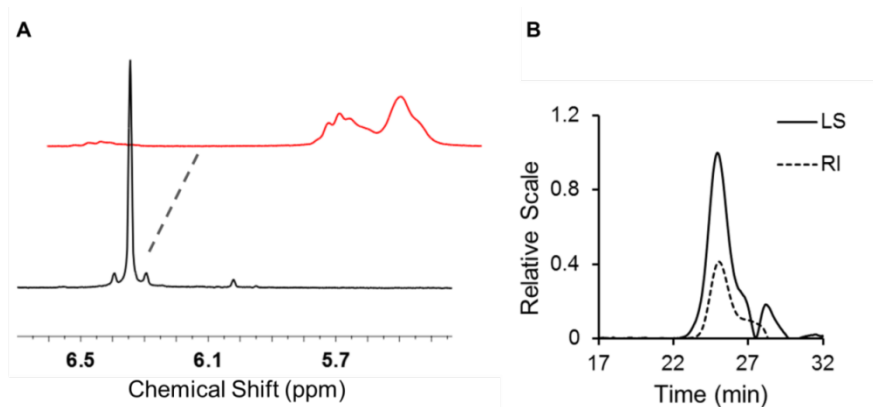
Figure 3 Characterization of Nor-biphenyl homopolymer *via* ^{1}H NMR and SEC-MALS, respectively. (A) Complete consumption of the norbornene olefin was observed after 30 min by monitoring the disappearance of the proton resonance at 6.34 ppm. (B) SEC-MALS characterization (dn/dc = 0.179, Mn = 4,302, Mn/Mw = 1.029); Degree of polymerization (DP) = 13.
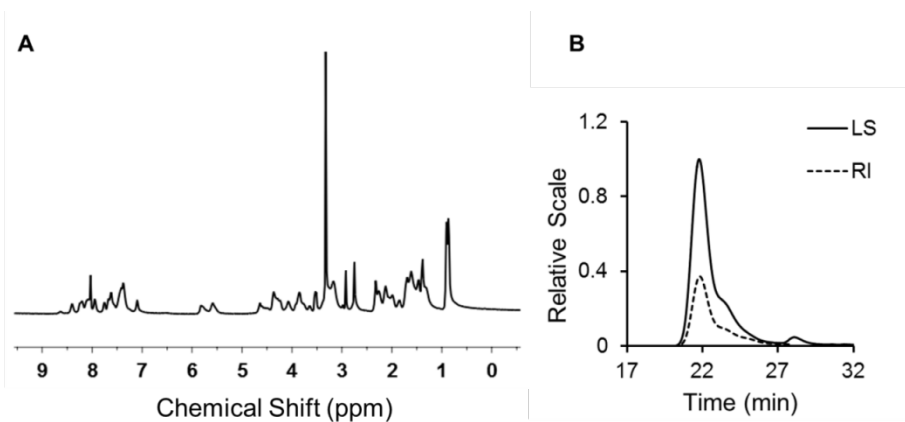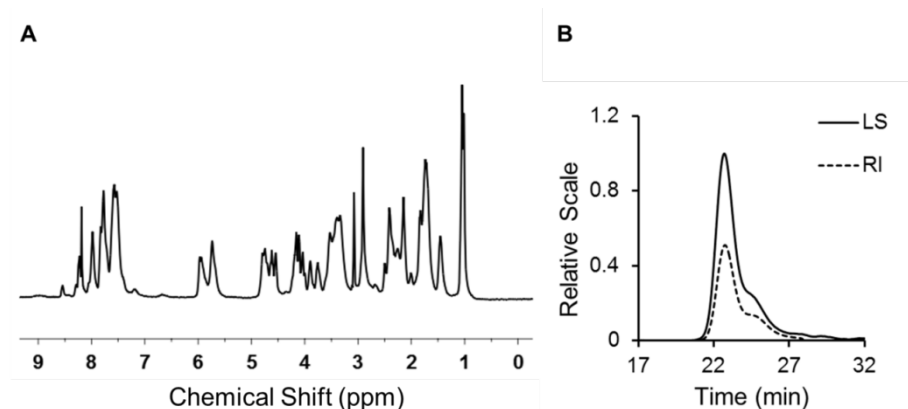

Figure 4 Characterization of PPA 1 block copolymer via ^{1}H NMR and SEC-MALS, respectively. (A) Complete consumption of the norbornene peptide monomer I olefin was observed after 1.5 hr. (B) SEC-MALS characterization (dn/dc = 0.179, M_n = 14,030, M_n/M_w = 1.007), DP = 13-*b*-9.
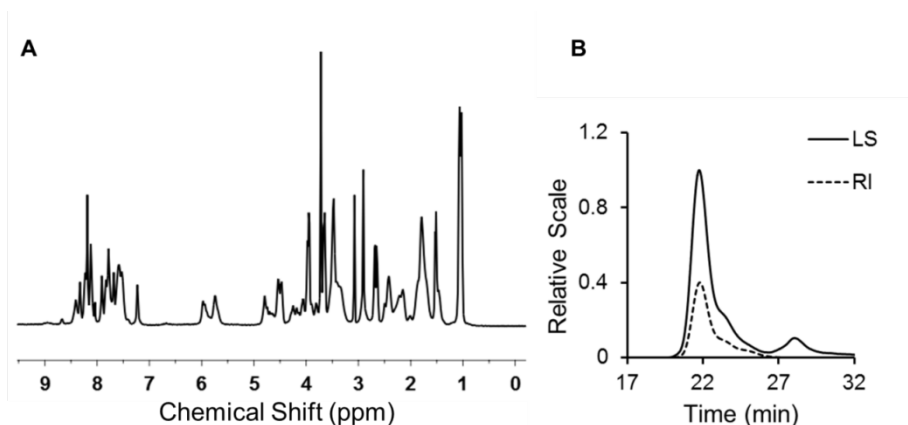
Figure 5 Characterization of PPA 2 block copolymer via ^{1}H NMR and SEC-MALS, respectively. (A) Complete consumption of the norbornene peptide monomer II olefin was observed after 1.5 hr. (B) SEC-MALS characterization (dn/dc = 0.179, M_n = 12,100, M_n/M_w = 1.007), DP = 13-*b*-7.

Figure 6 Characterization of PPA 3 block copolymer via ^{1}H NMR and SEC-MALS, respectively. (A) Complete consumption of the norbornene peptide monomer III olefin was observed after 1.5 hr. (B) SEC-MALS characterization (dn/dc = 0.179, M_n = 8,027, M_n/M_w = 1.010), DP = 13-*b*-6.

Preparation of LC emulsions

10 mM PBS (prepared from powder packets obtained from Sigma-Aldrich) used throughout our experiments contained 0.5 mM calcium chloride ($CaCl_2$ dihydrate from Sigma-Aldrich), which was added to ensure the structural stability of Thermolysin. The pH of the PBS was adjusted with concentrated HCl (25 vol. % from Fisher Scientific) and 2 M NaOH (Fisher Scientific) as needed. To prepare PPA-decorated microdroplets of 5CB (4-cyano-4'-pentylbiphenyl, Merck), 10 μL of the PPA in methanol (HPLC grade from Fisher Scientific) at 1 mg/mL PPA was added to 1 μL 5CB in disposable glass culture tubes (VWR), then the PPA doped 5CB was dried under a gentle

stream of nitrogen and placed under vacuum for 1 hr. Following removal of all volatiles, 1 mL PBS at pH 7.4 was added to the PPA doped 5CB for emulsification. The two-phase system was emulsified by repeated cycles of vortexing (2500 rpm for 10 s.) and sonication (1 min.) until the solution became milky white in appearance. Note: the water for the sonication bath (2 L) was replaced with the recommended volume fresh to ensure homogeneity between emulsion batches.

Thermolysin treatment of PPA-laden 5CB droplets

Thermolysin (purchased from Promega) was reconstituted in PBS at pH 7.4 and stored at -20 °C for a maximum duration of two weeks. The reconstituted Thermolysin was equilibrated to room temperature for a minimum of 30 min. prior to use. Thermolysin was then added to emulsions that had equilibrated for at least 15 min to obtain a final Thermolysin concentration of 0.2 µM in the emulsions. The Thermolysin-containing emulsions were then gently inverted several times to distribute the enzyme throughout the emulsions. Emulsions were incubated in the presence of Thermolysin at room temperature with periodic gentle mixing of the reaction to prevent sedimentation. 20 µL of 0.5 M ethylenediaminetetraacetic acid (EDTA, Sigma-Aldrich) in aqueous at pH 8 was added to 100 µL of the enzyme-treated emulsions to quench the reaction at the desired incubation times. After quenching the enzyme reaction, the emulsion was lyophilized for storage. To determine the percent conversion of the peptide substrates displayed on the PPAs, the lyophilized samples were reconstituted in 0.1 mL H_2O and then monitored *via* RP-HPLC. Percent conversion was calculated from the concentration of product determined against standard curves of the authentic cleaved peptide fragments. The peaks corresponding to the enzymatically cleaved products were collected from RP-HPLC and the fragment identities were confirmed by ESI-MS. A binary gradient was used (2 - 50 % buffer B over 30 minutes) for sample analysis.
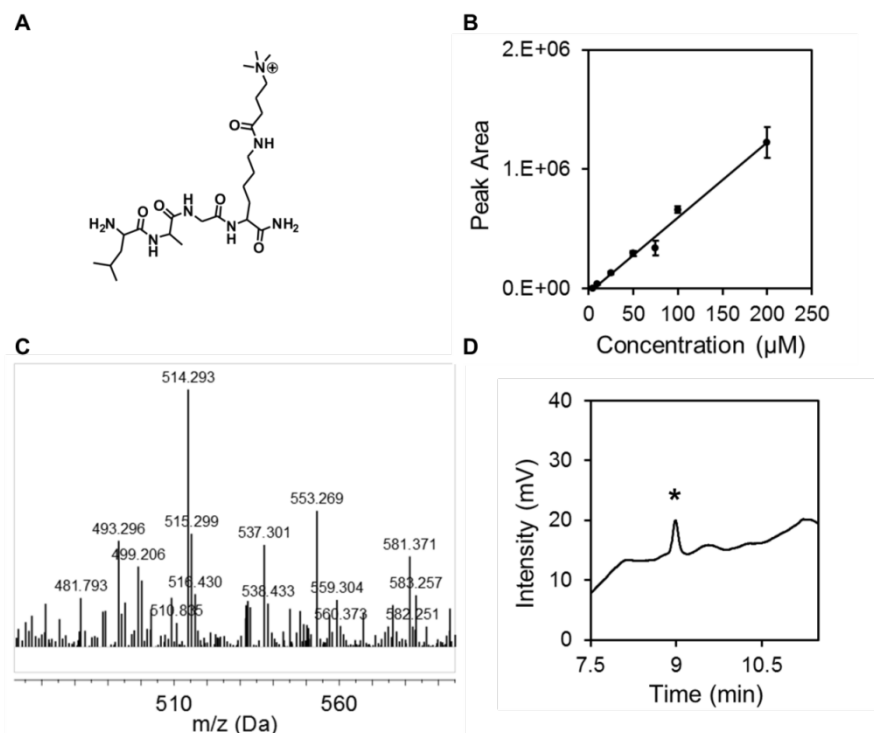
Figure 7 Analysis of Thermolysin-treated PPA 1-laden 5CB droplets. (A) Chemical structure of the cleaved peptide fragment from PPA 1. (B) Standard curve of the authentically cleaved peptide fragment performed in triplicate. (C) ESI-MS confirming the enzymatically cleaved peptide identity of the peak collected from RP-HPLC. ESI-MS: Mass calcd: 514.37; Mass obs: $[M]^+$ 514.29. (D) Peak corresponding the enzymatically cleaved product as indicated from RP-HPLC.

Figure 8 Analysis of Thermolysin-incubated PPA 2-laden 5CB droplets. (A) Chemical structure of the cleaved peptide fragment from PPA 2. (B) Standard curve of the authentically cleaved peptide fragment performed in triplicate. (C) ESI-MS confirming the enzymatically cleaved peptide identity of the peak collected from RP-HPLC. ESI-MS: Mass calcd: 545.32; Mass obs: $[M + H]^+$ 546.29. (D) Peak corresponding to the enzymatically cleaved product as indicated from RP-HPLC.

Amphiphilic development with surfactants

The Triton X-100, dodecyltrimethylammonium bromide (DTAB), and sodium dodecylsulfate (SDS) were purchased from Sigma-Aldrich and used without further purification. For amphiphilic development, 2 mM surfactant solutions in PBS at the corresponding emulsion pH were diluted into the appropriate emulsions to obtain a final surfactant concentration of 1 mM.

LC droplet characterization with microscopy

LC droplets were imaged using an Olympus IX71 inverted microscope with either a 60 x objective or 100 x oil immersion objective. Bright-field and polarized light micrographs of the LC droplets were collected with a Hamamtsu 1394 ORCAER CCD camera connected to a computer and controlled through SimplePCI imaging software. LC droplet characterization was limited to only LC droplets that were diffusing (translating and/or rotating).

Surface pressure-area isotherms

Langmuir films of the PPAs were formed at the PBS/air interface on a Nima 602A film balance equipped with a Wilhelmy plate (filter paper) to monitor the surface pressure. Prior to depositing the PPA onto the PBS/air interface, the Wilhelmy plate (filter paper) was equilibrated in PBS for 30 min. No significant surface pressure was observed from full compression of the bare PBS/air interface. A known volume of PPA solution in methanol was then spread uniformly across the PBS/air interface in a drop wise fashion. A 20 min equilibration period followed before film compression began. Symmetric compression of the PPA films, at a rate of 35 cm^2/min with the PBS subphase maintained at 25 °C, was used to collect the surface pressure-area isotherms.

References

1.   Boal, A. K. Self-assembly of nanoparticles into structured spherical and network aggregates. *Nature* **404,** 746–748 (2000).

2.   Randolph, L. M. Biological stimuli and biomolecules in the assembly and manipulation of nanoscale polymeric particles. *Chem. Sci.* **3,** 1363 (2012).

3.   Ringsdorf, H., Schlarb, B. & Venzmer, J. Molecular Architecture and Function of Polymeric Oriented Systems: Models for the Study of Organization, Surface Recognition, and Dynamics of Biomembranes. *Angew. Chemie Int. Ed. English* **27,** 113–158 (1988).

4.   Carlton, R. J. Chemical and biological sensing using liquid crystals. *Liq. Cryst. Rev.* **1,** 29–51 (2013).

5.   Aliño, V. J., Pang, J. & Yang, K.-L. Liquid Crystal Droplets as a Hosting and Sensing Platform for Developing Immunoassays. *Langmuir* **27,** 11784–11789 (2011).
6.   Bai, Y. & Abbott, N. L. Enantiomeric Interactions between Liquid Crystals and Organized Monolayers of Tyrosine-Containing Dipeptides. *J. Am. Chem. Soc.* **134,** 548–558 (2012).

7.   Brake, J. M., Daschner, M. K., Luk, Y.-Y. & Abbott, N. L. Biomolecular interactions at phospholipid-decorated surfaces of liquid crystals. *Science* **302,** 2094–7 (2003).

8.   Noonan, P. S., Roberts, R. H. & Schwartz, D. K. Liquid Crystal Reorientation Induced by Aptamer Conformational Changes. *J. Am. Chem. Soc.* **135,** 5183–5189 (2013).

9.   Price, A. D. & Schwartz, D. K. DNA Hybridization-Induced

Reorientation of Liquid Crystal Anchoring at the Nematic Liquid Crystal/Aqueous Interface. *J. Am. Chem. Soc.* **130,** 8188–8194 (2008).

10. Hahn, M. E., Randolph, L. M., Adamiak, L., Thompson, M. P. & Gianneschi, N. C. Polymerization of a peptide-based enzyme substrate. *Chem. Commun.* **49,** 2873–2875 (2013).

11. Ku, T.-H. Controlling and Switching the Morphology of Micellar Nanoparticles with Enzymes. *J. Am. Chem. Soc.* **133,** 8392–8395 (2011).

12. Alexandridis, P. & Alan Hatton, T. Poly(ethylene oxide) poly(propylene oxide) poly(ethylene oxide) block copolymer surfactants in aqueous solutions and at interfaces: thermodynamics, structure, dynamics, and modeling. *Colloids Surfaces A Physicochem. Eng. Asp.* **96,** 1–46 (1995).

13. Biggs, S., Selb, J. & Candau, F. Effect of surfactant on the solution properties of hydrophobically modified polyacrylamide. *Langmuir* **8,** 838–847 (1992).

14. Guillemet, F. & Piculell, L. Interactions in Aqueous Mixtures of Hydrophobically Modified Polyelectrolyte and Oppositely Charged Surfactant. Mixed Micelle Formation and Associative Phase Separation. *J. Phys. Chem.* **99,** 9201–9209 (1995).

15. Hansson, P. & Lindman, B. Surfactant-polymer interactions. *Curr. Opin. Colloid Interface Sci.* **1,** 604–613 (1996).

16. Piculell, L., Guillemet, F., Thuresson, K., Shubin, V. & Ericsson, O. Binding of surfactants to hydrophobically modified polymers. *Adv. Colloid Interface Sci.* **63,** 1–21 (1996).

17. Tanaka, R., Meadows, J., Williams, P. A. & Phillips, G. O. Interaction of hydrophobically modified hydroxyethyl cellulose with various added surfactants. *Macromolecules* **25,** 1304–1310 (1992).

18. Yekta, A., Duhamel, J., Brochard, P., Adiwidjaja, H. & Winnik, M. A. A fluorescent probe study of micelle-like cluster formation in aqueous solutions of hydrophobically modified poly(ethylene oxide). *Macromolecules* **26,** 1829–1836 (1993).

19. Khan, W. Microfluidic formation of pH responsive 5CB droplets decorated with PAA-b-LCP. *Lab Chip* **11,** 3493 (2011).

20. Kinsinger, M. I., Buck, M. E., Campos, F., Lynn, D. M. & Abbott, N. L.

Dynamic Ordering Transitions of Liquid Crystals Driven by Interfacial Complexes Formed between Polyanions and Amphiphilic Polyamines. *Langmuir* **24,** 13231–13236 (2008).

21.   Kinsinger, M. I., Sun, B., Abbott, N. L. & Lynn, D. M. Reversible Control of Ordering Transitions at Aqueous/Liquid Crystal Interfaces Using Functional Amphiphilic Polymers. *Adv. Mater.* **19,** 4208–4212 (2007).

22.   Lee, D.-Y. pH-responsive aqueous/LC interfaces using SGLCP-b-polyacrylic acid block copolymers. *Soft Matter* **6,** 1964 (2010).

23.   Seo, J.-M., Khan, W. & Park, S.-Y. Protein detection using aqueous/LC interfaces decorated with a novel polyacrylic acid block liquid crystalline polymer. *Soft Matter* **8,** 198–203 (2012).

24.   Kinsinger, M. I., Buck, M. E., Abbott, N. L. & Lynn, D. M. Immobilization of Polymer-Decorated Liquid Crystal Droplets on Chemically Tailored Surfaces. *Langmuir* **26,** 10234–10242 (2010).

25.   Miller, D. S., Wang, X., Buchen, J., Lavrentovich, O. D. & Abbott, N. L. Analysis of the internal configurations of droplets of liquid crystal using flow cytometry. *Anal. Chem.* **85,** 10296–303 (2013).

26.   Lin, I.-H. Endotoxin-induced structural transformations in liquid crystalline droplets. *Science* **332,** 1297–300 (2011).

27.   Smith, D., Pentzer, E. B. & Nguyen, S. T. Bioactive and Therapeutic ROMP Polymers. *J. Macromol. Sci. Part C Polym. Rev.* (2007).

28.   Sanford, M. S., Love, J. A. & Grubbs, R. H. A Versatile Precursor for the Synthesis of New Ruthenium Olefin Metathesis Catalysts. *Organometallics* **20,** 5314–5318 (2001).

29.   Bielawski, C. W. & Grubbs, R. H. Living ring-opening metathesis polymerization. *Prog. Polym. Sci.* **32,** 1–29 (2007).

30.   Kammeyer, J. K., Blum, A. P., Adamiak, L., Hahn, M. E. & Gianneschi, N. C. Polymerization of protecting-group-free peptides via ROMP. *Polym. Chem.* **4,** 3929–3933 (2013).

31.   van den Burg, B. & Eijsink, V. in *Handbook of Proteolytic Enzymes* 540–553 (2013). doi:10.1016/B978-0-12-382219-2.00111-3

32.   Tian, C. S. & Shen, Y. R. Structure and charging of hydrophobic material/water interfaces studied by phase-sensitive sum-frequency vibrational

spectroscopy. *Proc. Natl. Acad. Sci.* **106,** 15148–15153 (2009).

33.   Vácha, R. The Orientation and Charge of Water at the Hydrophobic Oil Droplet–Water Interface. *J. Am. Chem. Soc.* **133,** 10204–10210 (2011).

34.   Zangi, R. & Engberts, J. B. F. N. Physisorption of Hydroxide Ions from Aqueous Solution to a Hydrophobic Surface. *J. Am. Chem. Soc.* **127,** 2272–2276 (2005).

35.   Lavrentovich, O. D. Topological defects in dispersed words and worlds around liquid crystals, or liquid crystal drops. *Liq. Cryst.* **24,** 117–126 (1998).

36.   Prishchepa, O. O., Shabanov, A. V. & Zyryanov, V. Y. Director configurations in nematic droplets with inhomogeneous boundary conditions. *Phys. Rev. E* **72,** 031712 (2005).

37.   Brake, J. M., Mezera, A. D. & Abbott, N. L. Effect of Surfactant Structure on the Orientation of Liquid Crystals at Aqueous−Liquid Crystal Interfaces [†]. *Langmuir* **19,** 6436–6442 (2003).

38.   Gupta, J. K., Zimmerman, J. S., de Pablo, J. J., Caruso, F. & Abbott, N. L. Characterization of Adsorbate-Induced Ordering Transitions of Liquid Crystals within Monodisperse Droplets. *Langmuir* **25,** 9016–9024 (2009).

39.   Lockwood, N. A., de Pablo, J. J. & Abbott, N. L. Influence of Surfactant Tail Branching and Organization on the Orientation of Liquid Crystals at Aqueous−Liquid Crystal Interfaces. *Langmuir* **21,** 6805–6814 (2005).

40.   Patel, P. R. Synthesis and Cell Adhesive Properties of Linear and Cyclic RGD Functionalized Polynorbornene Thin Films. *Biomacromolecules* **13,** 2546–2553 (2012).

41.   Makino, K. & Ohshima, H. Electrophoretic Mobility of a Colloidal Particle with Constant Surface Charge Density. *Langmuir* **26,** 18016–18019 (2010).

42.   Hiemenz, P. C. & Rajagopalan, R. *Principles of colloid and surface chemistry.*   (Marcel   Dekker,   1997)

SECTION 2: Design of Triggerable Amphiphiles with Mesogenic Side Chains for Multi-Scale Responses with Liquid Crystals

Introduction

Recent studies have emerged that describe the use of responsive amphiphilic copolymers to generate stimuli-responsive liquid crystal (LC) systems.[1,2] Among those reported, several incorporate chemical functionality which enable a response to changes in pH,[1–4] the presence of polyelectrolytes of opposite charge,[5] or enzymatic cleavage.[6] A common strategy to this end is the design of block copolymers consisting of a "LC-philic" unit (highlighted in blue) and a responsive hydrophilic block (Figure 1). For example, Lee and coworkers synthesized the block copolymer, PAA-*b*-LCP, using reversible addition-fragmentation chain transfer (RAFT) polymerization consisting of polyacrylic acid (PAA) as the pH-responsive component and the hydrophobic unit consisting of the mesogenic side-chain 4-cyanobiphenyl-4'-oxyundecrylacrylate (LCP) (Figure 1A).[4] This side-chain mesogen, which is closely related to the liquid crystal, 4'-undecyloxy-biphenyl-4-carbonitrile (commonly known as 11OCB), was incorporated with a side-chain ratio (PAA : LCP units) of 0.93:0.07. In this study, the interface of a 5CB LC film was decorated with PAA-*b*-LCP by way of a Langmuir-Schaefer transfer with an interfacial density of ~1271 $Å^2$ per polymer or ~84.7 $Å^2$ per LCP group. The LC film decorated with PAA-*b*-LCP responded to changes in the bulk aqueous pH; specifically, the copolymer transitioned from planar anchoring at pH 2 to homeotropic anchoring at pH 10, enabling the LC geometry transition from bipolar to radial, respectively. Kinsinger and coworkers designed amine-based amphiphilic polymers with aliphatic side-chains to design LCs that amplify changes in the aqueous solution pH[2] or electrolyte composition[5] into optical outputs (Figure 1B). To decorate 5CB films, Kinsinger performed a Langmuir-Schaefer transfer of the random copolymer (Figure 1B left structure), supported on a PBS subphase at pH 5, onto the interface of a 5CB film at surface densities of ~38 Å2, 40-48 Å2, or 52 Å2 per aliphatic group and observed that the LC anchoring at the polymer decorated interface was homeotropic, tilted and planar, respectively. Sodium poly(styrene sulfonate), a strong anionic polyelectrolyte, was applied to the aqueous subphase and a homeotropic to planar anchoring transition was observed over the course of 15 minutes.[5] Further, LC films decorated with a similar copolymer were sensitive to pH changes in the aqueous phase.[2] An alternative random copolymer (Figure 1B, right structure), was also used to immobilize LC droplets on chemically functionalized surfaces.[7] A change in the LC droplet anchoring was found to depend on the nature of the surface at which the droplets were immobilized. Ma and coworkers used amphiphilic block copolymers (PPA1-3) synthesized by ring opening metathesis polymerization (ROMP), which incorporate biphenyl and peptide-based side-chains, to design responsive PPA-coated LC droplets (Figure 1C).[6] The peptide sequences (GPLGLAGK and GPLGLAG-Ebes-G) were designed to be enzymatically processed by thermolysin, resulting in truncation of the peptide sequence to yield a pH-responsive carboxylate-containing product (Figure 1C). In order to discern proteolytically-driven changes in the LC ordering of PPA-decorated LC droplets, sodium dodecyl sulfate (SDS) was added and the aqueous solution was acidified to pH 3 post enzyme treatment. Applying these conditions provoked LC droplets decorated by cleaved and uncleaved PPAs to adopt distinct configurations.
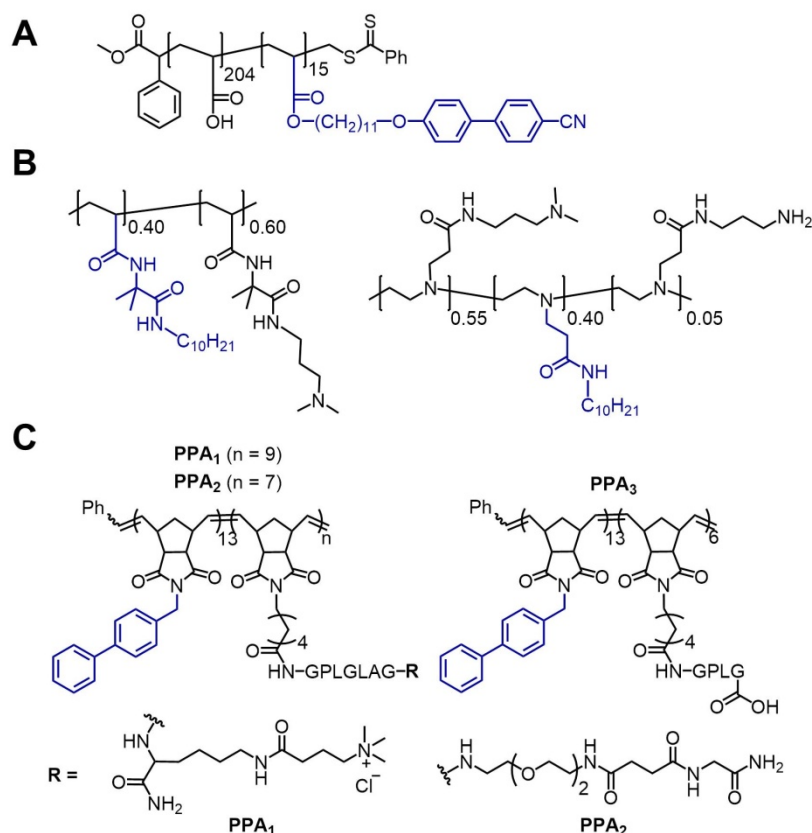
Figure 1 Examples of amphiphilic copolymers reported in previous studies. The mesogenic side chains used are (A) hendecaoxycyanobiphenyl (11OCB),[3,8] (B) linear aliphatic tails,[2,7] and (C) biphenyl.[6]

When collectively considered, these previous studies generate a number of questions related to the structure and architecture of the amphiphilic polymers and their specific interactions with LCs. First, we note that two classes of amphiphilic polymers; one with LC-like (Figure 1A) and one with surfactant-like (Figure 1B) side chains were able to anchor perpendicular (homeotropic anchoring) to LC surfaces, resulting in a radial configuration of the LC. Interestingly, however, LC-like polymers were shown to be more capable of generating homeotropic LCs at a lower surface density of hydrophobic units (1 unit per 84.7 Å^2) compared to aliphatic side-chain polymers (1 unit per 38 Å^2). This suggests that amphiphilic polymers with LC-like side-chains are more effective than polymers with aliphatic side chains in inducing homeotropic anchoring. In contrast, the biphenyl side-chain used in the PPA shown in Figure 1C was unable to generate homeotropic anchoring of the LC. This inconsistency may stem from the short single methylene spacer connecting the mesogen to the rather rigid backbone of the polymer, which restricts perpendicular anchoring of the side chains to the LC interface.

By comparing the LC-like side-chain containing polymers (Figure 1A and 1C), we note three main differences. First, the length of the aliphatic chain linking the biphenyl gives rise to greater degrees of freedom of the LCP unit (C11 for ether-nitrile biphenyl and C1 for 4-phenylbenzyl, Figure 1A and 1C, respectively. Second, the functional group connectivity of the biphenyl, for example the ether functional group in Figure 1A, extends

the rigidity of the mesogen[9] compared to the benzyl group in Figure 1C; and third, the presence or absence of a nitrile terminal group on the biphenyl unit (Figure 1A and 1C, respectively). Next, by comparing these polymer architectures, we observe that the ratio of the hydrophobic: hydrophilic blocks are very different (15: 204 and 13: 9, Figure 1A and 1C, respectively). In addition, we note that these two polymers were synthesized using different methods (RAFT or ROMP, respectively), each of which generates distinct polymer backbone chemistry (and polymer flexibility) and may play an important role in polymer-LC interactions. Finally, amphiphilic copolymers in Figure 1A and 1B were synthesized as block and random copolymers, respectively. These two architectures are varied in the spatial density of mesogens along the polymer backbone, which also may dramatically affect polymer-LC interactions. To illustrate this point, a block copolymer oriented along a LC interface will display regions of hydrophobic-rich and hydrophobic-poor domains. Comparatively, a random copolymer with a stochastic arrangement of hydrophobic and hydrophilic units along the polymer backbone has a homogeneous hydrophobic unit density along the LC interface.

In general, the impact of polymer composition and architecture on the interfacial ordering of polymers at LC interfaces is not understood. The work described in this report was initially motivated by the need to identify a set of design principles for amphiphilic copolymers that can be used to rationally tailor anchoring transitions at aqueous interfaces of LCs. To this end, we used ROMP as a synthetic method to enable the design of responsive polymers and the development of structure-property relationships for triggering ordering transitions in LC systems. Polymers of various architectures, such as homopolymers, block and random copolymers, can be readily prepared by this method using the bipyridyl Grubb's catalyst, which is known for its high-functional group tolerance and ability to incorporate peptides and other functionally complex molecules in a graft-through approach (Scheme 1).[10] As a living polymerization technique, ROMP has the additional advantage of producing high molecular weight polymers with low dispersity, a feature that is generally more difficult to achieve with reversible deactivation radical polymerization (RDRP) methods such as RAFT and atom transfer radical polymerization (ATRP). Utilizing ROMP, we synthesized a library of polymers probing polymer composition as well as architecture on triggering LC ordering transitions.
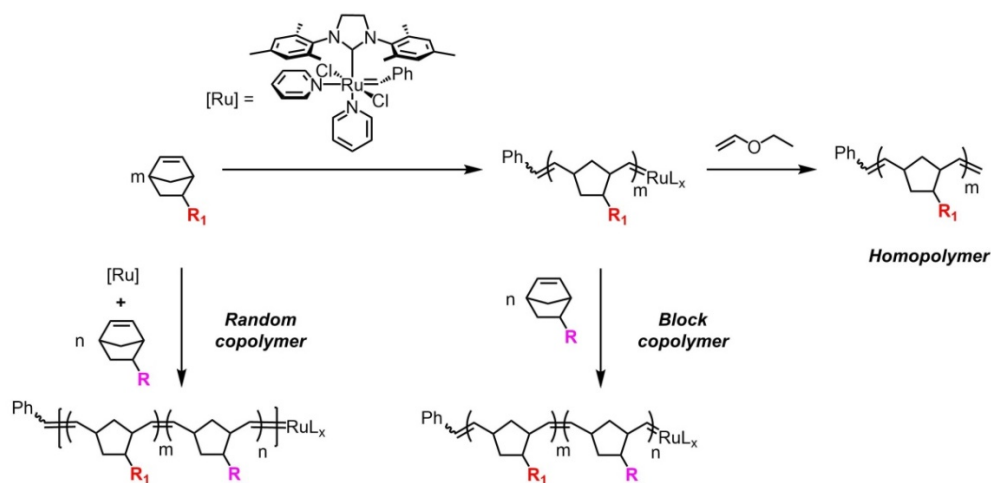
Scheme 1 Synthesis of homopolymers, block and random copolymers using ROMP

First, we report a systematic study on the effect of mesogen side-chain structure on homopolymer anchoring at the LC/aqueous interface (Figure 2). From this survey, we identified a mesogen that is efficient at triggering homeotropic anchoring of LCs, and can be readily incorporated into copolymer structures that contain hydrophilic units. Second, we studied the effect of polymer architecture on LC ordering at the aqueous interface of polymer decorated LC droplets. Block and random copolymers bearing poly(ethylene glycol) (PEG) as the hydrophilic block and the optimized mesogen as the hydrophobic block, were prepared as model systems. Third, we study the effect of copolymer composition on LC ordering, specifically the presence of a nitrile functional groups on the biphenyl as well as functional group conjugation (ether or amide) to the polymer (Figure 2). Finally, by leveraging the design principles that emerge from the above studies, we report the design of copolymers incorporating a peptide hydrophilic unit that triggers ordering transitions in LC droplets when the peptide is processed by enzymatic hydrolysis.
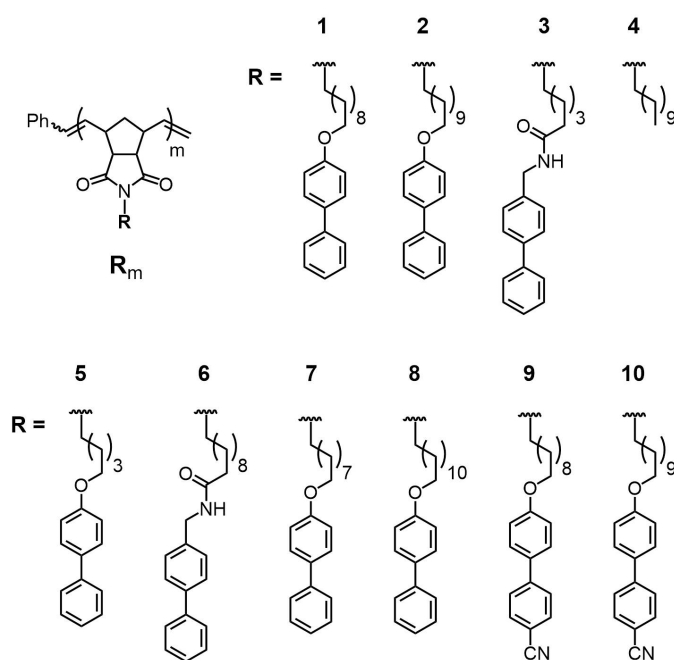
Figure 9 The catalogue of homopolymers utilized to determine the optimal mesogenic side-chain structure for triggering LC geometry changes at the liquid crystal interface.

Identifying LC configurations of polymer-decorated LC droplet emulsions by flow cytometry

In this work, we examine polymer-driven perturbations in the ordering of the LC within polymer-decorated LC droplets. In an aqueous environment, LCs form spherical droplets to minimize the interfacial area. The anchoring of LC molecules at the undecorated LC/aqueous interface is tangential, or planar.[11–13] Due to the spherical geometry of the droplet and a minimization of the elastic and surface anchoring energy at the interface of the droplet, the LC adopts a bipolar droplet configuration, with two diametrically opposite defects called boojums (Figure 3B). These droplets can be driven from a bipolar configuration to a radial configuration (with one point defect located at the center of the droplet) through a change in LC anchoring from planar to perpendicular or homeotropic

(Figure 3A). The size at which the droplet configuration is most sensitive is when the elastic energy and the anchoring energy are comparable, which is determined by setting the elastic energy, $E_k \propto KR$, equal to the anchoring energy, $E_W \propto WR^2$. This leads to a critical radius of $R = K \cdot W^{-1}$, where $K = 10^{-11}$ $J \cdot m^{-1}$ and $W = 10^{-5}$-10^{-6} $J \cdot m^{-2}$ (weak anchoring), which are typical values for thermotropic LCs when the radius is between 1 and 10 µm. Droplets of this size may change configuration through a change in the LC anchoring strength by decorating the droplet interface with amphiphiles. Therefore, by choosing an amphiphile with a suitable mesogen, the hydrophobic moieties can interdigitate with the LC at the droplet interface, causing an anchoring change from planar to homeotropic.
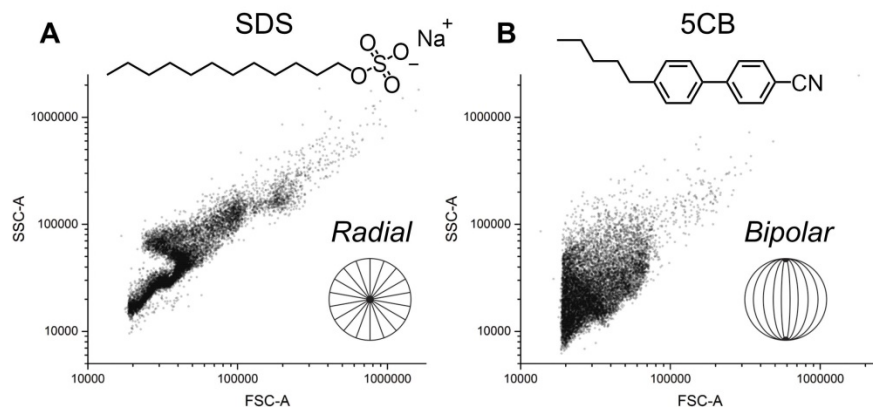
Figure 10 Liquid crystal droplets of 5CB exhibit different droplet configurations (detectable by flow cytometry scatter plots) in the (A) presence and (B) absence of surfactants, such as the single-tailed surfactant SDS. Perpendicular or homeotropic anchoring of SDS results in a change in the LC droplet geometry from (B) bipolar to (A) radial.

This change in anchoring propagates through the bulk of the LC droplet transforming the droplet from a bipolar configuration to a radial configuration (Figure 3). Furthermore, these two droplet configurations (bipolar and radial) are cylindrically and spherically symmetric, respectively. As such, we can readily measure the droplet configuration through the use of flow cytometry. A flow cytometer measures forward scattered light (related to the droplet volume or size) and side scattered light (related to the internal complexity). For radial droplets, we observe an "S" shaped scatter plot (Figure 3A), due to the spherical symmetry of the droplet, while for bipolar droplets, we observe a more broad scatter plot (Figure 5.3B), due to the rotational freedom of the droplet and varying optical indices at the droplet interface.

Studying the effects of polymer side chain structure on polymer-LC interactions

To provide insight into mesogen side-chain structures that cause homeotropic anchoring of LCs, we first tested four designs based on the previously mentioned studies (Figure 1). Homopolymers with the desired mesogen were dispersed into the LC prior to emulsification in PBS. The side-chain functionalities of homopolymers, $\mathbf{1}_{18}$, $\mathbf{2}_{18}$ and $\mathbf{3}_{21}$ all include biphenyl (Figure 4), a common rigid functional group in many mesogens such as 5CB; however the side chains differ in the design of the linker between the mesogen and

backbone of the polymer. Homopolymers 1_{18} and 2_{18} differ by one carbon in the hydrocarbon linker length. Specifically, 1_{18} and 2_{18} have a C10 and C11 linear alkyl chain, respectively. Homopolymer 3_{21} has an amide linking the biphenyl to the backbone along with a C5 linear alkyl spacer. Homopolymer 4_{15} is a simple linear C11 hydrocarbon. The degree of polymerization (DP, m~20) and molecular weights of homopolymers 1_{18}, 2_{18}, 3_{21} and 4_{15} are approximately similar (4-9 kDa), which enables a direct comparison of the hydrophobic side-chain structure of the homopolymers on the interactions with the LC droplet.
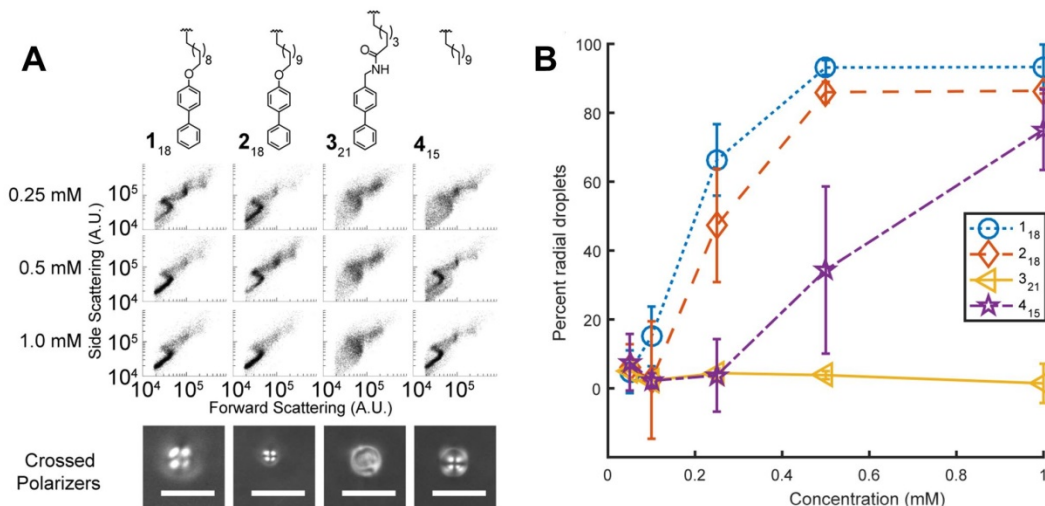
Figure 11 (A) Scatter plots generated from flow cytometry of LC droplets decorated with polymers 1-4 (Fig. 1-4) and crossed polarized microscopy images. (B) The percentage of radial droplets generated as a function of the polymer and polymer concentration, calculated from the scatter plots.

The percentage of radial droplets was dependent upon the polymer concentration (Figure 4A), likely due to a higher number density of hydrophobic side-chains at the LC droplet interface. We found that LC droplets decorated with 4_{15} required a higher homopolymer concentration than droplets decorated with 1_{18} or 2_{18} in order to transform the droplets to a radial configuration. The LC droplet configurations of droplets decorated with 1_{18} or 2_{18} was similar, so we speculate that either of these homopolymers, which differ by only one carbon in the alkyl linker, is sufficient for homeotropic anchoring. The LC droplet configuration was, however, sensitive to the structure of the hydrophobic side-chain. We observed that homopolymers 1_{18}, 2_{18} and 4_{15} were able to generate radial droplets at the range of concentrations tested (0.25 to 1 mM); however, 3_{21} was unable to generate radial droplets (Figure 4A). Both flow cytometry scatter plots and optical micrographs collected under crossed polarizers verified these observations. Within the scope of substrates tested, it remains unclear whether the short alkyl linker or the amide functional group prevents homeotropic anchoring (a point of discussion that is revisited later). Considering the surface area of an LC droplet and the assumption that all polymer chains adsorb to the droplet interface, we calculated that all homopolymers cause homeotropic anchoring at approximately the same side chain density. Specifically, we calculate an average surface area per hydrophobic unit of ~30.6 ± 7.4, 35.3 ± 1.4, 23.3 ± 2.3 and 54.8 ± 21.8 Å2 for 1_{18}, 2_{18} and 3_{21} and 4_{15} at 0.25 mM (moles of polymer with

respect to 5CB volume), respectively. Comparison of these surface area values for the area per hydrophobic unit of the homopolymers (at 0.25 mM, ~20-55 Å^2), to the limiting area per classical single tail surfactants, such as SDS or CnTAB (~40-70 Å^2); it is somewhat perplexing that the surfactant-like 4_{15} is unable to generate radial droplets at surface coverages comparable to those of small molecule surfactants.

To determine the underlying inability of homopolymer 3_{21} to generate radial droplets, we synthesized homopolymers 5_{20} and 6_{16} (Figure 5.2). For homopolymers 1_{18} and 5_{20} we observed that the length of the alkyl chain linking the biphenyl to the main chain affects the percentage of radial droplets generated (Figure 5). Specifically, 1_{18}, bearing a C8 alkyl linker can generate approximately 25 % more radial droplets than 5_{20}, which consists of a C5 alkyl linker. This observation is consistent with previous reports on the alkyl length dependence of surfactants on the anchoring of LC at the LC/aqueous interface.[14] Further, these results indicate that the earlier ROMP-based copolymers bearing the short 4-phenylbenzyl side-chains would be unable to generate radial droplets under these conditions, as observed emperically.[6]
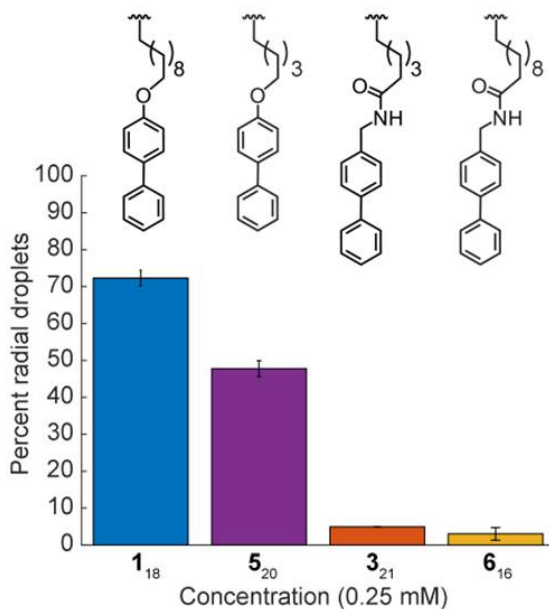
Figure 12 Percentage of radial configuration generated from LC droplets decorated with homopolymers 1_{18}, 5_{20}, 3_{21}, and 6_{16}.

By contrast, homopolymers 3_{21} and 6_{16} generate a small percentage of radial droplets (Figure 5). These results indicate that ether biphenyl mesogens are more effective at homeotropic anchoring and thereby generating radial droplets than the amide biphenyl mesogens. Several reasons could explain this phenomenon, one being the large lateral dipole moment of the amide, which is perpendicular to the longitudinal axis of the biphenyl side-chain. The dipole moment could perhaps bury itself in the dielectric medium (the LC), which would require the side-chain to lay parallel to the LC/aqueous interface. This side-chain ordering (planar to the LC interface), would be conducive to a bipolar, rather than a radial, droplet configuration. Indeed, the absence of a significant radial droplet population generated by homopolymers 3_{21} and 6_{16} suggests that the amide dipole is dominating the interactions of the polymer side-chains with the LC. This

also illustrates the high sensitivity of the LC ordering to the structure of the hydrophobic side-chain. As such, when synthesizing functional polymers, the hydrophobic side chain structure must be carefully considered to enable productive interactions with the LC.

Closer inspection of Figure 4 reveals a small difference in the percentage of droplets that assume a radial configuration in the presence of 1_{18} and 2_{18}. Furthermore, the results of Figure 5 show an alkyl chain-length dependence on the LC droplet configuration. Since homopolymers 1_{18} and 2_{18} have side chains that differ in length by one carbon, we synthesized homopolymers 7_{16} and 8_{16} to determine if this difference can be attributed to an odd or even alkyl chain length (Figure 2). Within this library, homopolymers 7_{16}, 1_{18}, 2_{18}, and 8_{16} have alkyl chain lengths of C9, C10, C11 and C12, respectively. At a concentration of 0.3 mM (moles of homopolymer with respect to 5CB volume), we observe a subtle difference in the ability of the homopolymers to generate radial droplets as a function of the alkyl chain length (Figure 6). When the linking aliphatic chain is C10, we observe a maximum percentage of droplets with a radial configuration compared to chain lengths of C5, C9, C11 or C12 (Figure 6). This results suggests that an even alkyl chain length is better than an odd alkyl chain length and specifically the hydrophobic side chain of 1_{18}, with an alkyl chain length of C10, is more effective at triggering homeotropic anchoring compared to 7_{16}, 2_{18}, and 8_{16}.
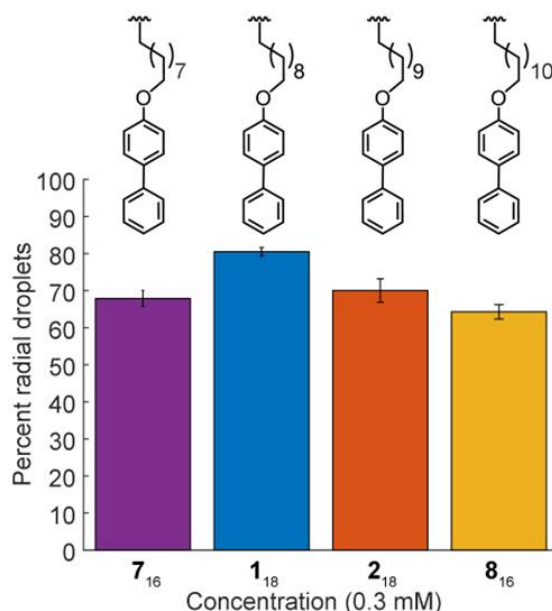
Figure 13 Percentage of radial configuration generated from LC droplets decorated with homopolymers 7_{16}, 1_{18}, 2_{18}, and 8_{16}.

Intrigued by the idea that subtle molecular changes in hydrophobic side chains can lead to drastic changes in the ordering of polymer-decorated LCs, we investigated the effect of the presence (9_{16} or 10_{19}) or absence (1_{18} or 2_{18}) of a nitrile terminal group on the ether-linked biphenyl side chain (Figure 2). Interestingly, we observed that side chains without a terminal nitrile functional group were able to generate a higher percentage of radial droplets than side chains bearing a nitrile group (Figure 7). This is a somewhat surprising result as we anticipated the presence of the nitrile group in the hydrophobic

side chain would enhance the interactions with the nitrile-containing 5CB molecules due to dipole-dipole interactions. Nevertheless, from these collective studies, we have generated a set of design parameters for hydrophobic polymer side chains that are able to generate strong homeotropic anchoring at the LC interface. Based on these measurements, the side chain structure should incorporate a rigid mesogenic component, such as a biphenyl moiety. A single-tailed surfactant-like side chain, as in the case of 4_{15}, was unable to generate radial droplets at low concentrations. Moreover, incorporation of an amide or terminal nitrile group is not suitable, perhaps due to dipole-dipole interactions and as such, an ether biphenyl side chain is optimal. Lastly, the length of the hydrocarbon spacer connecting the rigid mesogenic component is vital for homeotropic anchoring of polymer decorated LCs; from these studies, a length of C10 was found to be best, inducing a higher percentage of droplets with radial configuration at lower concentrations (Figure 6). Based on these results, we conclude that the side chain used in 1_{18} is the optimal structure to trigger ordering transitions in the LC. In the next set of studies, we incorporated this mesogenic group into copolymers bearing hydrophilic moieties in order to probe the effect of copolymer composition and architecture on polymer-LC interactions.
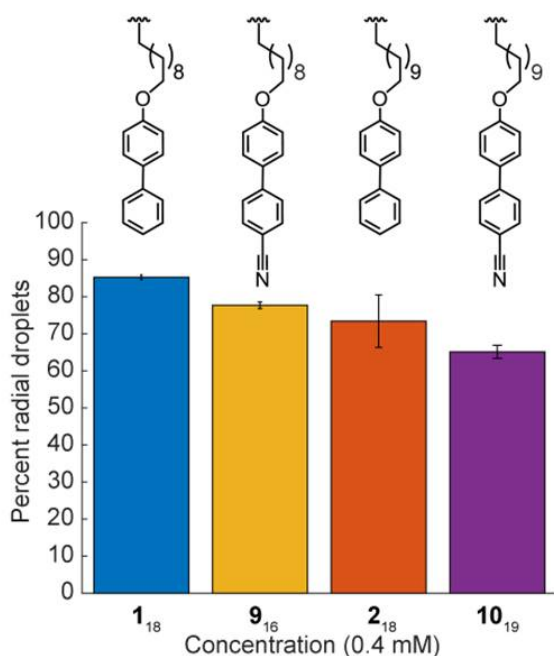
Figure 14 Percentage of radial configuration generated from LC droplets decorated with homopolymers 1_{18}, 9_{16}, 2_{18}, and 10_{19}.

Copolymer composition and architecture on LC ordering

Utilizing monomer **1**, the ether biphenyl rigid core identical to the hydrophobic side chain of 1_{18}, we synthesized block and random copolymers consisting of poly(ethylene glycol) (12 repeat units), PEG12, as the hydrophilic unit (Figure 8, Table 1). Guided by the results described above, we used **1** as it was found to be effective at generating homeotropic anchoring of LCs. PEG12 was used simply as a model system.
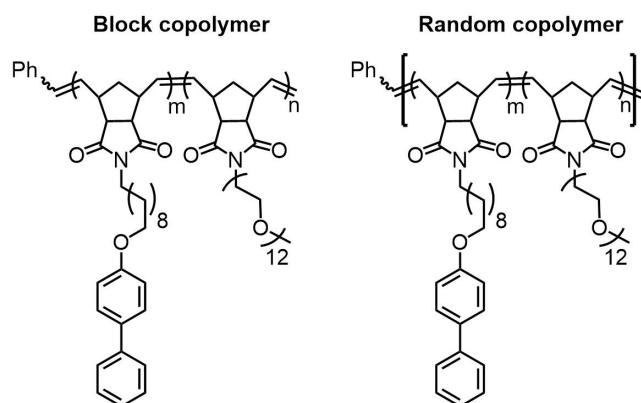
Figure 15 Chemical structures of copolymers synthesized by ROMP used in this study

We varied the the ratio of hydrophobic, m, to hydrophilic, n, units of random and block copolymers to compare the effect of copolymer architectures of similar compositions (Figure 8). For both copolymer architectures, we hypothesized that copolymers rich in mesogenic repeat units will generate radial droplets at low concentrations. First, we examined the effect of block copolymer composition on its ability to generate radial droplets. Based on previous work, we expected that even at high hydrophilic compositions, radial droplet configurations would predominantly form.[3]

Table 1 Copolymer library for examining copolymer-LC interactions

entry	UPAC	M_n (Da)[a]	M_w/M_n[b]	DP (m)[c]	DP (n)[d]	Wt. fraction[e]
1	1_{17}-b-PEG12$_{29}$	27,680	1.02	17 (30)	29 (10)	0.29
2	1_{30}-b-PEG12$_{26}$	32,350	1.02	30 (27)	26 (13)	0.53
3	1_{26}-b-PEG12$_{16}$	22,970	1.01	26 (20)	16 (20)	0.43
4	1_{47}-b-PEG12$_{15}$	32,170	1.02	47 (32)	15 (8)	0.68
5	1_{12}-ran-PEG12$_{20}$	19,290	1.02	12 (13)	20 (27)	0.29
6	1_{14}-ran-PEG12$_{17}$	18,650	1.01	14 (20)	17 (20)	0.35
7	1_{26}-ran-PEG12$_{19}$	25,240	1.02	26 (27)	19 (13)	0.48
8	1_{33}-ran-PEG12$_{17}$	27,090	1.02	33 (32)	17 (8)	0.57

[a] M_n denotes number-average molecular weight. [b] M_w denotes weight-average molecular weight. [c] DP$_m$ denotes degree of polymerization of the first block, **1**; (m) denotes the theoretical DP of the first block. [d] DP$_n$ denotes degree of polymerization of the second block, **PEG12**; (n) denotes the theoretical DP of the second block. [e] weight fraction of the hydrophobic block.

The block copolymers did not generate a substantial population of radial droplet configurations (Figure 9). The most hydrophobic composition (**1$_{47}$-b-PEG12$_{15}$**) generates a small number of radial droplets (~20%) at a polymer concentration of 1mM (Figure 9A). Comparing the surface area available per hydrophobic unit of the block copolymer (at 1 mM) and the homopolymer **1$_{18}$**, we find the surface density of hydrophobic repeat units to be somewhat comparable. For example, the hydrophobic surface densities of the block copolymer and the homopolymer were calculated as 3.0 Å^2 and 10.6 Å^2, respectively.

This suggests that the hydrophobic units of the block copolymer are unable to interdigitate with the LC.

Random copolymers were synthesized (Figure 8) to test whether dispersing the mesogenic components within the hydrophilic units can lead to homeotropic anchoring and the generation of radial droplets.   Intriguingly, random copolymers with a smaller hydrophobic weight (wt.) fraction (1_{26}-*ran*-**PEG12$_{19}$** and 1_{14}-*ran*-**PEG12$_{17}$** with 0.48 and 0.35 respectively) were able to generate radial droplets at 1 mM copolymer concentration (Figure 9B). The random copolymer with the lowest hydrophobic wt. fraction (1_{12}-*b*-**PEG12$_{20}$**, 0.29 wt. fraction) was unable to generate radial droplets. This suggests that the minimum hydrophobic wt. fraction required to generate radial droplets is 0.35 for the random copolymer architecture. For 1 mM random copolymer (with respect to the volume of 5CB), with a hydrophobicity index of 0.35, we calculate the hydrophobic surface density as 16.9 Å^2. This is more comparable to the hydrophobic surface density calculated for homopolymer 1_{18}, (10.6 Å^2).
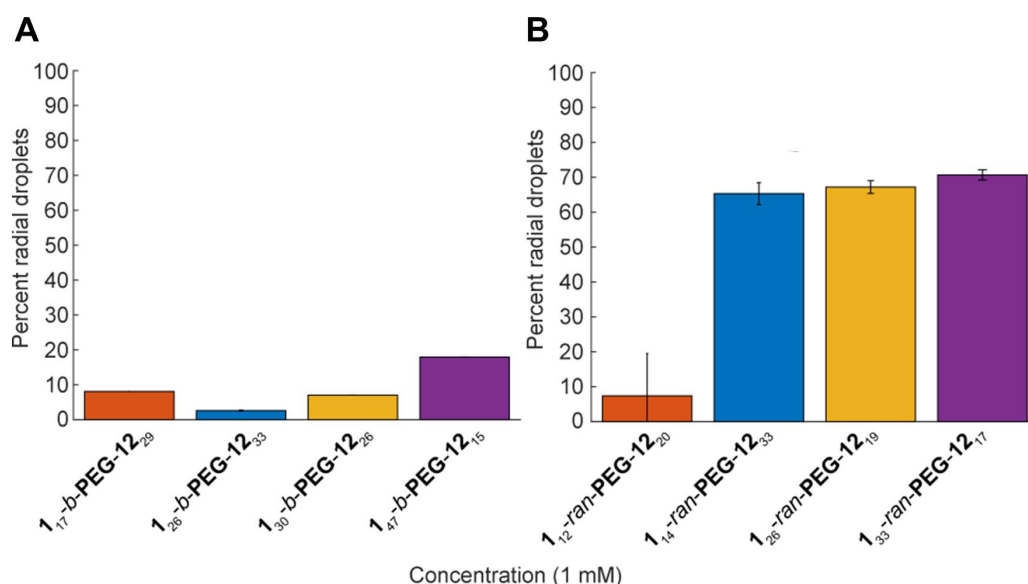
Figure 16 The percentage of radial droplets generated for (A) block copolymer-decorated LC droplets and (B) random copolymer-decorated LC droplets at 1 mM copolymer concentration. The block copolymer was unable to generate a significant amount of radial droplets even for copolymers of high mesogen content (~20 %). In contrast, random copolymers of varying mesogen content were able to generate a significant number of droplets (> 70 %) with radial configuration.

Comparing the block and random copolymer architectures with similar compositions at 1 mM, we observed that the random copolymer is suitable to generate radial droplet configurations. We then examined the effect of composition (using block and random copolymers of 0.53 and 0.57 hydrophobic mol percent, respectively) on a range of copolymer concentrations (Figure 10). Intriguingly, the random copolymer, 1_{33}-*ran*-**PEG12$_{17}$**, was able to generate radial droplets at low concentrations (0.1 mM). In contrast, the block copolymer of similar composition generated droplets with approximately 10 % radial configuration, even at the highest concentration tested (1 mM), similar to the previous measurements (Figure 9). These results demonstrate that random

copolymers are able to trigger changes in the LC geometry more effectively than block copolymers.
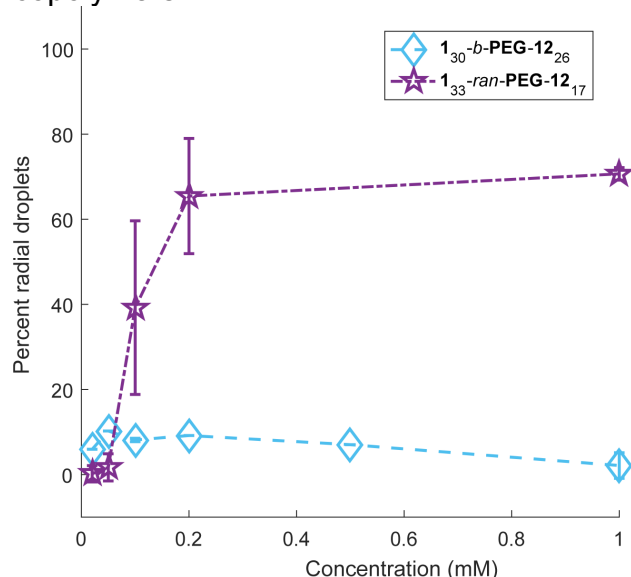
Figure 17 Comparison of the random and block copolymer architectures with a similar hydrophobic index (ratio of hydrophobic to hydrophilic). The random copolymer is able to generate radial droplets at a much lower concentration (with respect to the 5CB volume) than the block copolymer of similar hydrophobic index.

The organization of copolymers at the air-water interface

Both the random and block copolymers possess sufficiently high numbers of hydrophobic repeat units (mesogens) to be able to trigger homeotropic anchoring of the LC, yet this is only observed with the random copolymer. The previous results suggest that the copolymers order at the interface of the LC droplet in a manner, which depends upon the copolymer architecture. Accordingly, we performed Langmuir isotherms to determine if differences in the organization of the random and block copolymers at the aqueous interface could be detected (Figure 11). To perform these experiments, 0.5 mg/mL of copolymer in chloroform was spread on an aqueous trough to produce a copolymer film at the aqueous/air interface. For the block copolymer (Figure 11A), we observed multiple features such as an initial rise in the pressure, a plateau, and finally a steep rise at small surface areas at the so-called "brush" region.[15] Upon completion of barrier compression (25 cm^2/min), the pressure dropped slowly. Furthermore, there was hysteresis in the expansion isotherm (-25 cm^2/min) upon expansion. A second compression of the copolymers **1$_{30}$-b-PEG12$_{26}$** and **1$_{47}$-b-PEG12$_{15}$** was performed (Figure 13). The second compression isotherms exhibited a lower pressure when compared to the first isotherm until the "brush" region was reached (at a similar area per molecule) wherein the pressures from the first and second compression isotherms overlapped. We did not observe the isotherm to depend on the rate of the compression (Figure 14).

Lee and coworkers were able to observe homeotropic anchoring with their block copolymers (Figure 1A) using a Langmuir-Schaefer transfer with a polymer density of

1271 Å^2 per copolymer, which corresponds to a surface area of ~84.7 Å^2 per hydrophobic unit. For the copolymers reported here, this would correspond to the "brush" region of the isotherm (Figure 11A). This hydrophobic surface density is much larger than that calculated for the ROMP polymer systems (3.0 Å^2 per hydrophobic unit) yet homeotropic anchoring was not observed for the ROMP copolymers. These differences in the hydrophobic surface densities of the copolymers and the inability to obtain homeotropic anchoring suggest that the ROMP copolymer backbone has a large effect on the organization of the copolymer at the LC/aqueous interface. Furthermore, when the isotherms were normalized by the number of mesogens in the block copolymer, we observed a ranking of the isotherms based on the area of the initial rise in the pressure. For example, the copolymer consisting of the largest number of mesogen units also exhibited the largest area per mesogen with the initial rise in pressure. For the random copolymers (Figure 11B), only one single rise in the surface pressure was observed. The area where this initial rise occurs, ~1500-3000 Å^2 per molecule, is smaller than that for most of the block copolymers (~5000-10000 Å^2 per molecule) with the exception of 1_{47}-b-PEG12$_{15}$. Nevertheless, when these isotherms were normalized by the number of mesogens, we observed a ranking similar to that of the block copolymers.
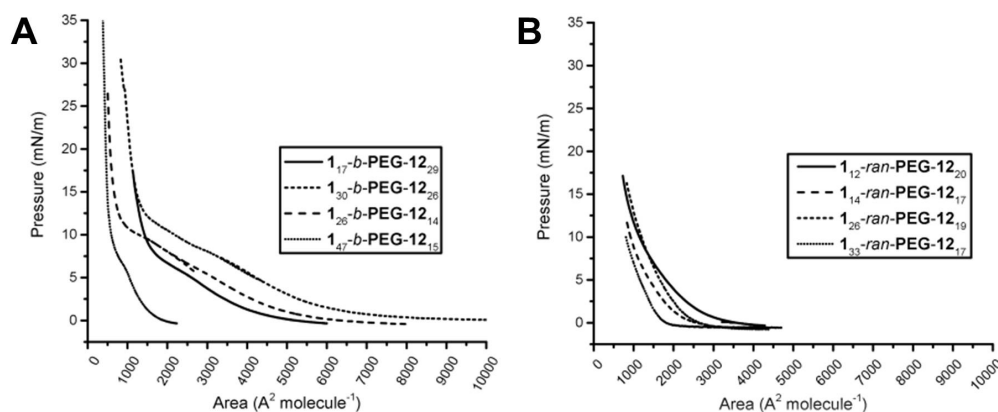
Figure 18 Langmuir surface pressure-area isotherms of (A) block and (B) random copolymers. Upon compression, the block copolymers exhibit an initial rise followed by a plateau region and finally a very steep rise. The random polymers do not exhibit these features and we observed the surface pressure to rise as the area decreases.

The previous studies provide evidence that a random copolymer architecture is able to organize at the LC interface in such a manner as to enable homeotropic anchoring, whereas a block copolymer architecture is incapable of doing so. We were encouraged to apply these findings to produce a responsive system, consisting of a random copolymer bearing a peptide moiety as the hydrophilic unit.

Enzyme-responsive copolymer-decorated LC droplets

By applying the optimized design parameters described in the previous sections, our goal was to produce a random copolymer that was capable of amplifying a targeted biomolecular event to the micron scale through interactions of the copolymer with LC droplets. Our previous results showed that the mesogenic side chain **1** (Figure 2) is the optimal hydrophobic structure to generate homeotropic anchoring. Furthermore, the

copolymer architecture and composition experiments indicated that a random copolymer with a hydrophobic wt. fraction ≥ 0.35 would yield radial droplets. As such, we were motivated to use these principles to improve the original ROMP-based design reported by Ma and coworkers,[6] by amplifying proteolytic cleavage events of a copolymer bearing peptides that are recognized by the enzyme, thermolysin. To determine if unprocessed (uncleaved) and enzymatically processed (cleaved) copolymers could give rise to dissimilar configurations of LC droplets, we synthesized an uncleaved and an authentically cleaved peptide polymer amphiphile (PPA) to simulate these structures (Figure 12). A random copolymer structure was utilized as this was determined to be the optimal architecture. For the uncleaved and cleaved peptide sequences, we used GPLGLAGK (containing a C-terminal amide), and GPLG (containing a C-terminal carboxylate), respectively. The resulting PPAs consisted of 0.65 and 0.68 hydrophobic wt. fraction, respectively.

First, we decorated LC droplets with the uncleaved and cleaved PPAs using a copolymer concentration of 1 mM. Using optical microscopy (under crossed polarizers), the number of droplets with a radial configuration were counted and compared to the total number of droplets in order to determine the percentage of radial droplets. A small majority of LC droplets decorated with the uncleaved PPA exhibited a radial configuration (~55%). LC droplets decorated with the cleaved PPA exhibited a significantly lower percentage of radial droplets (~20%). This result suggests that when the uncleaved PPA is enzymatically processed by thermolysin, the PPA structural change is amplified *via* the LC to produce an optically detectable change in droplet configuration. Ongoing work is now aimed at characterizing and detecting the *in situ* enzyme cleavage of peptide-containing copolymers.
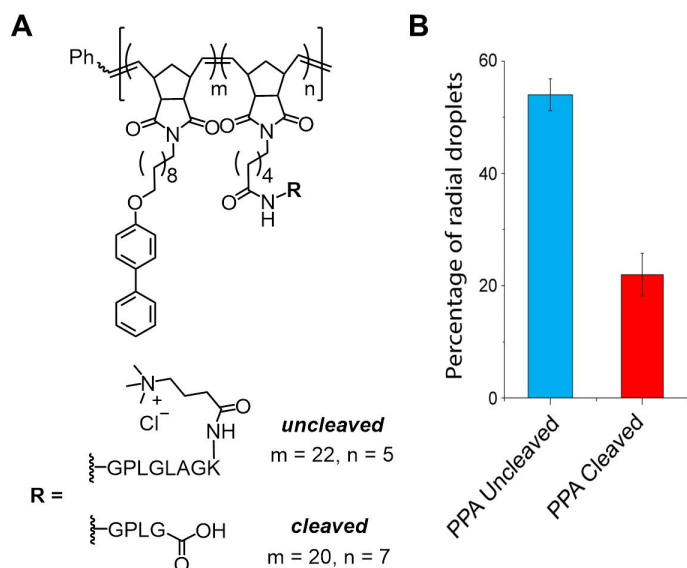
Figure 19 Peptide polymer amphiphiles (PPAs), synthesized as random copolymers, which incorporate either cleaved or uncleaved peptides to simulate copolymer structures prior to and after thermolysin cleavage. (A) Chemical structures of PPAs. The uncleaved and cleaved PPA consist of 0.65 and 0.68 wt. fraction hydrophobic side chain, respectively. (B) The percentage of LC droplets with a radial configuration from 5CB decorated with either uncleaved or cleaved PPAs (1 mM).

Conclusion and future outlook

Herein, we report a systematic study, which identified a set of rational design principles for amphiphilic polymers derived by ROMP that can trigger responses in LC systems. The ability to tailor not only the selectivity of the response but also the rate of the response by incorporating a variable number of reactive side chains and without compromising polymer-LC interactions, is an immense challenge. First, we investigated the effect of the hydrophobic side chain on homopolymer anchoring at the LC/aqueous interface. We identified an optimal structure that proved efficient at triggering homeotropic anchoring of LCs. Incorporating this optimized mesogen in either block or random copolymers, we found a clear difference in the ability of copolymers of different architectures to generate radial droplets. Specifically, block copolymers were unable to generate a significant population of radial droplets even for the hydrophobic-rich compositions (< 20% for 0.68 hydrophobic wt. fraction) and at high concentrations (1 mM). Conversely, the random copolymer was able to generate radial droplets for both hydrophobic-rich and poor compositions (0.35 wt. fraction). The inability of the ROMP block copolymers to generate radial droplets is interesting when compared to block copolymers synthesized by RAFT polymerization, which were able to generate a radial configuration despite having a small wt. fraction of hydrophobic units (0.07).[4] In this work, Lee proposed that the polymer backbone along with hydrophobic side chains was able to penetrate the LC, while the hydrophilic block dissolved in the continuous phase. One key difference between the two types of copolymers is the backbone chemistry, which appears to have a significant impact on polymer organization at the LC/aqueous interface. The ROMP backbone, for example, is bulky and rigid, which restricts the rotational motion of the copolymer and may limit its ability to insert the backbone and hydrophobic side chains into the LC. Nevertheless, this behavior does not appear to be dependent upon the density of hydrophobic units at the interface of the droplets, which suggests that ROMP copolymers order differently depending on the polymer architecture. This finding was corroborated by Langmuir isotherms of block and random copolymers, which reorganize differently in response to isotherm compression.

Finally, in employing these design principles, we investigated random copolymer-decorated LC droplets, comprised of peptide polymer amphiphiles (PPas) that trigger ordering transitions in the LC when the peptide side chain is processed by the enzyme thermolysin. We observed a greater percentage of radial droplets for the uncleaved PPA-decorated LC droplets than for the cleaved PPA decorated droplets. Further experiments will focus on *in situ* cleavage of the PPAs and the observation of biomolecular event-triggered LC ordering transitions. The ability to vary the number of hydrophilic units within the random copolymer and still generate radial droplets should not be understated. Ultimately, we may find that the ROMP architecture is not practical for integrating with the LC for future applications. Alternate strategies may need to be considered in this regard, such as reducing the polyolefin backbone *via* common methods such as Pd-catalyzed hydrogenation to instill greater polymer flexibility or employing different

polymerization methods. Despite these shortcomings, ROMP affords the ability to incorporate complex functionality with ease and high reproducibility, which makes it a method that is ideally suited, at present, for the design of bioactive systems for technological applications.

This report contains material that is currently being prepared for submission for publication: "Design of Triggerable Amphiphiles with Mesogenic Side-Chains for Multi-Scale Responses with Liquid Crystals," Joel Pendery, Lisa Adamiak, Jiawei Sun, Nathan C. Gianneschi, and Nicholas L. Abbott. Methods

Materials

Reagents were purchased from Sigma-Aldrich, Fisher Scientific, TCI, and Acros and were used without further purification unless otherwise specified. Sealed ampules of CDCl3 or DMF-d7 (Cambridge Isotopes) for monitoring polymerization reactions were used without further modification. Reactions were monitored with analytical TLC (glass plate 60 F254, Merck). Column chromatography was performed using silica gel 60 (230 - 400 mesh, 40 – 63 μm). N-(hexanoic acid)-cis-5-norbornene-exo-dicarboximide was prepared as previously described.[16] $(H_2IMes)(pyr)_2Cl_2Ru=CHPh$ was prepared from $(H_2IMes)(PCy_3)Cl_2Ru=CHPh$ according to a literature procedure.[10] Peptides were synthesized by standard solid phase peptide chemistry on rink amide resin (100-200 mesh, Aapptec) using an APPTTEC Focus XC automated synthesizer following previously published procedures.[6] cis-5-Norbornene-exo-2,3-dicarboxylic anhydride, 4-phenylphenol, 4-phenylbenzylamine, 4′-Hydroxy-4-biphenylcarbonitrile, decylamine, and undecylamine were purchased from commercial sources and used without further purification.

General Methods

NMR spectra were recorded on a Varian Mercury 400 MHz, Bruker AVA 300 MHz, and a Varian VX 500 MHz in DMF-d7, CD2Cl2, or CDCl3 and referenced to the residual protons. HR and EI-MS (electron impact mass spectrometry) data were obtained on an Agilent 6230 HR-ESI-TOF MS and a Thermo Trace Plus GC-MS (70 eV) at the Molecular Mass Spectrometry Facility at the UCSD Chemistry and Biochemistry Department. For EI-MS, the molecular fragments are listed as the mass and charge ratio (m/z), followed by the intensities as a percentage value relative to the intensity of the base peak (100%). The molecular ion obtains the abbreviation [M+]. All Polymerizations were conducted in J Young NMR tubes (5 mm diameter) for monitoring via 1H-NMR or in vials in a glove box under dinitrogen atmosphere at room temperature. Polymer dispersities and molecular weights were determined by size-exclusion chromatography (Phenomenex Phenogel 5u 10, 1K-75K, 300 x 7.80 mm in series with a Phenomex Phenogel 5u 10, 10K-1000K, 300 x 7.80 mm (0.05 M LiBr in DMF)) using a Shimadzu LC-AT-VP pump equipped with a multi-angle light scattering detector (DAWN-HELIOS: Wyatt Technology), a refractive index detector (Hitachi L-2490) and a UV-Vis detector (Shimadzu SPD-10AVP) normalized to a 30,000 MW polystyrene standard (Flow rate: 0.75 mL/min). RP-HPLC analyses were performed on a Jupiter Proteo90A phenomenex column (150 x 4.60 mm) using a Hitachi-Elite LaChrom L-2130 pump equipped with a UV-Vis detector (Hitachi-Elite LaChrome L-2420) using a binary gradient (Buffer A: 0.1%

TFA in water; Buffer B: 0.1% TFA in acetonitrile; Flow rate: 1 mL/min). Peptides were purified using a Jupiter Proteo90A Phenomenex column (2050 x 25.0 mm) on a Waters DeltaPrep 300 system using a binary gradient (Buffers A and B; Flow rate: 22 mL/min).

Characterization of LC droplets with optical microscopy

LC droplets were imaged using an Olympus IX71 inverted microscope with either a 60x objective or 100x oil immersion objective. Bright-field and polarized light micrographs of the LC droplets were collected with a Hamamtsu 1394 ORCAER CCD camera connected to a computer and controlled through SimplePCI imaging software. LC droplet characterization was limited to only LC droplets that were diffusing (translating and/or rotating).

Surface-pressure area isotherm measurements
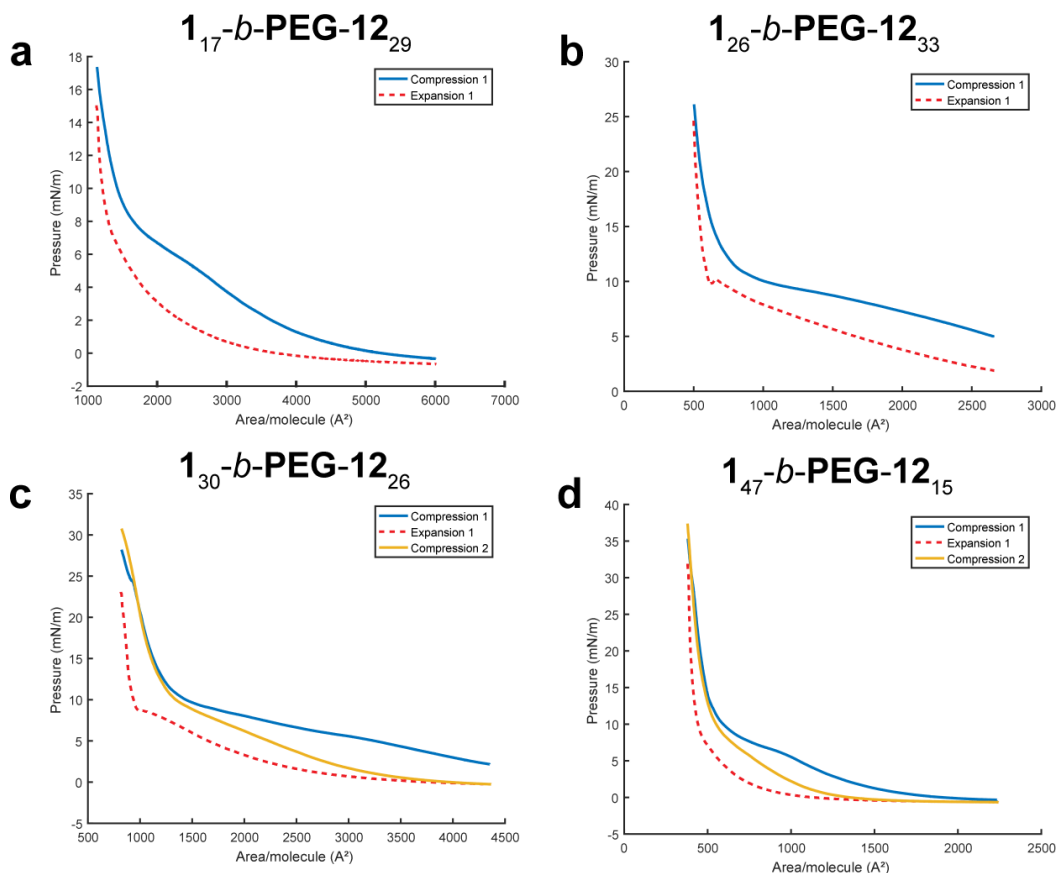
Figure 20 Langmuir isotherms for block copolymers polymers (A) **1₁₇-*b*-PEG12₂₉**, (B) **1₂₆-*b*-PEG12₃₃**, (C) **1₃₀-*b*-PEG12₂₆** and (D) **1₄₇-*b*-PEG12₁₅** exhibit hysteresis. Upon expansion, at high pressures the isotherm drops rapidly before leveling off and approaching zero. A second compression was performed for (C) and (D), which shows a deviation of the pressure of the isotherm from the first compression until the "brush" region is observed and then the pressures match again.
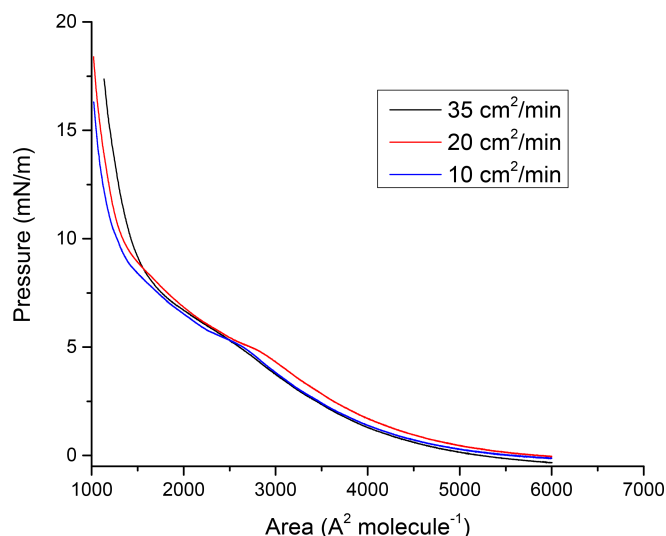
Figure 21 Langmuir isotherms for **1**$_{17}$-***b***-**PEG12**$_{29}$ at various compression rates. All features were observed (initial rise, "plateau" and "brush" regions) and there were no major deviations of the isotherm as a function of barrier speed.

Representative homopolymer procedure

Grubbs' modified second generation catalyst (H_2IMes)(pyr)$_2$Cl$_2$Ru=CHPh (1 equiv) was dissolved in anhydrous CDCl3 and added to 1 (20 equiv) in CDCl3 to a final volume of 450 µL in a J Young NMR tube. The tube was inverted several times to ensure mixing. A 1H NMR spectrum was recorded to confirm complete monomer consumption after 30 min. The homopolymer was terminated with 150 µL EVE and an aliquot (15 µL) was removed to characterize the polymer molecular weight and dispersity (Đ or Mw/Mn) via SEC-MALS. The homopolymer was precipitated using cold Et2O and centrifuged at 3000 rpm for 7 min. The Et2O was decanted and the pellet was triturated two times with DMF and cold Et2O, followed by centrifugation. The remaining pellet was washed several times with Et2O and dried in vacuo or dissolved in water with a minimal amount of ACN and lyophilized to afford a white solid.

Representative block copolymer procedure

Grubbs' modified second generation catalyst (1 equiv) was dissolved in anhydrous CDCl3 and added to **1** (20 equiv) in CDCl3 to a final volume of 400 µL. After 1 h, an aliquot (15 µL) of the homopolymer was removed from the glove box and terminated with EVE (20 µL) for SEC-MALS analysis (first block). **PEG12** or peptide monomer (100 µL, 20 equiv) in CDCl3 or DMF, respectively, was added to the solution. The copolymer was terminated with EVE (150 µL) after 2 h and analyzed by SEC-MALS. Purification was carried out as described in the homopolymer procedure.

Representative random copolymer procedure with PEG12 monomer

Grubbs' modified second generation catalyst (1 equiv) was dissolved in anhydrous CDCl3 and added to a solution containing **1** (20 equiv) and **PEG12** (20 equiv) in CDCl3 to a final volume of 400 µL. After 1 h, a 1H NMR spectrum was recorded to confirm

complete monomer consumption. The random copolymer was terminated with EVE (150 µL), followed by SEC-MALS analysis. Purification was carried out as described in the homopolymer procedure.

Representative random copolymer procedure using peptide monomer

Grubbs' modified second generation catalyst (1 equiv) was dissolved in anhydrous DMF-d7 and added to a solution containing peptide (250 µL, 10 equiv) in DMF-d7. An aliquot from a solution of **1** (12 µL, 1.7 equiv) in CDCl3 was added to the reaction every five minutes over the course of an hour to reach a final volume of 450 µL. After 2 h, a 1H NMR spectrum was recorded to confirm the complete consumption of both monomers and to estimate monomer ratios from the relative integration of biphenyl proton resonances and polymer backbone olefin protons. The random copolymer was terminated with EVE (150 µL), followed by SEC-MALS analysis. Purification was carried out as described in the homopolymer procedure.
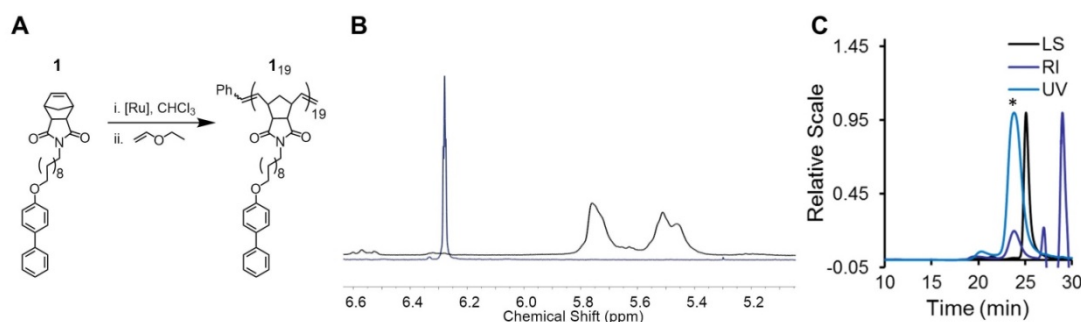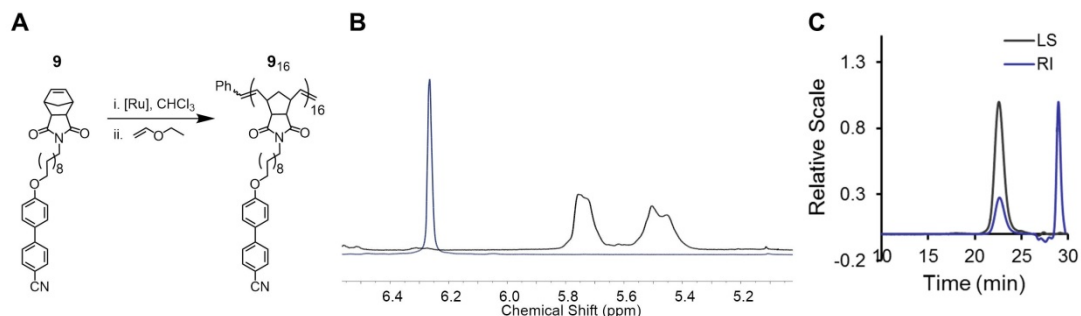

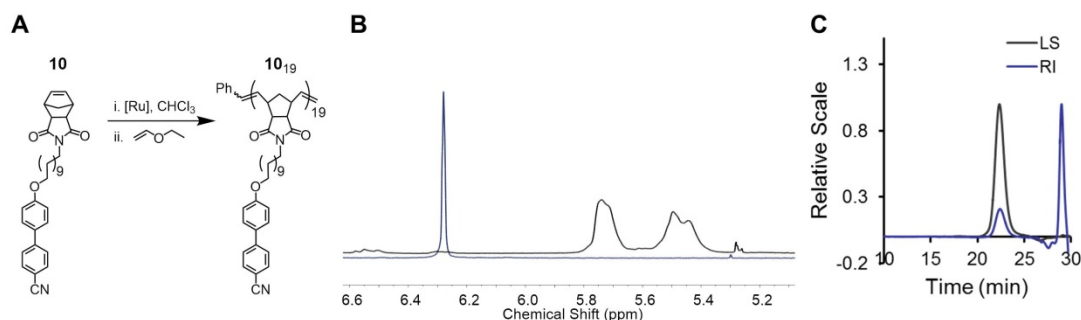**Figure 22** Polymerization and characterization of **1₁₉**. (A) Polymerization of monomer 1 to afford homopolymer **1₁₉**. (B) 1H-NMR of **1** to confirm complete polymerization (M:I = 20:1). Spectra of the monomer and polymer depict olefin resonances and are shown in blue and black, respectively. (C) SEC-MALS data of polymer **1₁₉**; M_n = 8,868 g/mol, M_w/M_n = 1.151, (dn/dc = 0.179). The peak analyzed is indicated by (*).
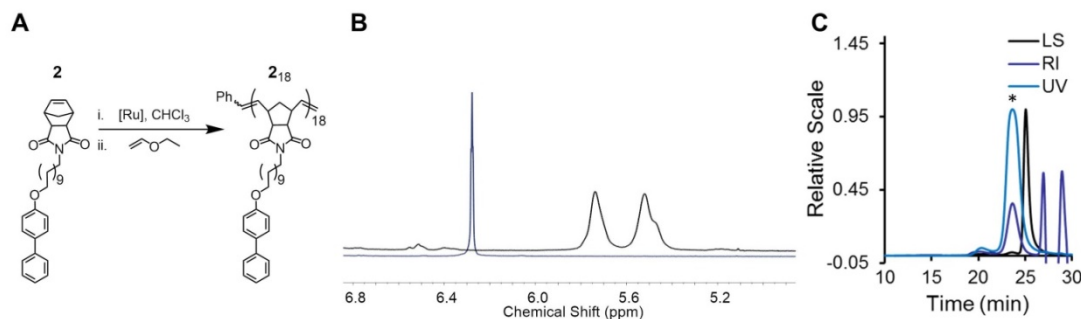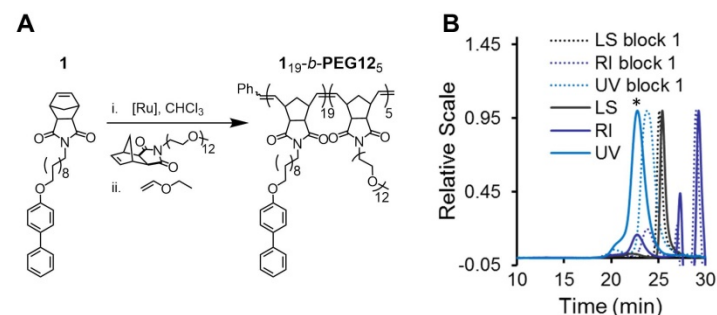

Figure 23 Polymerization and characterization of **2₁₈**. (A) Polymerization of monomer 2 to afford homopolymer **2₁₈**. (B) 1H-NMR of **2** to confirm complete polymerization (M:I = 20:1). Spectra of the monomer and polymer depict olefin resonances and are shown in

blue and black, respectively. (C) SEC-MALS data of polymer 2_{18}; Mn = 8,525 g/mol, Mw/Mn = 1.040, (dn/dc = 0.179). The peak analyzed is indicated by (*).
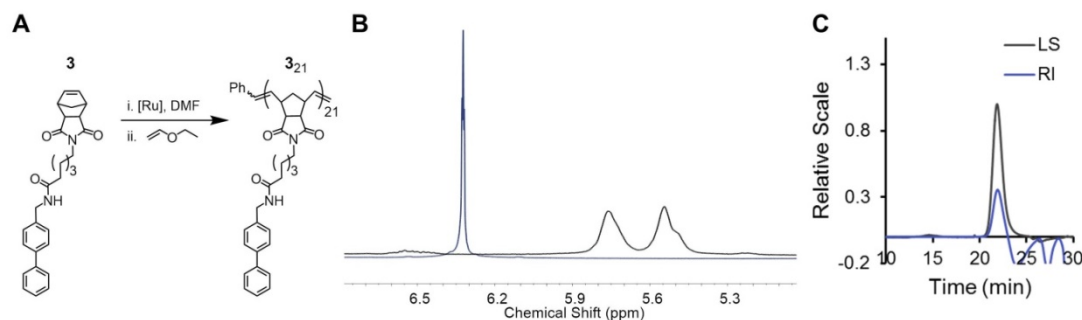
Figure 24 Polymerization and characterization of 3_{21}. (A) Polymerization of monomer **3** to afford homopolymer 3_{21}. (B) 1H-NMR of **3** to confirm complete polymerization (M:I = 20:1). Spectra of the monomer and polymer depict olefin resonances and are shown in blue and black, respectively. (C) SEC-MALS data of polymer 3_{21}; Mn = 9,426 g/mol, Mw/Mn = 1.010, (dn/dc = 0.179).
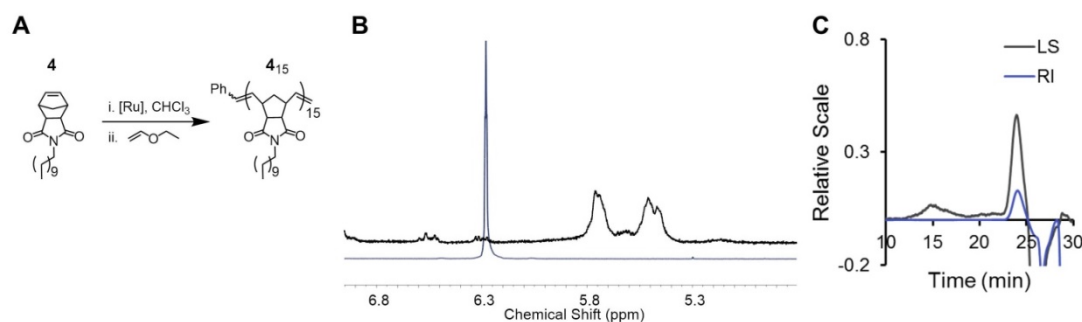
Figure 25 Polymerization and characterization of 4_{15}. (A) Polymerization of monomer **4** to afford homopolymer 4_{15}. (B) 1H-NMR of **4** to confirm complete polymerization (M:I = 20:1). Spectra of the monomer and polymer depict olefin resonances and are shown in blue and black, respectively. (C) SEC-MALS data of polymer 4_{15}; Mn = 4,726 g/mol, Mw/Mn = 1.437, (dn/dc = 0.179).
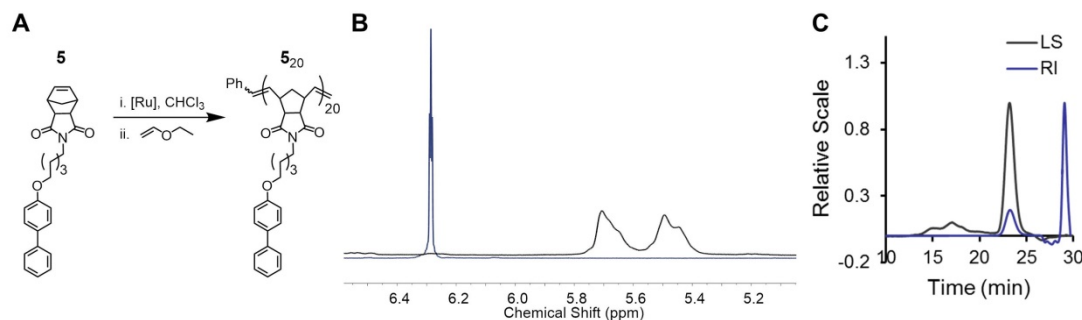
Figure 26 Polymerization and characterization of 5_{20}. (A) Polymerization of monomer **5** to afford homopolymer 5_{20}. (B) 1H-NMR of **5** to confirm complete polymerization (M:I =

20:1). Spectra of the monomer and polymer depict olefin resonances and are shown in blue and black, respectively. (C) SEC-MALS data of polymer 5_{20}; Mn = 7,880 g/mol, Mw/Mn = 1.035, (dn/dc = 0.179).
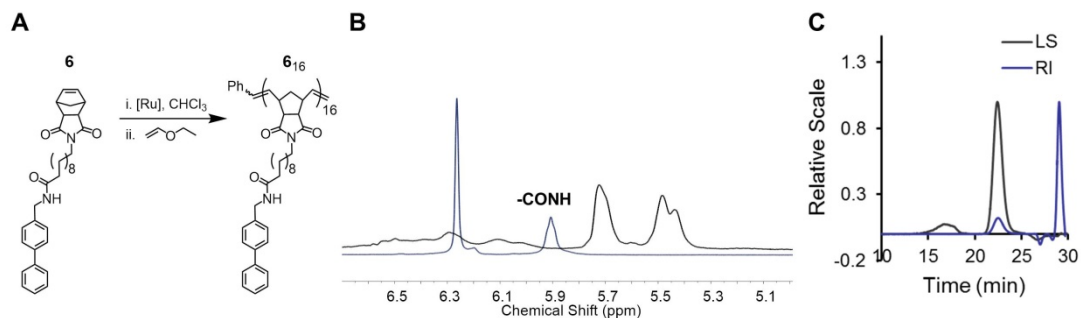
Figure 27 Polymerization and characterization of 6_{16}. (A) Polymerization of monomer 10 to afford homopolymer 6_{16}. (B) 1H-NMR of **6** to confirm complete polymerization (M:I = 20:1). Spectra of the monomer and polymer depict olefin resonances and are shown in blue and black, respectively. The amide resonance in the monomer spectrum is indicated (-CONH).
(C) SEC-MALS data of polymer 6_{16}; Mn = 8,011 g/mol, Mw/Mn = 1.063, (dn/dc = 0.179).
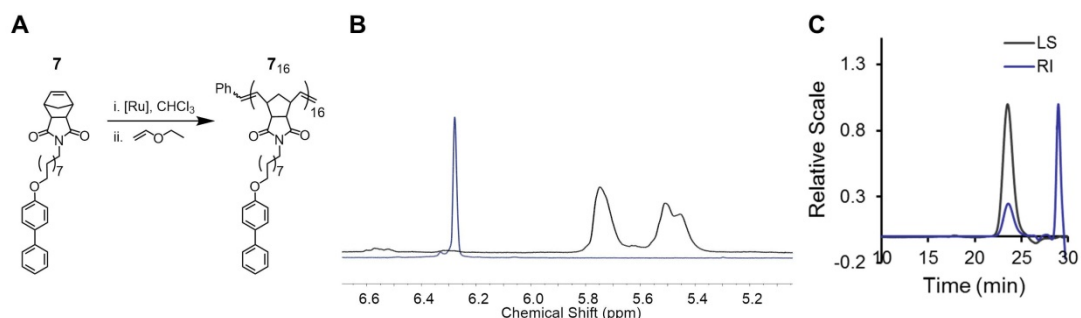
Figure 28 P Polymerization and characterization of 7_{16}. (A) Polymerization of monomer 5 to afford homopolymer 7_{16}. (B) 1H-NMR of **7** to confirm complete polymerization (M:I = 20:1). Spectra of the monomer and polymer depict olefin resonances and are shown in blue and black, respectively. (C) SEC-MALS data of polymer 7_{16}; Mn = 7,142 g/mol, Mw/Mn = 1.024, (dn/dc = 0.179).
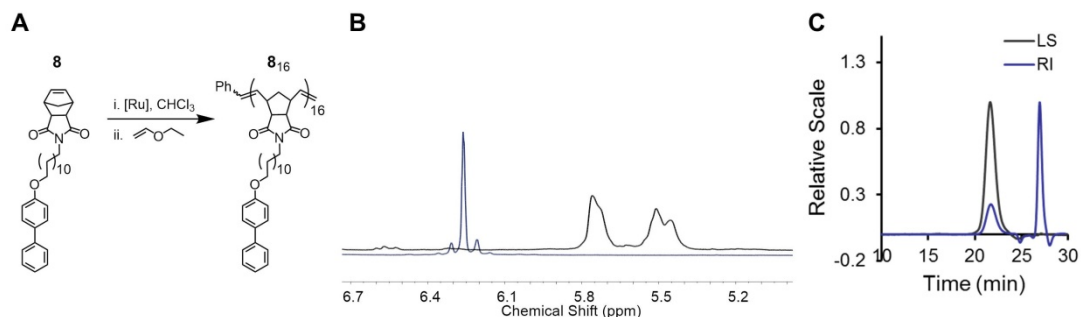
Figure 29 Polymerization and characterization of 8_{16}. (A) Polymerization of monomer **8** to afford homopolymer 8_{16}. (B) 1H-NMR of **8** to confirm complete polymerization (M:I = 20:1). Spectra of the monomer and polymer depict olefin resonances and are shown in

blue and black, respectively. (C) SEC-MALS data of polymer **8₁₆**; Mn = 8,139 g/mol, Mw/Mn = 1.017, (dn/dc = 0.179).

Figure 30 P Polymerization and characterization of **9₁₆**. A) Polymerization of monomer **9** to afford homopolymer **9₁₆**. (B) 1H-NMR of **9** to confirm complete polymerization (M:I = 20:1). Spectra of the monomer and polymer depict olefin resonances and are shown in blue and black, respectively. (C) SEC-MALS data of polymer **9₁₆**; Mn = 8,077 g/mol, Mw/Mn = 1.017, (dn/dc = 0.179).

Figure 31 Polymerization and characterization of **10₁₉**. (A) Polymerization of monomer 8 to afford homopolymer **10₁₉**. (B) 1H-NMR of **10** to confirm complete polymerization (M:I = 20:1). Spectra of the monomer and polymer depict olefin resonances and are shown in blue and black, respectively. (C) SEC-MALS data of polymer 819; Mn = 9,746 g/mol, Mw/Mn = 1.021, (dn/dc = 0.179).
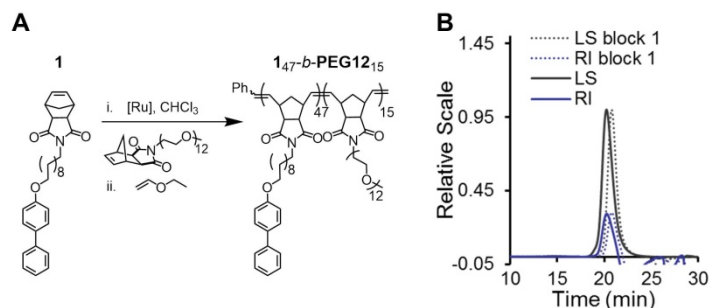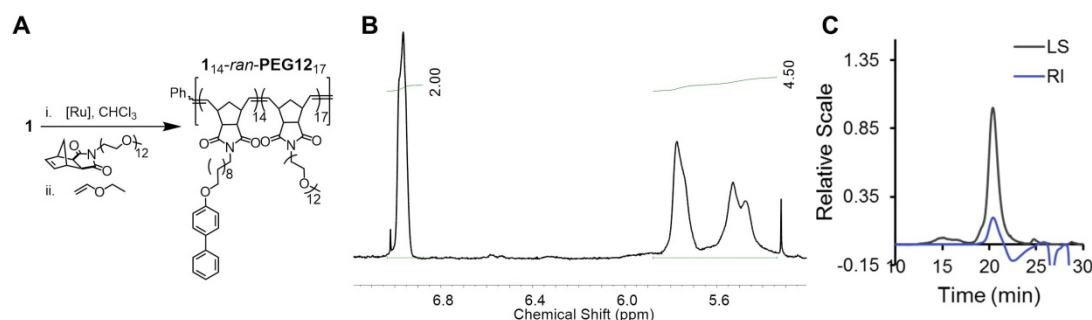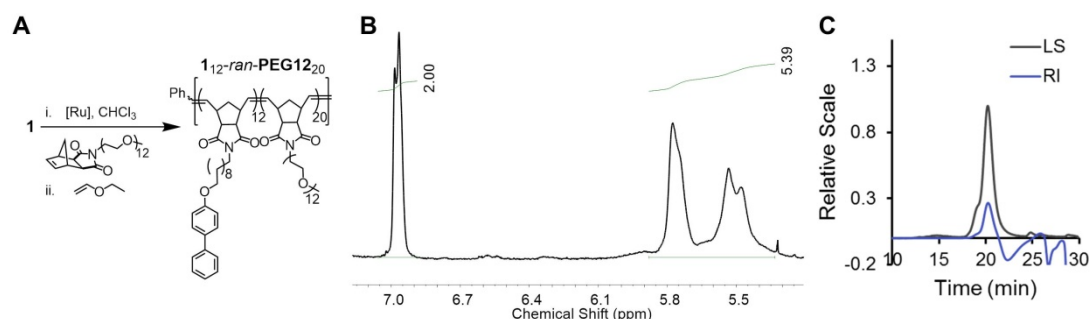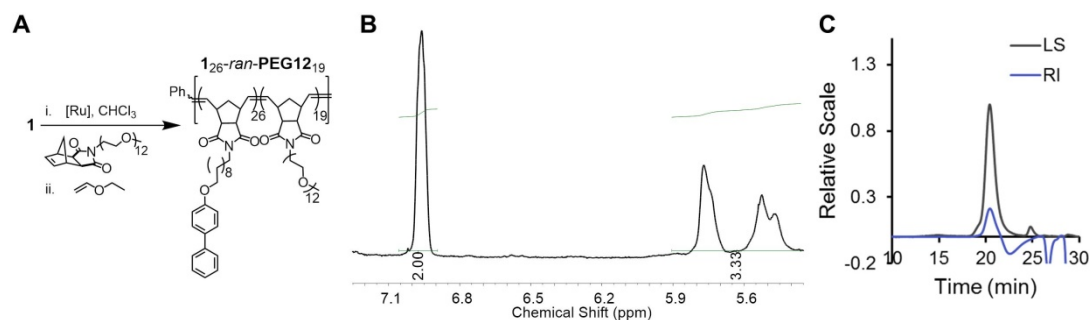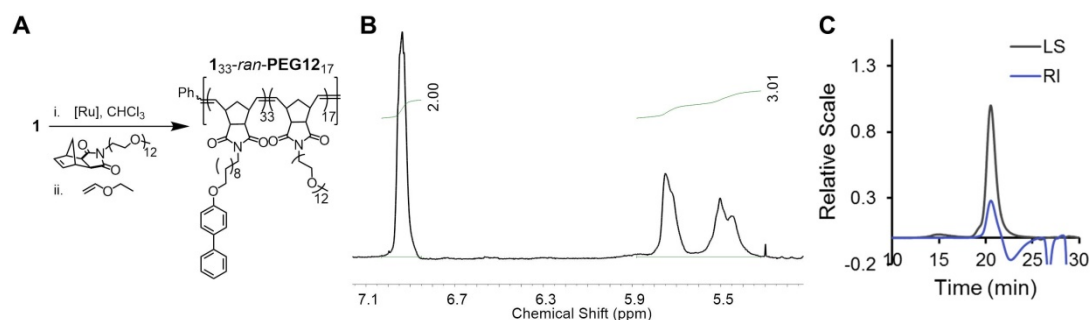

Figure 32 Polymerization and characterization of **1₁₉-b-PEG12₅**. (A) Polymerization of monomers **1** and **PEG12** to afford block copolymer **1₁₉-b-PEG12₅**. (B) 1H-NMR of **1₁₉-b-PEG12₅** to confirm complete polymerization (**1:PEG12:I** = 15:10:1). (C) SEC-MALS data of copolymer **1₁₉-b-PEG12₅**; Mn = 12,660 g/mol, Mn/Mw = 1.196, (dn/dc = 0.1375);

Block 1: Mn = 8,868 g/mol, Mw/Mn = 1.151, (dn/dc = 0.179).). The copolymer peak analyzed is indicated by (*).
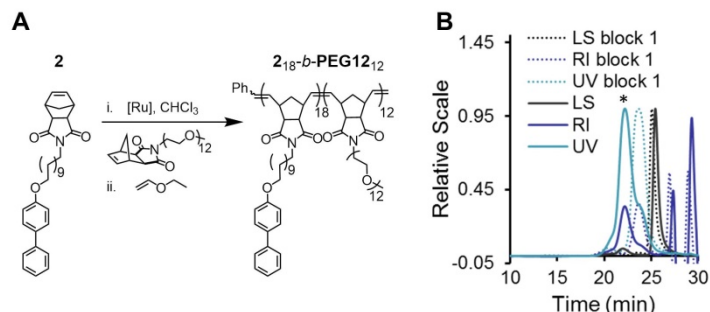
Figure 33 Polymerization and characterization of **2$_{18}$-*b*-PEG12$_{12}$**. (A) Polymerization of monomers **2** and **PEG12** to afford block copolymer **2$_{18}$-*b*-PEG12$_{12}$**. (B) 1H-NMR of **2$_{18}$-*b*-PEG12$_{12}$** to confirm complete polymerization (**2:PEG12**:I = 15:10:1). (C) SEC-MALS data of copolymer **2$_{18}$-*b*-PEG12$_{12}$**; Mn = 16,660 g/mol, Mw/Mn = 1.082, (dn/dc = 0.1375); Block 1: Mn = 8,525 g/mol, Mn/Mw = 1.040, (dn/dc = 0.179). The copolymer peak analyzed is indicated by (*).
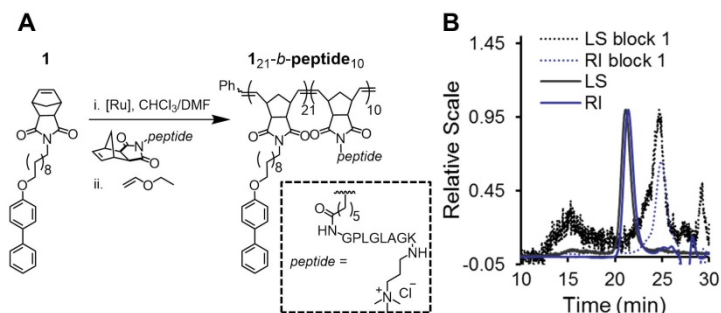
Figure 34 Polymerization and characterization of **1$_{21}$-*b*-peptide$_{10}$**. (A) Polymerization of monomers **1** and **peptide** to afford block copolymer **1$_{21}$-*b*-peptide$_{10}$**. (B) 1H-NMR of **1$_{21}$-*b*-peptide$_{10}$** to confirm complete polymerization (**1:peptide**:I = 15:15:1). (C) SEC-MALS data of copolymer **1$_{21}$-*b*-peptide$_{10}$**; Mn = 20,250 g/mol, Mw/Mn = 1.169, (dn/dc = 0.179). Block 1: Mn = 11,720 g/mol, Mn/Mw = 1.276, (dn/dc = 0.179).
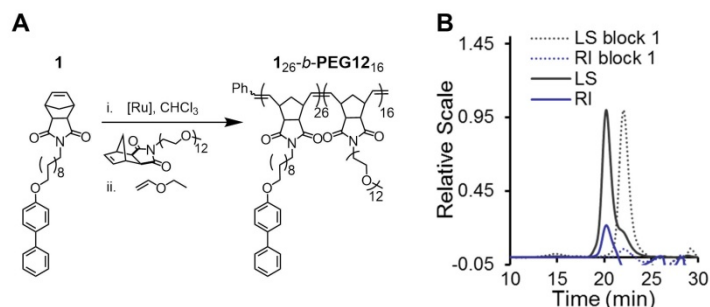
Figure 35 Polymerization and characterization of **1$_{26}$-*b*-PEG12$_{16}$**. (A) Polymerization of monomers **1** and **PEG12** to afford block copolymer **1$_{26}$-*b*-PEG12$_{16}$**. (B) 1H-NMR of **1$_{26}$-*b*-PEG12$_{16}$** to confirm complete polymerization (**1:PEG12**:I = 20:20:1). (C) SEC-MALS data of copolymer **1$_{26}$-*b*-PEG12$_{16}$**; Mn = 22,970 g/mol, Mn/Mw = 1.011, (dn/dc = 0.1375); Block 1: Mn = 12,090 g/mol, Mw/Mn = 1.021, (dn/dc = 0.179).
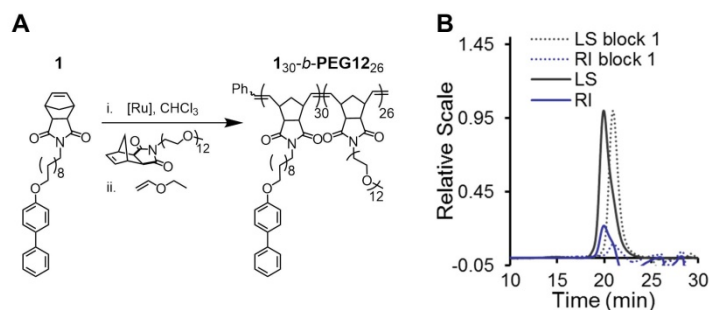
Figure 36 Polymerization and characterization of $\mathbf{1}_{30}$-*b*-**PEG12**$_{26}$. (A) Polymerization of monomers **1** and **PEG12** to afford block copolymer $\mathbf{1}_{30}$-*b*-**PEG12**$_{26}$. (B) 1H-NMR of $\mathbf{1}_{30}$-*b*-**PEG12**$_{26}$to confirm complete polymerization (**1**:**PEG12**:I = 27:13:1). (C) SEC-MALS data of copolymer $\mathbf{1}_{30}$-*b*-**PEG12**$_{26}$; Mn = 32,350 g/mol, Mn/Mw = 1.022, (dn/dc = 0.1375); Block 1: Mn = 13,990 g/mol, Mn/Mw = 1.073, (dn/dc = 0.179).
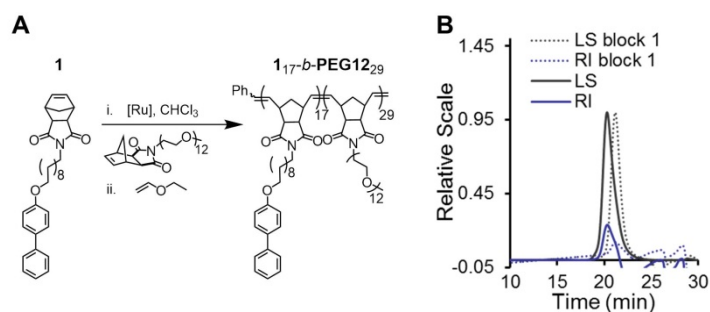
Figure 37 Polymerization and characterization of $\mathbf{1}_{17}$-*b*-**PEG12**$_{29}$. (A) Polymerization of monomers **1** and **PEG12** to afford block copolymer $\mathbf{1}_{17}$-*b*-**PEG12**$_{29}$. (B) 1H-NMR of $\mathbf{1}_{17}$-*b*-**PEG12**$_{29}$to confirm complete polymerization (**1**:**PEG12**:I = 30:10:1). (C) SEC-MALS data of copolymer $\mathbf{1}_{17}$-*b*-**PEG12**$_{29}$; Mn = 27,680 g/mol, Mn/Mw = 1.018, (dn/dc = 0.1375); Block 1: Mn = 7,860 g/mol, Mn/Mw = 1.131, (dn/dc = 0.179).

Figure 38 Polymerization and characterization of $\mathbf{1}_{47}$-*b*-**PEG12**$_{15}$. (A) Polymerization of monomers **1** and **PEG12** to afford block copolymer $\mathbf{1}_{47}$-*b*-**PEG12**$_{15}$. (B) 1H-NMR of $\mathbf{1}_{47}$-*b*-**PEG12**$_{15}$to confirm complete polymerization (**1**:**PEG12**:I = 32:8:1). (C) SEC-MALS data of copolymer $\mathbf{1}_{47}$-*b*-**PEG12**$_{15}$; Mn = 32,170 g/mol, Mn/Mw = 1.016, (dn/dc = 0.1375); Block 1: Mn = 22,020 g/mol, Mw/Mn = 1.009, (dn/dc = 0.179).
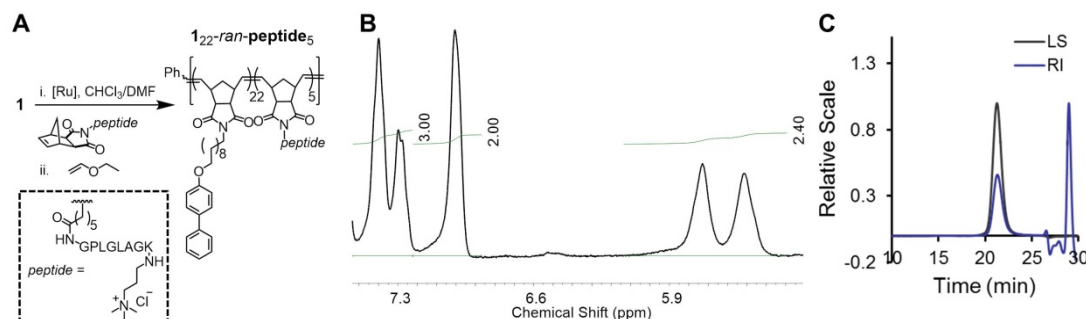
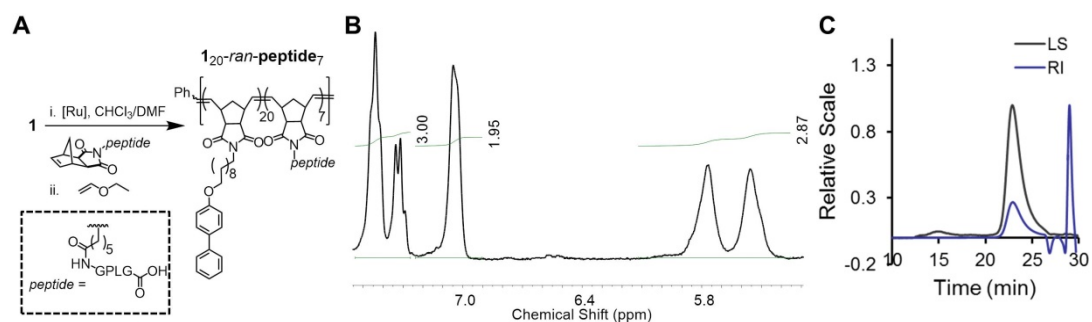**Figure 39** Polymerization and characterization of **1₁₄**-*ran*-**PEG12₁₇**. (A) Polymerization of monomers **1** and **PEG12** to afford random copolymer **1₁₄**-*ran*-**PEG12₁₇**. (B) 1H-NMR of **1₁₄**-*ran*-**PEG12₁₇** to confirm complete polymerization (**1**:**PEG12**:I = 20:20:1). Monomer ratios are estimated from the relative integration of biphenyl proton resonances and polymer backbone olefin protons. (C) SEC-MALS data of copolymer **1₁₄**-*ran*-**PEG12₁₇**; Mn = 18,650 g/mol, Mw/Mn = 1.009, (dn/dc = 0.1375).


Figure 40 Polymerization and characterization of **1₁₂**-*ran*-**PEG12₂₀**. (A) Polymerization of monomers **1** and **PEG12** to afford random copolymer **1₁₂**-*ran*-**PEG12₂₀**. (B) 1H-NMR of **1₁₂**-*ran*-**PEG12₂₀** to confirm complete polymerization (**1**:**PEG12**:I = 13:27:1). Monomer ratios are estimated from the relative integration of biphenyl proton resonances and polymer backbone olefin protons. (C) SEC-MALS data of copolymer **1₁₂**-*ran*-**PEG12₂₀**; Mn = 19,290 g/mol, Mw/Mn = 1.024, (dn/dc = 0.1375).

Figure 41 Polymerization and characterization of **1₂₆**-*ran*-**PEG12₁₉**. (A) Polymerization of monomers **1** and **PEG12** to afford random copolymer **1₂₆**-*ran*-**PEG12₁₉**. (B) 1H-NMR of **1₂₆**-*ran*-**PEG12₁₉** to confirm complete polymerization (**1**:**PEG12**:I = 27:13:1). Monomer ratios are estimated from the relative integration of biphenyl proton resonances and polymer backbone olefin protons. (C) SEC-MALS data of copolymer **1₂₆**-*ran*-**PEG12₁₉**; Mn = 25,240 g/mol, Mw/Mn = 1.019, (dn/dc = 0.1375).

Figure 42 Polymerization and characterization of **1**$_{33}$-*ran*-**PEG12**$_{17}$. (A) Polymerization of monomers **1** and **PEG12** to afford random copolymer **1**$_{33}$-*ran*-**PEG12**$_{17}$. (B) 1H-NMR of **1**$_{33}$-*ran*-**PEG12**$_{17}$to confirm complete polymerization (**1**:**PEG12**:I = 32:8:1). Monomer ratios are estimated from the relative integration of biphenyl proton resonances and polymer backbone olefin protons. (C) SEC-MALS data of copolymer **1**$_{33}$-*ran*-**PEG12**$_{17}$; Mn = 27,090 g/mol, Mw/Mn = 1.019, (dn/dc = 0.1375).

Figure 43 Polymerization and characterization of **1**$_{22}$-*ran*-**peptide**$_5$. (A) Polymerization of monomers 1 and peptide to afford random copolymer **1**$_{22}$-*ran*-**peptide**$_5$. (B) 1H-NMR of **1**$_{22}$-*ran*-**peptide**$_5$to confirm complete polymerization (**1**:**peptide**:I = 20:10:1). Monomer ratios are estimated from the relative integration of biphenyl proton resonances and polymer backbone olefin protons. (C) SEC-MALS data of copolymer **1**$_{22}$-*ran*-**peptide**$_5$; Mn = 15,800 g/mol, Mw/Mn = 1.015, (dn/dc = 0.179).

Figure 44 Polymerization and characterization of **1**$_{20}$-*ran*-**peptide**$_7$. (A) Polymerization of monomers **1** and **peptide** to afford random copolymer **1**$_{20}$-*ran*-**peptide**$_7$. (B) 1H-NMR of **1**$_{20}$-*ran*-**peptide**$_7$ to confirm complete polymerization (**1**:**peptide**:I = 20:10:1). Monomer ratios are estimated from the relative integration of biphenyl proton resonances and polymer backbone olefin protons. (C) SEC-MALS data of copolymer **1**$_{20}$-*ran*-**peptide**$_7$; Mn = 13,680 g/mol, Mw/Mn = 1.006, (dn/dc = 0.179).
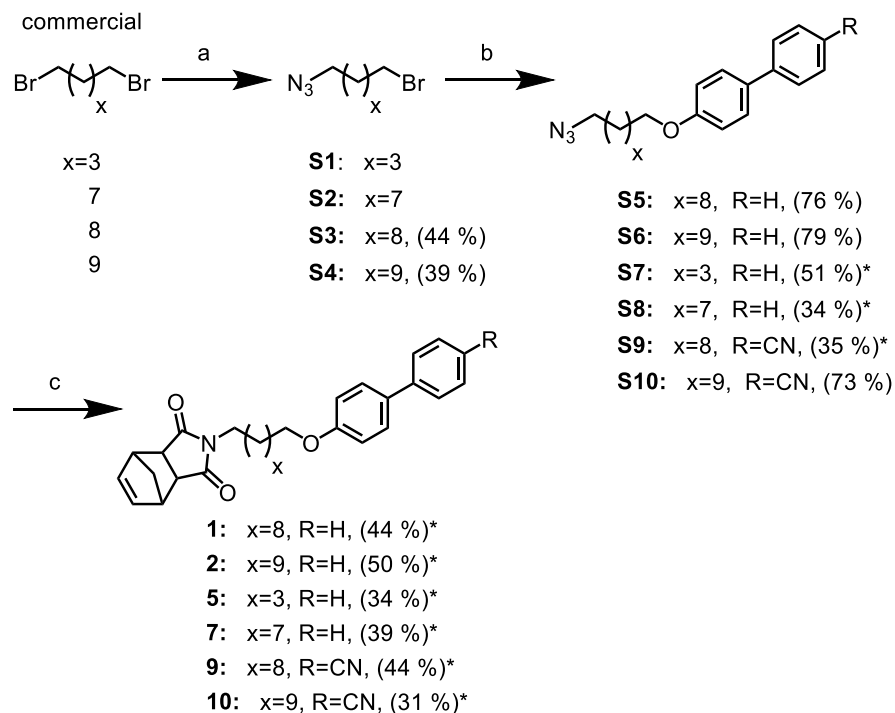
Scheme 2 Synthesis of norbornene monomers **1**, **2**, **5**, **7**, **9**, and **10**
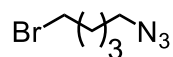
1-azido-5-bromopentane (S1). A round-bottom flask was charged with 1,5-dibromopentane (2.0 g, 8.7 mmol) and sodium azide (0.57 g, 8.7 mmol). To the solid mixture was added DMSO (35 mL). The solution was stirred vigorously at room temperature for 20 h. The solution was diluted with water (30 mL) and was allowed to cool. The aqueous phase was extracted with ether (3 x 30 mL) and the combined organic phase was washed with water (2 x 20 mL), dried over MgSO4, filtered, and concentrated under reduced pressure. The reaction mixture was run through a silica plug (SiO2, 3:1 hexanes:EtOAc, Rf = 0.69) to afford the crude product (1.53 g) as a pale yellow oil that was used without further purification. The analytical data of S1 were in agreement with those reported previously.17
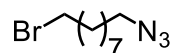
1-azido-9-bromononane (S2). A round-bottom flask was charged with 1,9-dibromononane (2.0 g, 6.99 mmol) and sodium azide (0.46 g, 6.99 mmol). To the solid mixture was added DMSO (35 mL). The solution was stirred vigorously at room temperature for 9 h. The solution was diluted with water (30 mL) and was allowed to cool.

The aqueous phase was extracted with ether (3 x 30 mL) and the combined organic phase was washed with water (2 x 20 mL), dried over MgSO4, filtered, and concentrated under reduced pressure to afford the crude product (2.33 g) as a pale yellow oil that was used without further purification. The analytical data of S2 were in agreement with those reported previously.[18]

Br～～(～)8～N3
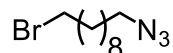
1-azido-10-bromodecane (S3). A round-bottom flask was charged with 1,10-dibromodecane (2.5 g, 8.33 mmol) and sodium azide (0.54 g, 8.33 mmol). To the solid mixture was added DMSO (40 mL). The solution was stirred vigorously at room temperature for 15 h. The solution was diluted with water (40 mL) and was allowed to cool. The aqueous phase was extracted with ether (3 x 30 mL) and the combined organic phase was washed with water (2 x 20 mL), dried over MgSO4, filtered, and concentrated under reduced pressure. The reaction mixture was purified by flash chromatography (SiO2, hexanes, Rf = 0.34) to afford the desired product (0.98 g, 44%) as a pale yellow oil: 1H NMR (400 MHz, CDCl3) δ 3.41 (t, J = 6.9 Hz, 2H), 3.26 (t, J = 6.9 Hz, 2H), 1.95 − 1.77 (m, 2H), 1.70 − 1.51 (m, 2H), 1.49 − 1.23 (m, 12H). 13C NMR (126 MHz, CDCl3) δ 51.58, 34.25, 32.91, 29.48, 29.44, 29.23, 28.95, 28.84, 28.26, 26.81. MS calcd: 261.08; EI-MS (70 eV), m/z (%): 70 (100) [C2H4N3+], 55 (48) [C3H5N], 84 (23) [C3H6N3+], 98 (6) [C4H8N3+], 120 (3) [C3H6Br+], 135 (6) [C4H8Br+], 232 (3) [M+ - N2, C10H19BrN].

Br～～(～)9～N3
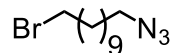
1-azido-11-bromoundecane (S4). A round-bottom flask was charged with 1,11-dibromoundecane (2.0 g, 6.37 mmol) and sodium azide (0.42 g, 6.37 mmol). To the solid mixture was added DMSO (35 mL). The solution was stirred vigorously at room temperature for 8 h. The solution was diluted with water (30 mL) and was allowed to cool. The aqueous phase was extracted with ether (3 x 30 mL) and the combined organic phase was washed with water (2 x 20 mL), dried over MgSO4, filtered, and concentrated under reduced pressure. The reaction mixture was purified by flash chromatography (SiO2, hexanes, Rf = 0.43) to afford the desired product (0.69 g, 39%) as a colorless oil: 1H NMR (400 MHz, CD2Cl2) δ 3.42 (t, J = 6.9 Hz, 2H), 3.25 (t, J = 6.9 Hz, 2H), 1.91 − 1.78 (m, 2H), 1.65 − 1.50 (m, 2H), 1.46 − 1.18 (m, 14H). 13C NMR (126 MHz, CDCl3) δ 51.60, 34.28, 32.94, 29.56, 29.54, 29.53, 29.27, 28.96, 28.88, 28.29, 26.84. MS calcd: 275.10; EI-MS (70 eV), m/z (%): 70 (100) [C2H4N3+], 55 (50) [C3H5N], 84 (25) [C3H6N3+], 98 (8) [C4H8N3+], 135 (7) [C4H8Br+], 166 (2) [M+ - Br, C11H20N+].

(biphenyl)—O～(～)8～N3
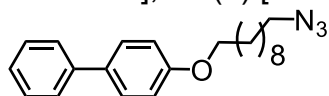
4-((10-azidodecyl)oxy)-biphenyl (S5). A round-bottom flask was charged with **S2** (0.46 g, 1.82 mmol), 4-phenylphenol (0.36 g, 2.18 mmol), and K2CO3 (1.21 g, 9.09 mmol). To the solid mixture was added acetone (40 mL) and the flask was heated to reflux for 21 h. The mixture was then allowed to cool to room temperature and concentrated. The residue was diluted with CHCl3 (40 mL) and washed with water (3 x 20 mL). The organic
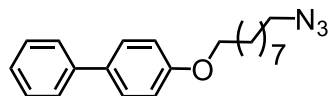
layer was dried over MgSO4, filtered, and concentrated under reduced pressure. The mixture was purified by flash chromatography (SiO2, 20% DCM in hexanes, Rf = 0.44) to afford the desired product (0.47 g, 76%) as a white solid: 1H NMR (400 MHz, CD2Cl2) δ 7.59 – 7.48 (m, 4H), 7.45 – 7.37 (m, 2H), 7.33 – 7.27 (m, 1H), 7.01 – 6.92 (m, 2H), 3.99 (t, J = 6.6 Hz, 2H), 3.26 (t, J = 7.0 Hz, 2H), 1.85 – 1.75 (m, 2H), 1.66 – 1.55 (m, 2H), 1.52 – 1.42 (m, 2H), 1.42 – 1.27 (m, 10H). 13C NMR (126 MHz, CDCl3) δ 158.79, 140.97, 133.62, 128.83, 128.23, 126.82, 126.72, 114.84, 68.14, 51.60, 29.59, 29.55, 29.49, 29.41, 29.28, 28.97, 26.84, 26.18.
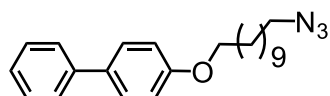
4-((11-azidoundecyl)oxy)-biphenyl (S6). A round-bottom flask was charged with **S4** (0.30 g, 1.09 mmol), 4-phenylphenol (0.22 g, 1.30 mmol), and K2CO3 (0.753 g, 5.45 mmol). To the solid mixture was added acetone (20 mL) and the flask was heated to reflux for 24 h. The mixture was then allowed to cool to room temperature and concentrated. The residue was diluted with CHCl3 (40 mL) and washed with water (2 x 20 mL). The organic layer was dried over MgSO4, filtered, and concentrated under reduced pressure. The mixture was purified by flash chromatography (SiO2, 20% DCM in hexanes, Rf = 0.43) to afford the desired product (0.31 g, 79%) as a white solid: 1H NMR (400 MHz, CD2Cl2) δ 7.64 – 7.47 (m, 4H), 7.44 – 7.38 (m, 2H), 7.35 – 7.24 (m, 1H), 6.99 – 6.93 (m, 2H), 4.00 (t, J = 6.6 Hz, 2H), 3.25 (t, J = 7.0 Hz, 2H), 1.84 – 1.74 (m, 2H), 1.65 – 1.54 (m, 2H), 1.51 – 1.43 (m, 2H), 1.42 – 1.26 (m, 12H). 13C NMR (126 MHz, CDCl3) δ 158.81, 140.99, 133.63, 128.84, 128.24, 126.84, 126.73, 114.85, 68.17, 51.62, 29.68, 29.61, 29.52, 29.42, 29.30, 28.98, 26.85, 26.19.
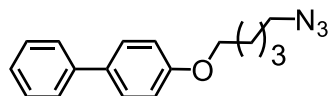
4-((5-azidopentyl)oxy)-biphenyl (S7). A round-bottom flask was charged with **S1** (1.53 g, 7.97 mmol), 4-phenylphenol (2.71 g, 15.9 mmol), and K2CO3 (5.51 g, 39.8 mmol). To the solid mixture was added acetone (40 mL) and the flask was heated to reflux for 15 h. The mixture was then allowed to cool to room temperature and concentrated. The residue was diluted with CHCl3 (40 mL) and washed with water (3 x 20 mL). The organic layer was dried over MgSO4, filtered, and concentrated under reduced pressure. The mixture was purified by flash chromatography (SiO2, 20% DCM in hexanes, Rf = 0.32) to afford the desired product (1.14 g, 51% over two steps) as a pale yellow oil: 1H NMR (400 MHz, CDCl3) δ 7.60 – 7.46 (m, 4H), 7.45 – 7.36 (m, 2H), 7.28 – 7.33 (m, 1H), 7.02 – 6.92 (m, 2H), 4.02 (t, J = 6.3 Hz, 2H), 3.32 (t, J = 6.8 Hz, 2H), 1.91 – 1.79 (m, 2H), 1.76 – 1.64 (m, 2H), 1.64 – 1.55 (m, 2H). 13C NMR (126 MHz, CDCl3) δ 158.63, 140.93, 133.81, 128.85, 128.28, 126.84, 126.77, 114.83, 67.74, 51.49, 28.98, 28.81, 23.55.

**4-((9-azidononyl)oxy)-biphenyl) (S8).** A round-bottom flask was charged with **S2** (1.74 g, 7.01 mmol), 4-phenylphenol (2.38 g, 13.9 mmol), and K2CO3 (4.74 g, 35.0 mmol). To the solid mixture was added acetone (25 mL) and the flask was heated to reflux for 21 h. The mixture was then allowed to cool to room temperature and concentrated. The residue was diluted with CHCl3 (40 mL) and washed with water (3 x 20 mL). The organic layer was dried over MgSO4, filtered, and concentrated under reduced pressure. The mixture was purified by flash chromatography (SiO2, 20% DCM in hexanes, Rf = 0.29) to afford the desired product (0.80 g, 34% over two steps) as a white solid: 1H NMR (400 MHz, CDCl3) δ 7.58 – 7.48 (m, 4H), 7.44 – 7.37 (m, 2H), 7.30 (t, J = 7.0 Hz, 1H), 7.00 – 6.93 (m, 2H), 4.00 (t, J = 6.5 Hz, 2H), 3.23 – 3.29 (m, 2H), 1.85 – 1.76 (m, 2H), 1.65 – 1.57 (m, 2H), 1.53 – 1.43 (m, 2H), 1.42 – 1.29 (m, 8H). 13C NMR (126 MHz, CDCl3) δ 158.79, 140.98, 133.65, 128.84, 128.24, 126.84, 126.73, 114.85, 68.13, 51.60, 29.55, 29.42, 29.41, 29.24, 28.97, 26.84, 26.17.
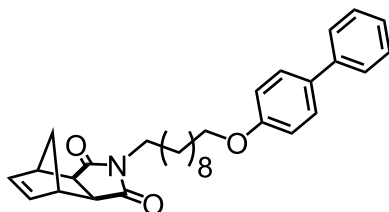
N-(4-decyloxy-biphenyl)-cis-5-norbornene-exo-dicarboximide (1). To a solution of **S5** (0.39 g, 1.10 mmol) in 4:1 THF:MeOH (15 mL) was added 10% Pd/C (5 mol% of S5). The flask was evacuated and backfilled with H2 (3 x) using a hydrogen balloon and the reaction was stirred at rt for 4 h. The reaction mixture was filtered through celite and washed using EtOAc. The filtrate was concentrated to give a white solid that was used in the next step without purification. A round-bottom flask was charged with the hydrogenated **S5** product (0.36 g, 1.1 mmol), and cis-5-norbornene-exo-2,3-dicarboxylic anhydride (0.152 g, 0.93 mmol). To the solid mixture was added toluene (20 mL). Et3N (15.5 µL, 0.11 mmol) was added. The flask was heated to reflux for 18 h. The mixture was then allowed to cool to room temperature and concentrated. The reaction mixture was diluted with CHCl3 (40 mL) and washed with 1 M aqueous HCl (2 x 20 mL). The organic layer was washed with saturated aqueous NaCl (20 mL), dried over MgSO4, filtered, and concentrated under reduced pressure. Purification by flash chromatography (SiO2, 5:1 hexanes:EtOAc, Rf = 0.29) gave the desired product (0.19 g, 44% over two steps) as a white solid: 1H-NMR (400 MHz, CDCl3) δ 7.59 – 7.48 (m, 4H), 7.45 – 7.37 (m, 2H), 7.33 – 7.27 (m, 1H), 7.00 – 6.93 (m, 2H), 6.28 (t, J = 1.9 Hz, 2H), 3.99 (t, J = 6.6 Hz, 2H), 3.49 – 3.42 (m, 2H), 3.25 – 3.30 (m, 2H), 2.67 (d, J = 1.3 Hz, 2H), 1.85 – 1.74 (m, 2H), 1.60 – 1.40 (m, 4H), 1.40 – 1.16 (m, 12H). 13C NMR (126 MHz, CDCl3) δ 178.29, 158.80, 141.00, 137.95, 133.60, 128.83, 128.23, 126.84, 126.71, 114.85, 68.16, 47.93, 45.29, 42.85, 38.89, 29.60, 29.52, 29.48, 29.42, 29.26, 27.91, 27.09, 26.18. HRMS (ESI) calcd for [C31H37NO3Na]+ : 494.2666, found: 494.2666 [M + Na]+
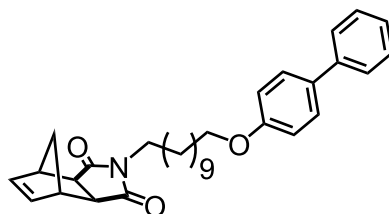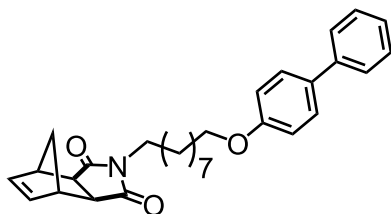
***N*-(4-undecyloxy-biphenyl)-*cis*-5-norbornene-*exo*-dicarboximide (2).** To a solution of **S6** (0.18 g, 0.492 mmol) in 4:1 THF:MeOH (15 mL) was added 10% Pd/C (5 mol% of S6). The flask was evacuated and backfilled with H2 (3 x) using a hydrogen balloon and the reaction was stirred at rt for 21 h. The reaction mixture was filtered through celite and washed using EtOAc. The filtrate was concentrated to give a white solid that was used in the next step without purification. A round-bottom flask was charged with the hydrogenated **S6** product (0.13 g, 0.38 mmol), and cis-5-norbornene-exo-2,3-dicarboxylic anhydride (0.052 g, 0.32 mmol). To the solid mixture was added toluene (15 mL). Et3N (6.4 µL, 0.05 mmol) was added. The flask was heated to reflux for 18 h. The mixture was then allowed to cool to room temperature and concentrated. The reaction mixture was diluted with CHCl3 (20 mL) and washed with 1 M aqueous HCl (2 x 15 mL). The organic layer was washed with saturated aqueous NaCl (15 mL), dried over MgSO4, filtered, and concentrated under reduced pressure. Purification by flash chromatography (SiO2, 4:1 hexanes:EtOAc, Rf = 0.39) gave the desired product (0.12 g, 50% over two steps) as a waxy pale yellow solid: 1H NMR (400 MHz, CDCl3) δ 7.60 – 7.47 (m, 4H), 7.46 – 7.36 (m, 2H), 7.34 – 7.26 (m, 1H), 7.02 – 6.91 (m, 2H), 6.28 (t, J = 1.8 Hz, 2H), 3.99 (t, J = 6.6 Hz, 2H), 3.45 (dd, J = 8.4, 6.6 Hz, 2H), 3.28 (dd, J = 9.9, 7.9 Hz, 2H), 2.66 (d, J = 1.1 Hz, 2H), 1.86 – 1.74 (m, 2H), 1.58 – 1.41 (m, 4H), 1.40 – 1.19 (m, 14H). 13C NMR (126 MHz, CDCl3) δ 178.17, 158.69, 140.87, 137.83, 133.47, 128.70, 128.10, 126.71, 126.59, 114.73, 68.05, 47.80, 45.16, 42.73, 38.78, 29.53, 29.48, 29.45, 29.40, 29.30, 29.15, 27.80, 26.97, 26.07. HRMS (ESI) calcd for [C32H39NO3Na]+: 508.2822, found: 508.2823 [M + Na]+
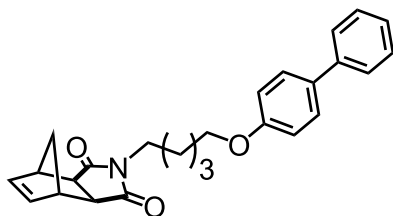

***N*-(4-pentyloxy-biphenyl)-*cis*-5-norbornene-*exo*-dicarboximide (5).** To a solution of **S7** (0.81 g, 2.89 mmol) in 4:1 THF:MeOH (35 mL) was added 10% Pd/C (5 mol% of S10). The flask was evacuated and backfilled with H2 (3 x) using a hydrogen balloon and the reaction was stirred at rt for 17 h. The reaction mixture was filtered through celite and washed using EtOAc. The filtrate was concentrated to give a white solid that was used in the next step without purification. A round-bottom flask was charged with the hydrogenated **S7** product (0.74 g, 2.89 mmol), and cis-5-norbornene-exo-2,3-dicarboxylic anhydride (0.39 g, 2.41 mmol). To the solid mixture was added toluene (50 mL). Et3N (40.3 µL, 0.29 mmol) was added. The flask was heated to reflux for 18 h. The mixture was then allowed to cool to room temperature and concentrated. The reaction mixture was diluted with CHCl3 (40 mL) and washed with 1 M aqueous HCl (2 x 20 mL). The organic layer was washed with saturated aqueous NaCl (20 mL), dried over MgSO4, filtered, and concentrated under reduced pressure. The residue was purified by flash chromatography (SiO2, 3:1, hexanes:EtOAc, Rf = 0.26) to afford the desired product

(0.33 g, 34% over two steps) as a white waxy solid 1H NMR (400 MHz, CDCl3) δ 7.60 – 7.48 (m, 4H), 7.45 – 7.36 (m, 2H), 7.34 – 7.27 (m, 1H), 6.97 – 6.93 (m, 2H), 6.29 (t, J = 1.8 Hz, 2H), 3.99 (t, J = 6.3 Hz, 2H), 3.54 – 3.48 (m, 2H), 3.30 – 3.26 (m, 2H), 2.68 (d, J = 1.3 Hz, 2H), 1.88 – 1.78 (m, 2H), 1.71 – 1.61 (m, 2H), 1.56 – 1.45 (m, 3H), 1.26 – 1.22 (m, 1H). 13C NMR (126 MHz, CDCl3) δ 178.24, 158.62, 140.94, 137.94, 133.70, 128.82, 128.23, 126.82, 126.72, 114.80, 67.64, 47.93, 45.27, 42.87, 38.67, 28.90, 27.65, 23.66. HRMS (ESI) calcd for [C26H27NO3Na]+: 424.1883, found: 424.1884 [M + Na]+

N-(4-nonyloxy-biphenyl)-*cis*-5-norbornene-*exo*-dicarboximide (7). To a solution of **S8** (0.58 g, 1.72 mmol) in 4:1 THF:MeOH (20 mL) was added 10% Pd/C (5 mol% of S7). The flask was evacuated and backfilled with H2 (3 x) using a hydrogen balloon and the reaction was stirred at rt for 4 h. The reaction mixture was filtered through celite and washed using EtOAc. The filtrate was concentrated to give a white solid that was used in the next step without purification. A round-bottom flask was charged with the hydrogenated **S8** product (0.44 g, 1.4 mmol), and cis-5-norbornene-exo-2,3-dicarboxylic anhydride (0.19 g, 1.1 mmol). To the solid mixture was added toluene (40 mL). Et3N (20 μL, 0.14 mmol) was added. The flask was heated to reflux for 4 h. The mixture was then allowed to cool to room temperature and concentrated. The reaction mixture was diluted with CHCl3 (40 mL) and washed with 1 M aqueous HCl (2 x 20 mL). The organic layer was washed with saturated aqueous NaCl (20 mL), dried over MgSO4, filtered, and concentrated under reduced pressure. The residue was purified by flash chromatography (SiO2, 5:1 hexanes:EtOAc, Rf = 0.21) to afford the desired product (0.21 g, 39% over two steps) as a white crystalline solid: 1H NMR (400 MHz, CDCl3) δ 7.60 – 7.47 (m, 4H), 7.45 – 7.36 (m, 2H), 7.33 – 7.27 (m, 1H), 7.00 – 6.91 (m, 2H), 6.24 – 6.31 (m, 2H), 3.99 (t, J = 6.6 Hz, 2H), 3.46 (t, J = 7.6 Hz, 2H), 3.31 – 3.23 (m, 2H), 2.71 – 2.63 (m, 2H), 1.86 – 1.73 (m, 2H), 1.61 – 1.40 (m, 4H), 1.39 – 1.17 (m, 10H). 13C NMR (126 MHz, CDCl3) δ 178.28, 158.79, 140.99, 137.95, 133.61, 128.83, 128.23, 126.84, 126.71, 114.85, 68.14, 47.93, 45.29, 42.85, 38.87, 29.51, 29.42, 29.40, 29.21, 27.90, 27.07, 26.14. HRMS (ESI) calcd for [C30H35NO3Na]+: 480.2509, found: 480.2507 [M + Na]+

3 (39 %)
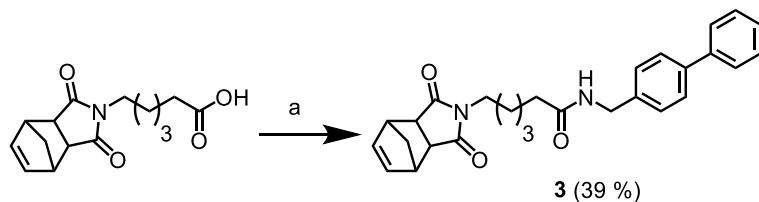
(a) 4-phenylbenzylamine, EDC, HOBt, DMF, 0 °C to rt.

Scheme 3 Synthesis of norbornene monomer **3**
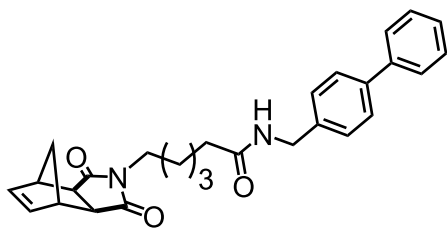
N-(4-phenylbenzyl-4-hexanamide)-*cis*-5-norbornene-*exo*-dicarboximide (3). To a solution of *N*-(hexanoic acid)-cis-5-norbornene-exo-dicarboximide (1.0 g, 3.61 mmol), EDC (0.84 g, 5.41 mmol), HOBt (0.73 g, 5.41 mmol) in DMF (30 mL) at 0 °C was added 4-phenylbenzylamine (0.99 g, 5.41 mmol). The ice bath was removed and the reaction mixture was stirred at room temperature overnight. DMF was removed in vacuo and the residue was diluted with CHCl3 (40 mL) and washed with 1 M aqueous HCl (2 x 20 mL). The organic layer was washed with saturated aqueous NaCl (20 mL), dried over MgSO4, filtered, and concentrated under reduced pressure. The residue was purified by flash chromatography (SiO2, 2:1 EtOAc:hexanes, Rf = 0.33) to afford the desired product (0.62 g, 39%) as a white waxy solid: 1H NMR (400 MHz, CDCl3) δ 7.62 – 7.50 (m, 4H), 7.48 – 7.39 (m, 2H), 7.39 – 7.30 (m, 3H), 6.26 (t, J = 1.9 Hz, 2H), 5.82 (t, J = 5.7 Hz, 1H), 4.48 (d, J = 5.7 Hz, 2H), 3.46 (t, J = 7.4 Hz, 2H), 3.27 – 3.23 (m, 2H), 2.64 (d, J = 1.6 Hz, 2H), 2.23 (t, J = 7.5 Hz 2H), 1.77 – 1.63 (m, 2H), 1.63 – 1.53 (m, 2H), 1.53 – 1.46 (m, 1H), 1.42 – 1.29 (m, 2H), 1.20 (dt, J = 9.9, 1.6 Hz, 1H). 13C NMR (126 MHz, CDCl3) δ 178.18, 172.67, 140.69, 140.44, 137.84, 137.51, 128.86, 128.32, 127.46, 127.42, 127.10, 47.84, 45.19, 43.29, 42.80, 38.44, 36.44, 27.53, 26.59, 25.17. HRMS (ESI) calcd for [C28H30N2O3Na]+: 465.2149, found: 465.2146 [M + Na]+
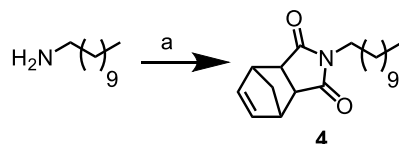
(a) *cis*-5-Norbornene-*exo*-2,3-dicarboxylic anhydride, TEA, Toluene, 110 °C.

Scheme 4 Synthesis of norbornene monomer **4**
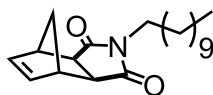
N-(undecyl)-*cis*-5-norbornene-*exo*-dicarboximide (4). A round-bottom flask was charged with undecan-1-amine (0.47 g, 2.74 mmol), and cis-5-norbornene-exo-2,3-

dicarboxylic anhydride (0.3 g, 1.83 mmol). To the solid mixture was added toluene (20 mL). Et3N (31 µL, 0.22 mmol) was added. The flask was heated to reflux overnight. The mixture was then allowed to cool to room temperature and concentrated. The residue was diluted with CHCl3 (40 mL) and washed with 1 M aqueous HCl (2 x 20 mL). The organic layer was washed with saturated aqueous NaCl (20 mL), dried over MgSO4, filtered, and concentrated under reduced pressure. The residue was then purified by flash chromatography (SiO2, 3:1 hexanes:EtOAc, Rf = 0.49) to afford the desired product as a pale yellow oil that was used without further purification: 1H NMR (400 MHz, CDCl3) δ 6.28 (t, J = 1.8 Hz, 2H), 3.48 – 3.42 (m, 2H), 3.30 – 3.23 (m, 2H), 2.67 (d, J = 1.1 Hz, 2H), 1.64 – 1.44 (m, 4H), 1.33 – 1.19 (m, 16H), 0.93 – 0.81 (m, 3H). HRMS (ESI) calcd for [C20H32NO2]+: 318.2428, found: 318.2429 [M + H]+
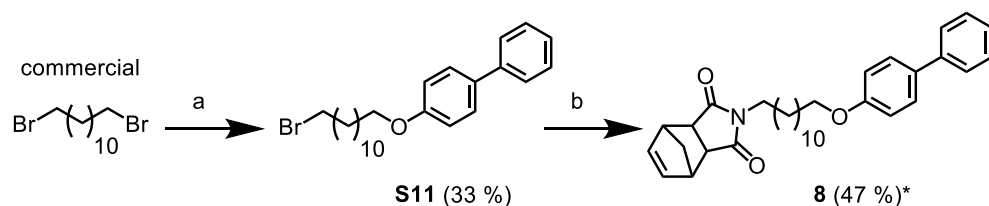
(a) 4-phenylphenol, K_2CO_3, Acetone, 56 °C. (b) i) NH_3 (g), MeOH, 0 °C to 65 °C;
ii) *cis*-5-Norbornene-*exo*-2,3-dicarboxylic anhydride, TEA, Toluene, 110 °C.
*denotes over two steps.

Scheme 5 Synthesis of norbornene monomer **8**
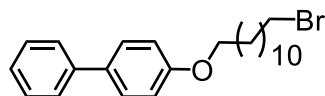
4-((12-bromododecyl)oxy)-biphenyl (S11). A round-bottom flask was charged with 1,12-dibromododecane (2.0 g, 6.10 mmol), 4-phenylphenol (1.24 g, 7.31 mmol), and K2CO3 (4.21 g, 30.5 mmol). To the solid mixture was added acetone (100 mL) and the flask was heated to reflux for 18 h. The mixture was then allowed to cool to room temperature and concentrated. The residue was diluted with CH2Cl2 (50 mL) and washed with water (3 x 30 mL). The organic layer was dried over MgSO4, filtered, and concentrated under reduced pressure. The crude solid was recrystallized using DCM to afford the desired product (0.84 g, 33%) as a silvery white solid: 1H NMR (400 MHz, CD2Cl2) δ 7.60 – 7.49 (m, 4H), 7.46 – 7.37 (m, 2H), 7.33 – 7.26 (m, 1H), 7.01 – 6.91 (m, 2H), 3.99 (t, J = 6.6 Hz, 2H), 3.42 (t, J = 6.8 Hz, 2H), 1.92 – 1.72 (m, 4H), 1.52 – 1.24 (m, 16H). ESI-MS calcd: 416.17, found: 417.18 [M + H]+; 13C NMR (126 MHz, CDCl3) δ 158.80, 140.98, 133.62, 128.84, 128.23, 126.83, 126.73, 114.85, 68.18, 34.31, 32.97, 29.70, 29.68, 29.67, 29.58, 29.54, 29.42, 28.91, 28.32, 26.20.
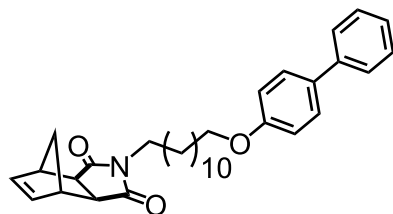
N-(4-dodecyloxy-biphenyl)-*cis*-5-norbornene-*exo*-dicarboximide (8). A pressure vial containing a solution of **S11** (0.30 g, 0.719 mmol) in MeOH (4 mL) at 0 °C was sparged with NH3 gas for 5 min. The vial was removed from the ice bath, capped, and heated to reflux for 17 h. The vial was allowed to cool to room temperature and opened at 0 °C. The reaction mixture was dried in vacuo and was used in the next step without purification. A round-bottom flask was charged with the hydrogenated S11 product (0.25 g, 0.72 mmol), and cis-5-norbornene-exo-2,3-dicarboxylic anhydride (0.098 g, 0.59 mmol). To the solid mixture was added toluene (20 mL). Et3N (12 μL, 0.086 mmol) was added. The flask was heated to reflux for 18 h. The mixture was then allowed to cool to room temperature and concentrated. The reaction mixture was diluted with CHCl3 (20 mL) and washed with 1 M aqueous HCl (2 x 15 mL). The organic layer was washed with saturated aqueous NaCl (15 mL), dried over MgSO4, filtered, and concentrated under reduced pressure. The residue was purified by flash chromatography (SiO2, 3:1 hexanes:EtOAc, Rf = 0.37) to afford the desired product (0.17 g, 47% over two steps) as a white solid: 1H NMR (400 MHz, CDCl3) δ 7.58 – 7.48 (m, 4H), 7.41 (t, J = 7.7 Hz, 2H), 7.33 – 7.27 (m, 1H), 7.01 – 6.92 (m, 2H), 6.28 (t, J = 1.9 Hz, 2H), 3.99 (t, J = 6.6 Hz, 2H), 3.51 – 3.39 (m, 2H), 3.30 – 3.24 (m, 2H), 2.67 (m, 2H), 1.87 – 1.74 (m, 2H), 1.62 – 1.41 (m, 4H), 1.40 – 1.19 (m, 16H). 13C NMR (126 MHz, CDCl3) δ 178.28, 158.81, 140.99, 137.95, 133.59, 128.82, 128.22, 126.83, 126.71, 114.85, 68.18, 47.92, 45.28, 42.85, 38.90, 29.86, 29.70, 29.67, 29.58, 29.54, 29.42, 29.28, 27.92, 27.10, 26.19. HRMS (ESI) calcd for [C33H41NO3Na]+: 522.2979, found: 522.2978 [M + Na]+
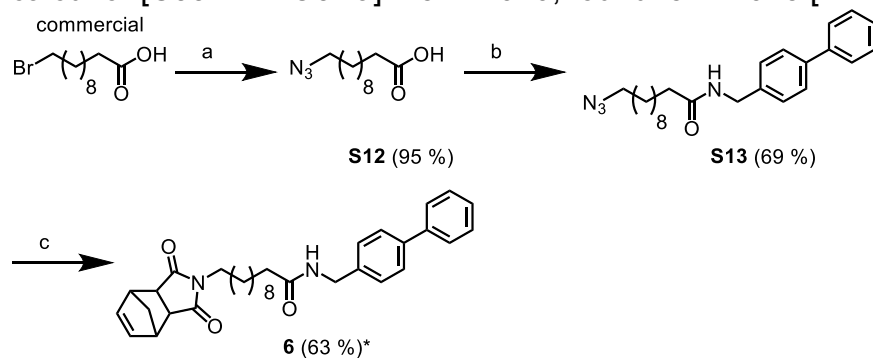
(a) NaN$_3$, DMSO, rt. (b) 4-phenylbenzylamine, EDC, HOBt, DCM, 0 $^{\circ}$C to rt. (c) i) 10 % Pd/C, H$_2$, 4:1 THF/MeOH, rt; ii) cis-5-norbornene-exo-2,3-dicarboxylic anhydride, TEA, Toluene, 110 $^{\circ}$C. *denotes over two steps.

Scheme 6 Synthesis of norbornene monomer **6**
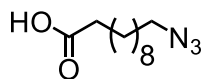
11-azidoundecanoic acid (S12). A round-bottom flask was charged with 11-Bromoundecanoic acid (1.0 g, 3.77 mmol), and sodium azide (0.49 g, 7.54 mmol). To the solid mixture was added DMSO (35 mL) and the solution was stirred overnight at room temperature. The reaction was diluted with water (75 mL) and was allowed to cool. The aqueous phase was then extracted with ether (3 x 100 mL) and the combined organic phase was washed with acidified brine at pH 2 (1 x 100 mL), dried over MgSO4, filtered, and concentrated under reduced pressure. The residue was purified by flash chromatography (SiO2, 1:1 hexanes:Et2O, Rf = 0.34) to afford the desired product (0.80 g, 95%) as a white, waxy solid. The analytical data of S12 were in agreement with those reported previously.[19]
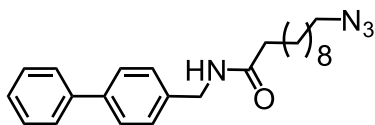
_N_-(4-phenylbenzyl)-11-azidoundecanamide (S13). To a solution of **S12** (0.70 g, 3.08 mmol), EDC (0.59 g, 3.08 mmol), HOBt (0.47 g, 3.08 mmol) in DCM (35 mL) at 0 °C was added 4-phenylbenzylamine (0.56 g, 3.08 mmol). The ice bath was removed and the reaction mixture was stirred at room temperature overnight. DCM was removed in vacuo and the residue was purified by flash chromatography (SiO2, DCM, Rf = 0.27) to afford the desired product (0.83 g, 69%) as a white waxy solid: 1H NMR (300 MHz, CDCl3) δ 7.62 – 7.52 (m, 4H), 7.48 – 7.40 (m, 2H), 7.39 – 7.30 (m, 3H), 5.57 (t, J = 5.9 Hz, 1H), 4.48 (d, J = 6.0 Hz, 2H), 3.24 (t, J = 6.9 Hz, 2H), 2.23 (t, J = 7.6 Hz, 2H), 1.78 – 1.50 (m, 4H), 1.45 – 1.16 (m, 12H). 13C NMR (126 MHz, CDCl3) δ 173.12, 140.76, 140.58, 137.56, 128.92, 128.40, 127.54, 127.49, 127.17, 51.57, 43.37, 36.94, 29.53, 29.48, 29.43, 29.42, 29.24, 28.94, 26.81, 25.88.
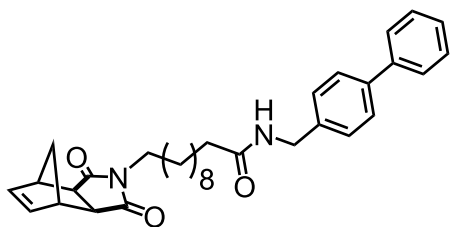
_N_-(4-phenylbenzyl-4-undecanamide)-_cis_-5-norbornene-_exo_-dicarboximide (6). To a solution of **S13** (0.57 g, 1.45 mmol) in 4:1 THF:MeOH (20 mL) was added 10% Pd/C (5 mol% of S13). The flask was evacuated and backfilled with H2 (3 x) using a hydrogen balloon and the reaction was stirred at rt for 19 h. The reaction mixture was filtered through celite and washed using EtOAc. The filtrate was concentrated to give a white solid that was used in the next step without purification. A round-bottom flask was charged with the hydrogenated **S13** product (0.38 g, 1.0 mmol), and cis-5-norbornene-exo-2,3-dicarboxylic anhydride (0.14 g, 0.86 mmol). To the solid mixture was added toluene (40 mL). Et3N (14 μL, 0.10 mmol) was added. The flask was heated to reflux for

18 h. The mixture was then allowed to cool to room temperature and concentrated. The residue was purified by flash chromatography (SiO2, 10% EtOAc in DCM, Rf = 0.34) to afford the desired product (0.28 g, 63% over two steps) as a white waxy solid: 1H NMR (400 MHz, CDCl3) δ 7.62 – 7.49 (m, 4H), 7.47 – 7.39 (m, 2H), 7.38 – 7.30 (m, 3H), 6.28 (t, J = 1.9 Hz, 2H), 5.81 (t, J = 5.9 Hz, 1H), 4.47 (dd, J = 12.3, 5.1 Hz, 2H), 3.42 (dd, J = 14.8, 7.2 Hz, 2H), 3.29 – 3.22 (m, 2H), 2.67 – 2.62 (m, 2H), 2.22 (t, J = 7.6 Hz, 2H), 1.72 – 1.61 (m, 2H), 1.57 – 1.45 (m, 2H), 1.37 – 1.16 (m, 14H). 13C NMR (126 MHz, CDCl3) δ 178.28, 173.15, 140.78, 140.59, 137.94, 137.59, 128.93, 128.42, 127.56, 127.49, 127.18, 47.91, 45.27, 43.39, 42.84, 38.85, 36.96, 29.42, 29.38, 29.35, 29.16, 27.84, 27.01, 25.88. HRMS (ESI) calcd for [C33H40N2O3Na]+: 535.2931, found: 535.2931 [M + Na]+
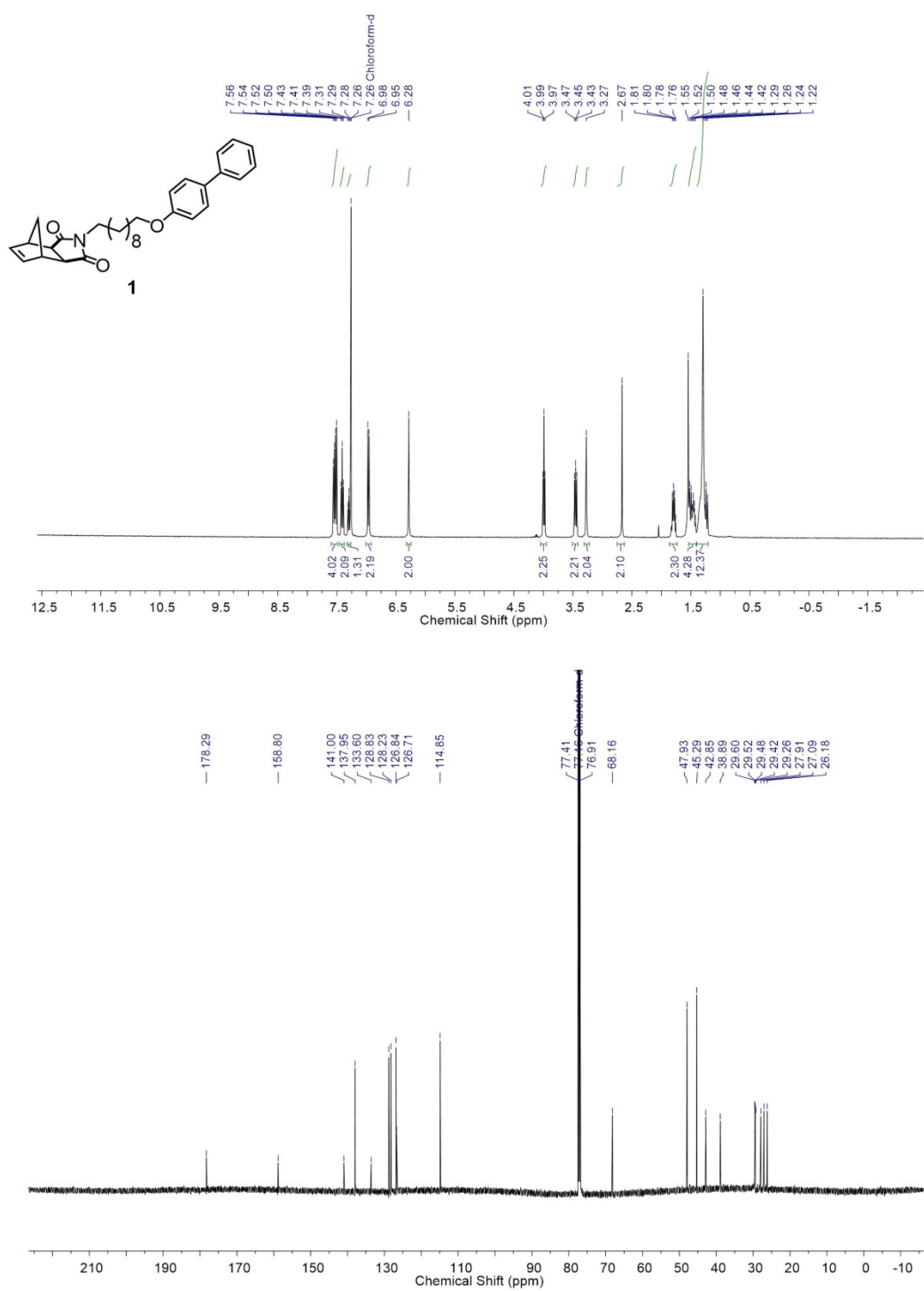
Figure 45 1H NMR and 13C NMR spectra of **1**
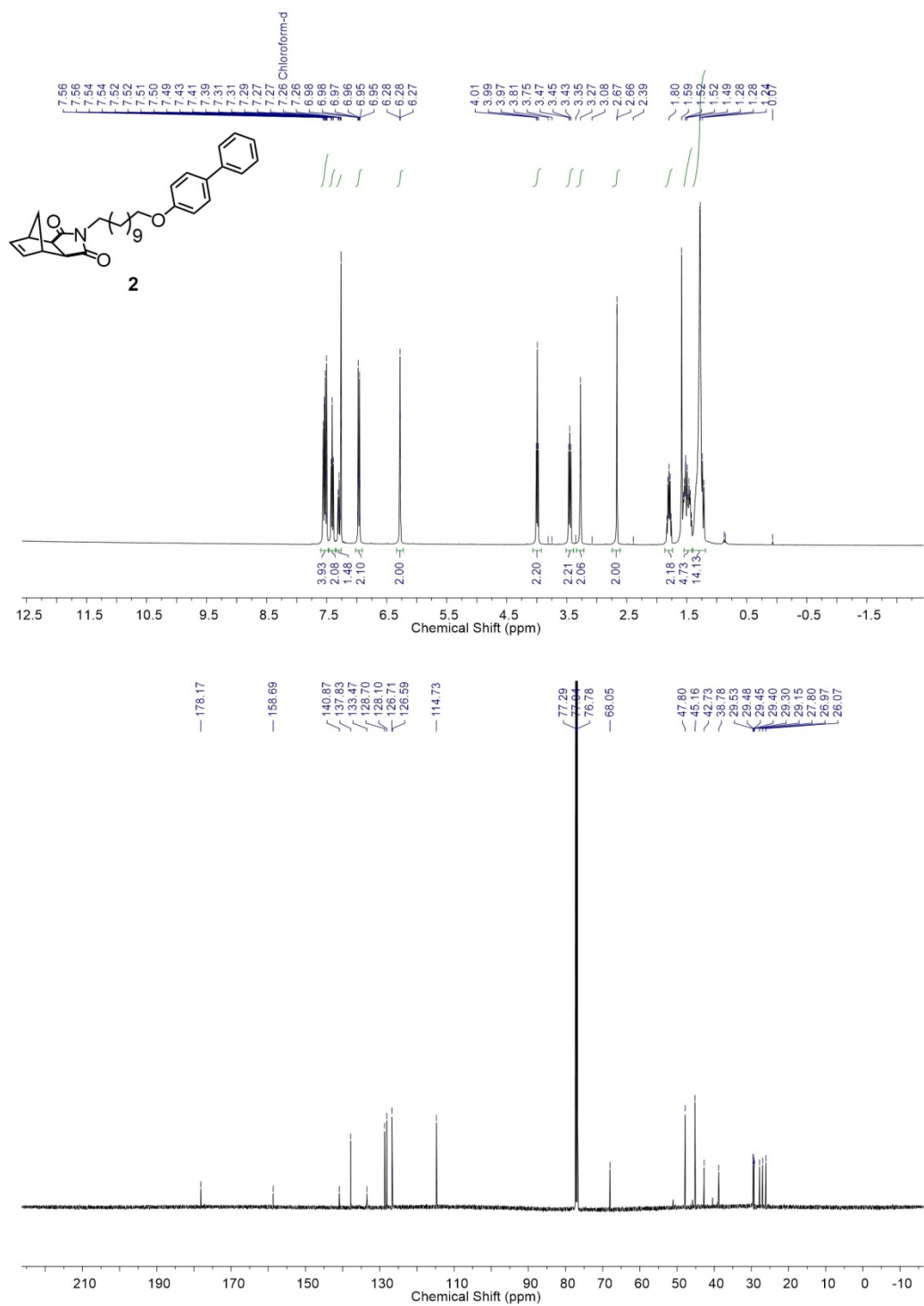
Figure 46 1H NMR and 13C NMR spectra of **2**
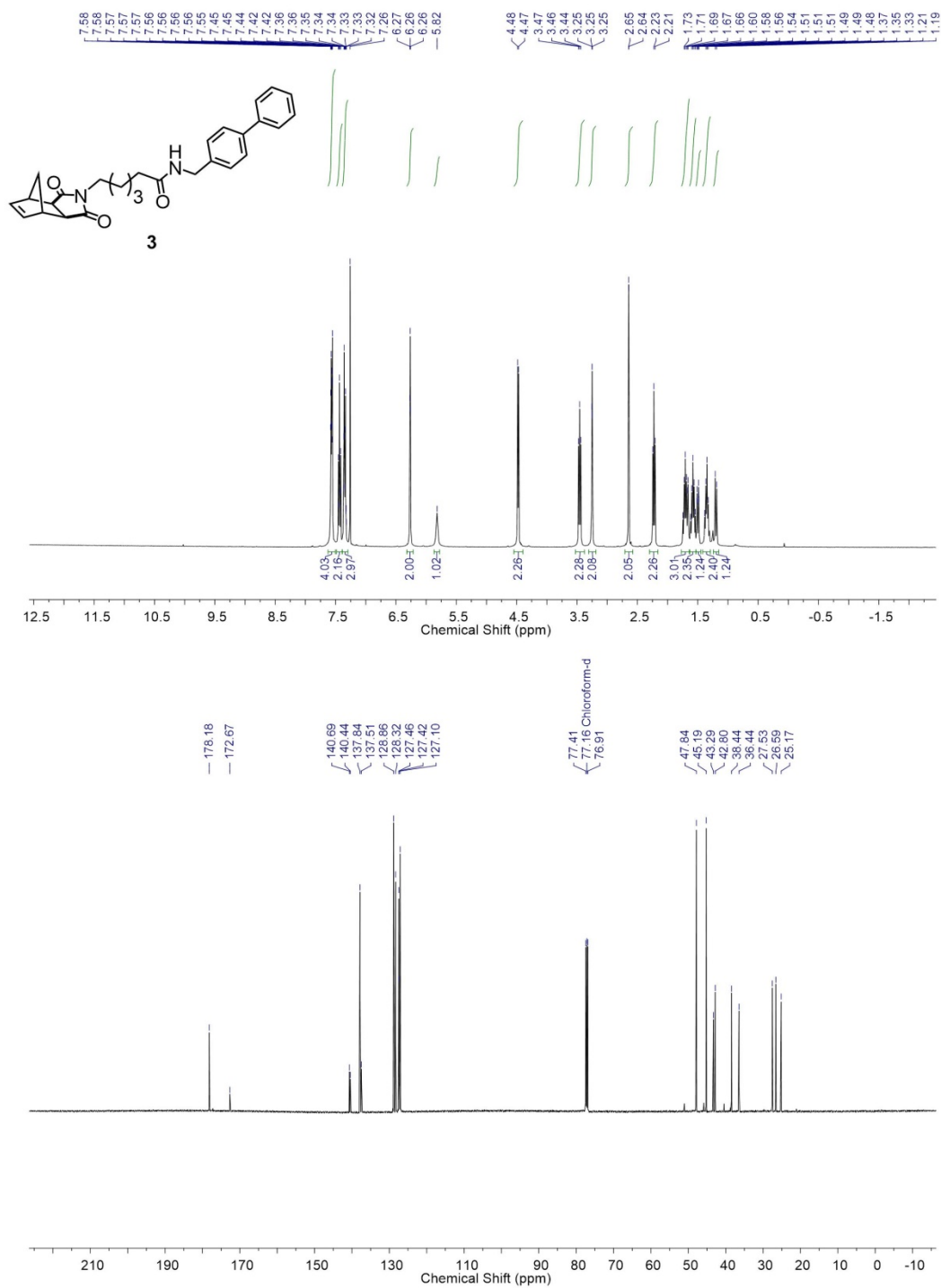
Figure 47 1H NMR and 13C NMR spectra of **3**
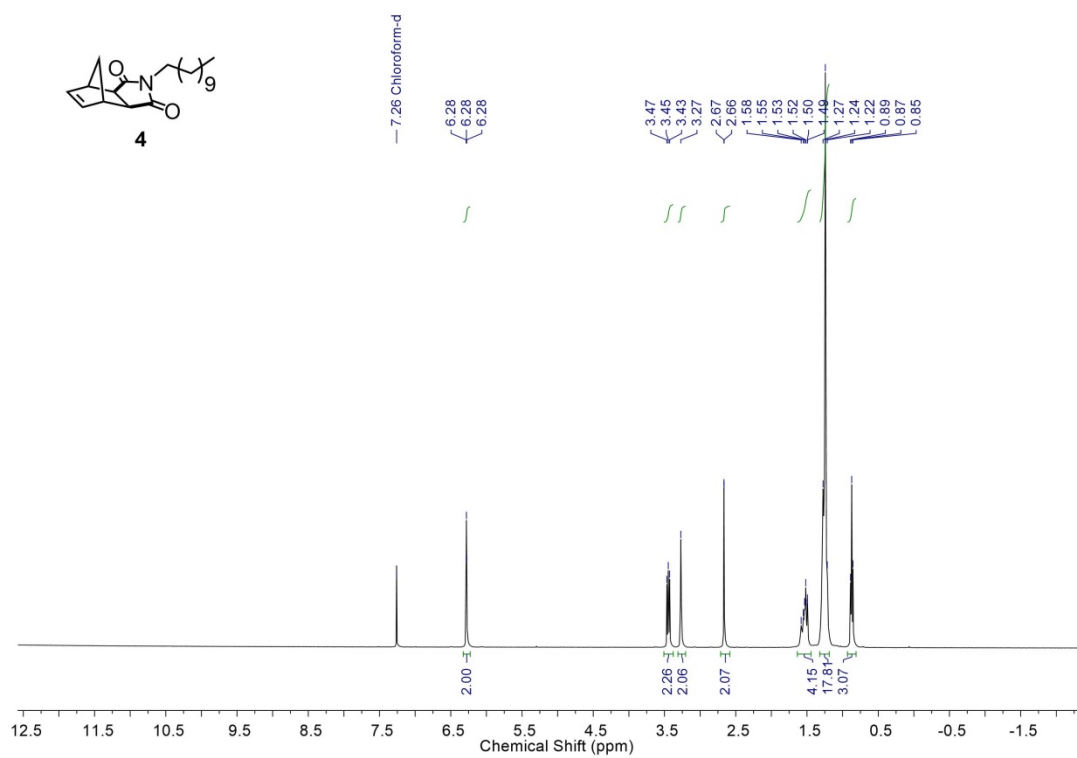
Figure 48 1H NMR spectrum of **4**

Figure 49 1H NMR and 13C NMR spectra of **5**
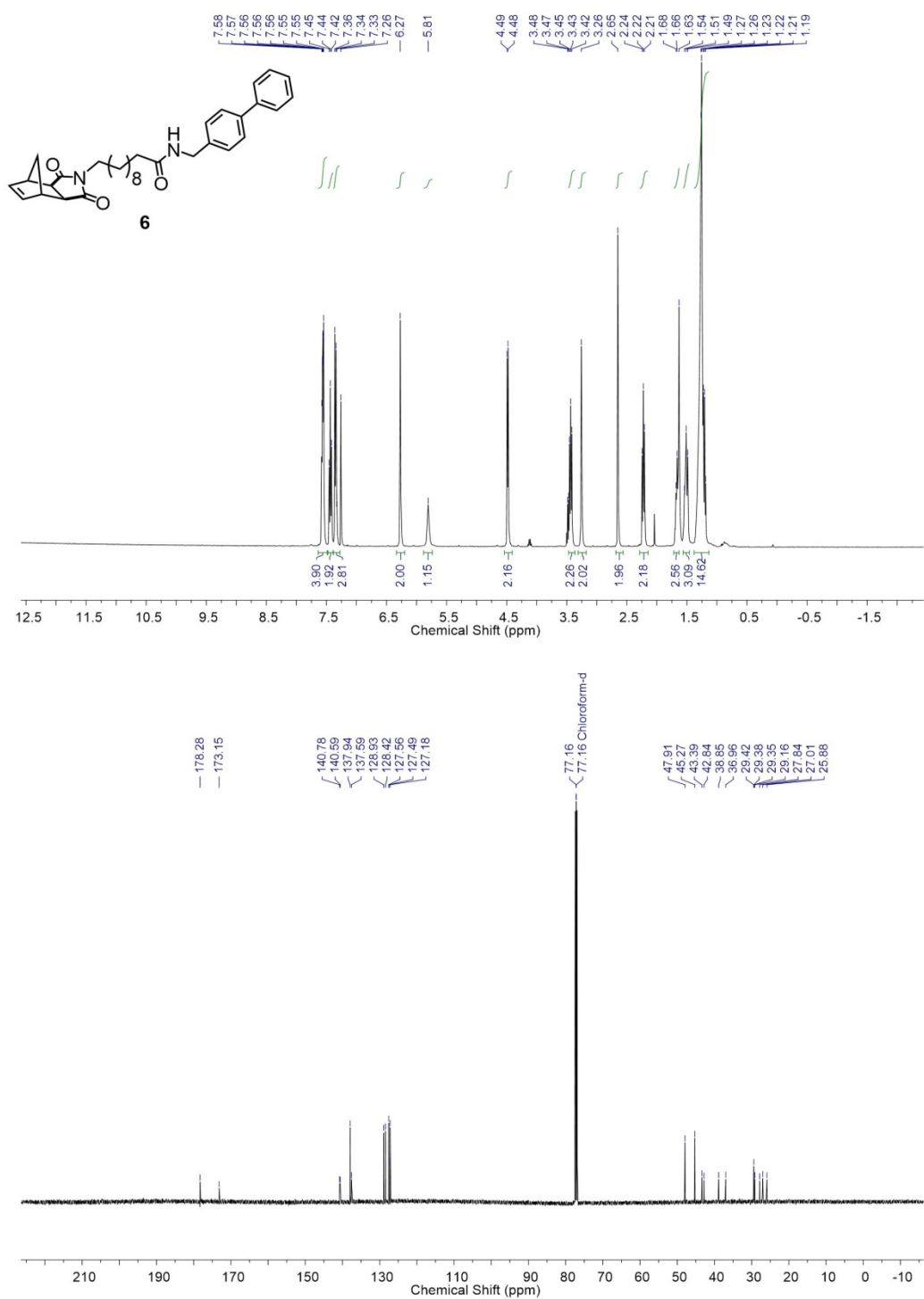
Figure 50 1H NMR and 13C NMR spectra of **6**
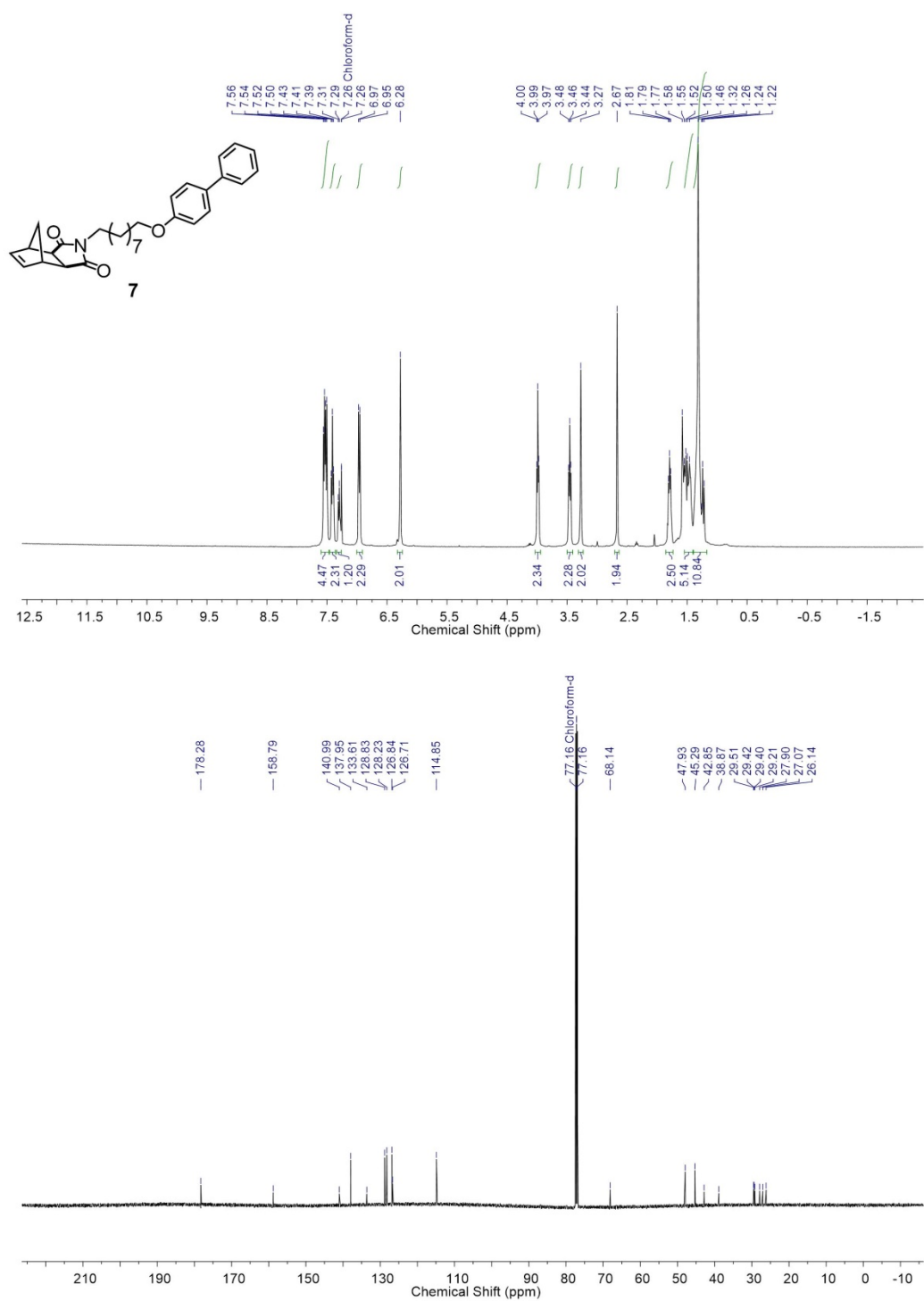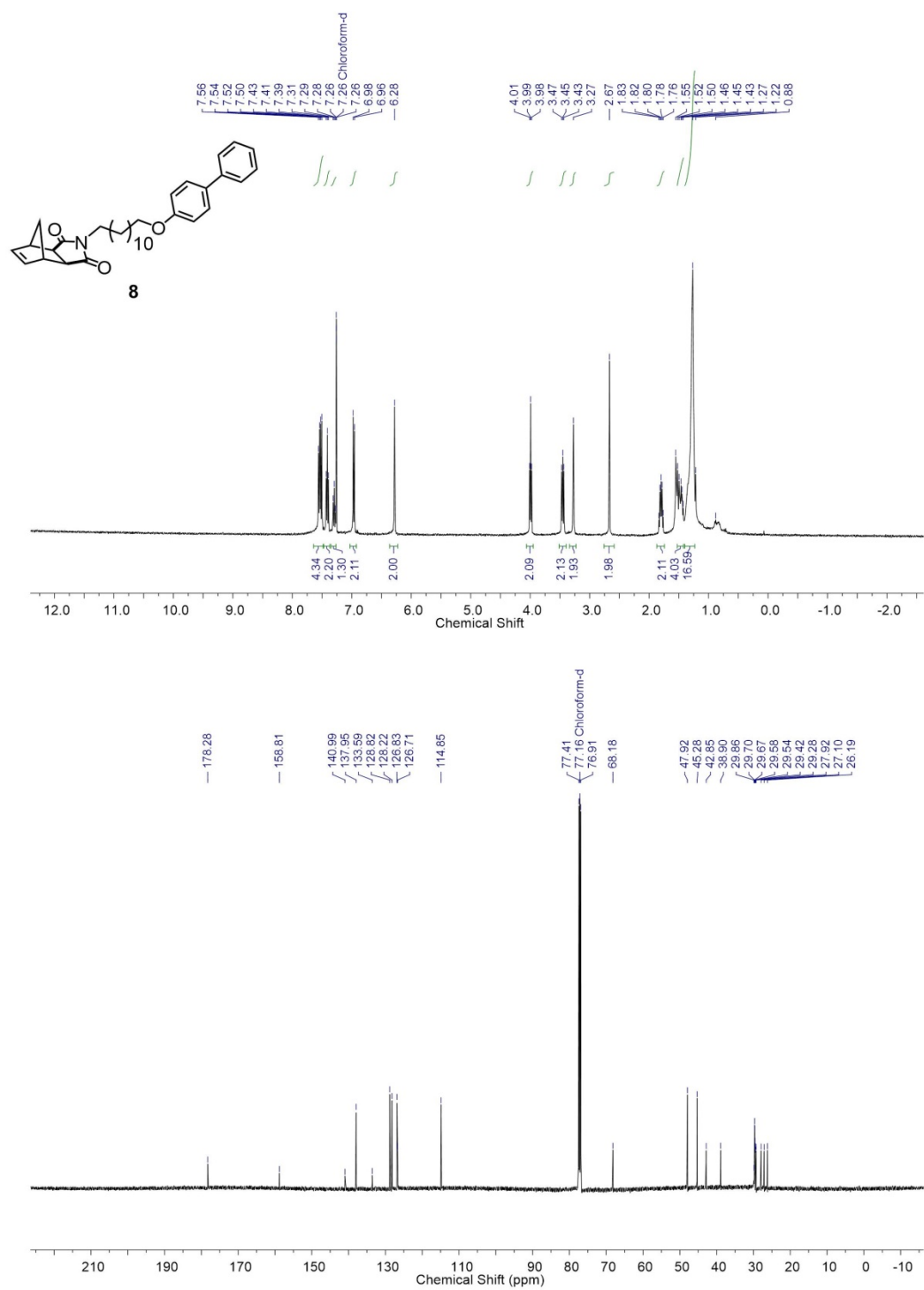
Figure 51 1H NMR and 13C NMR spectra of **7**

Figure 52 1H NMR and 13C NMR spectra of **8**
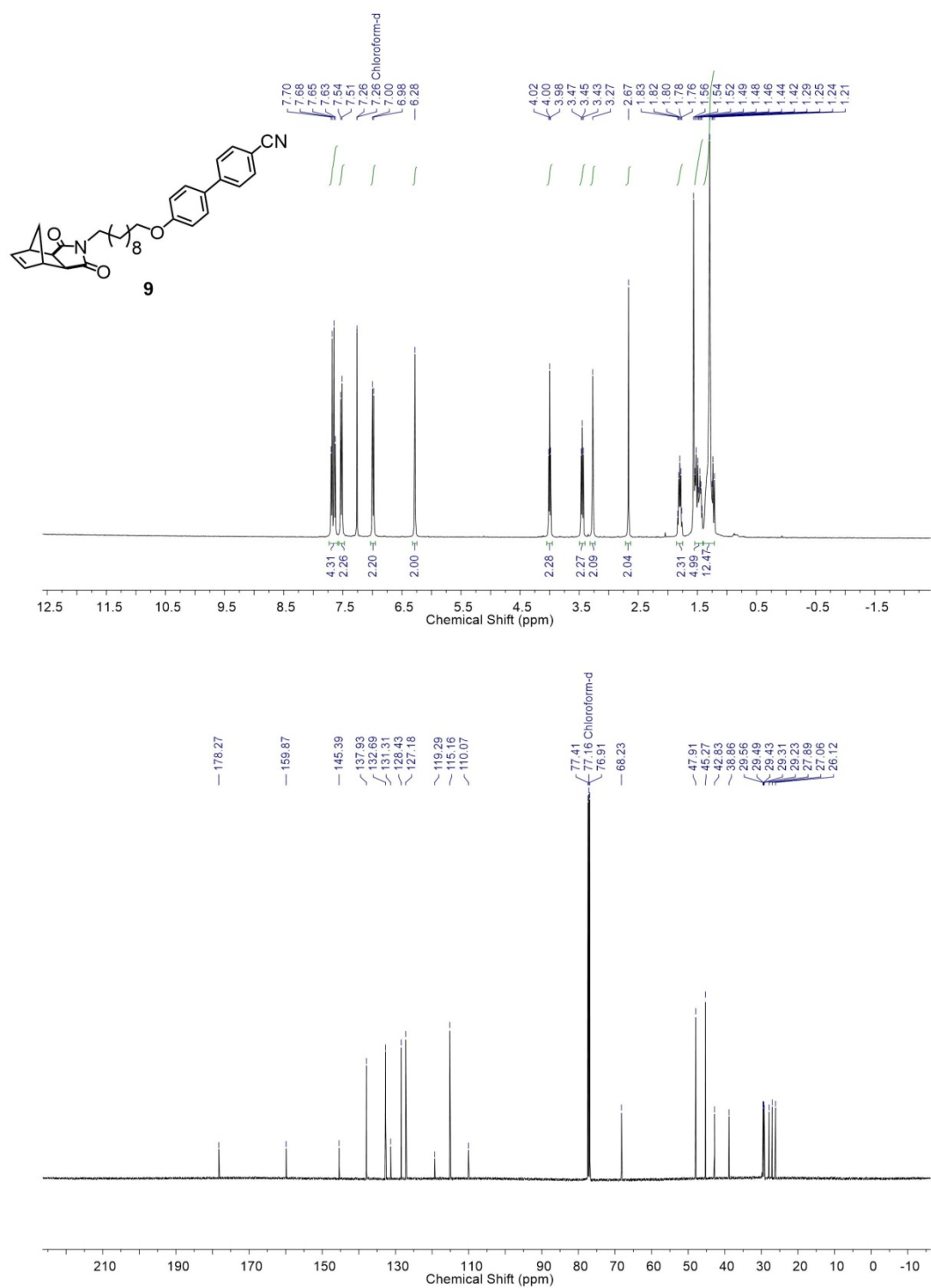
Figure 53 1H NMR and 13C NMR spectra of **9**
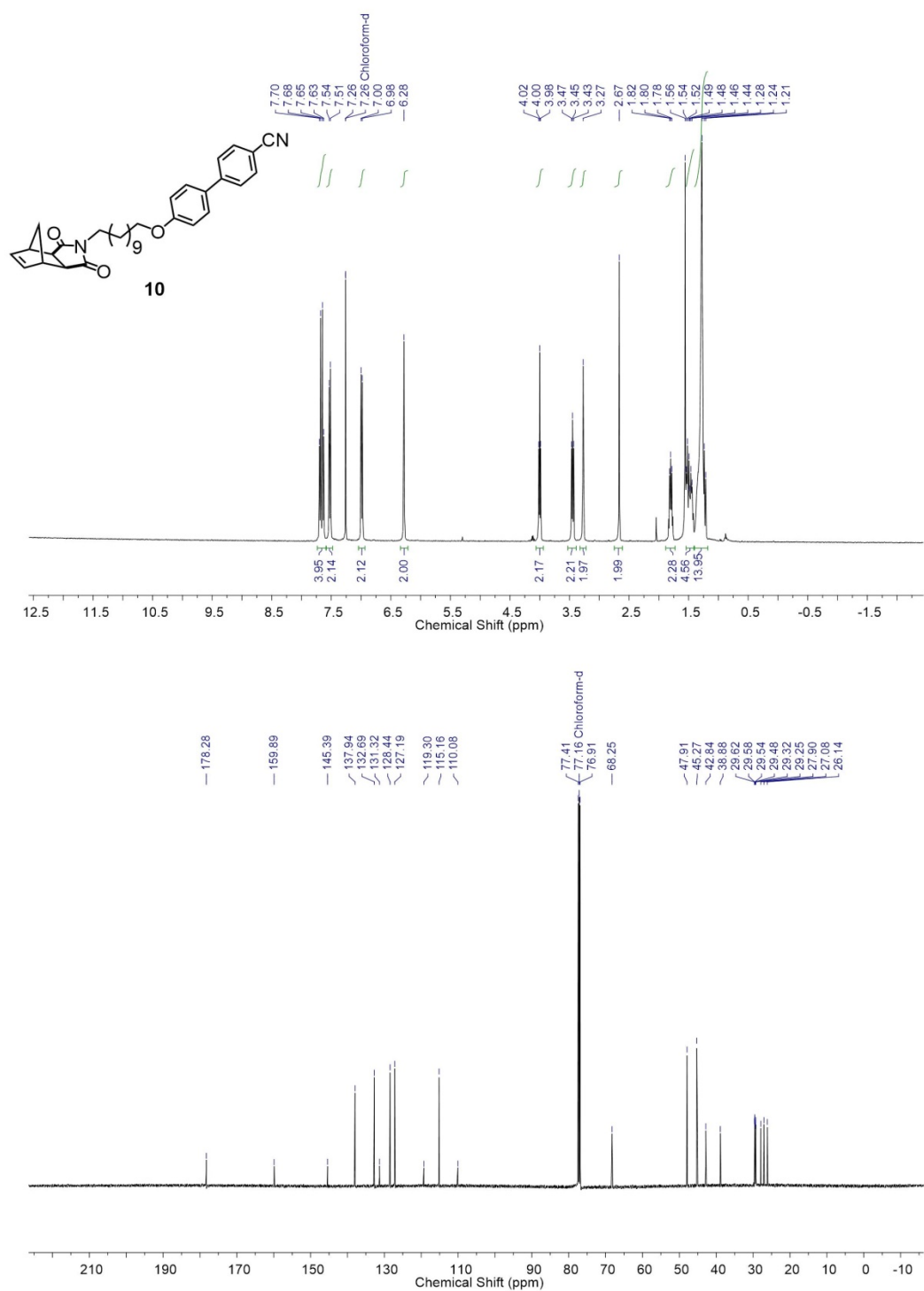
Figure 54 1H NMR and 13C NMR spectra of **10**

Br $\left(\begin{array}{c}\\\end{array}\right)_8$ N$_3$

S3
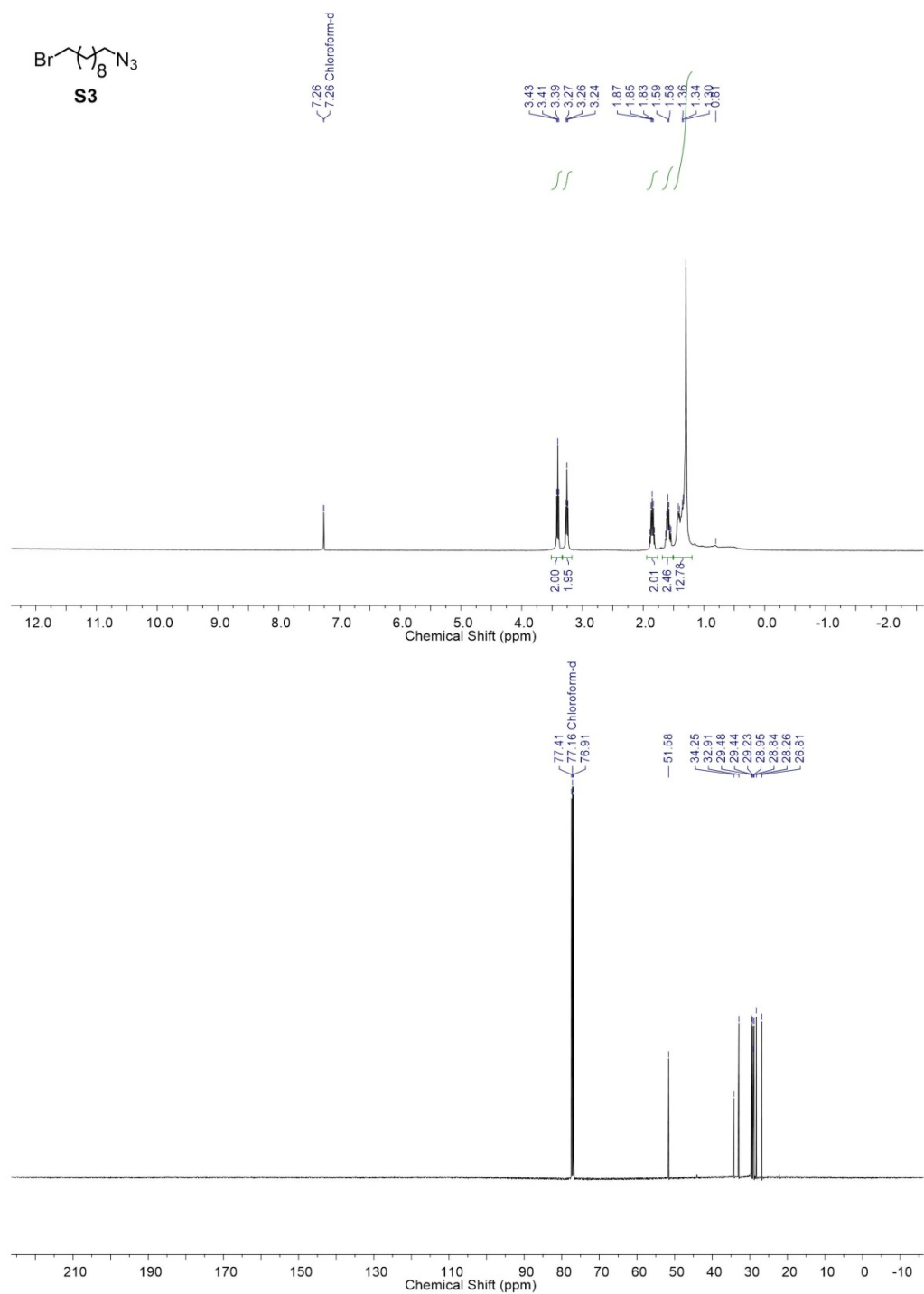
Figure 55 1H NMR and 13C NMR spectra of **S3**
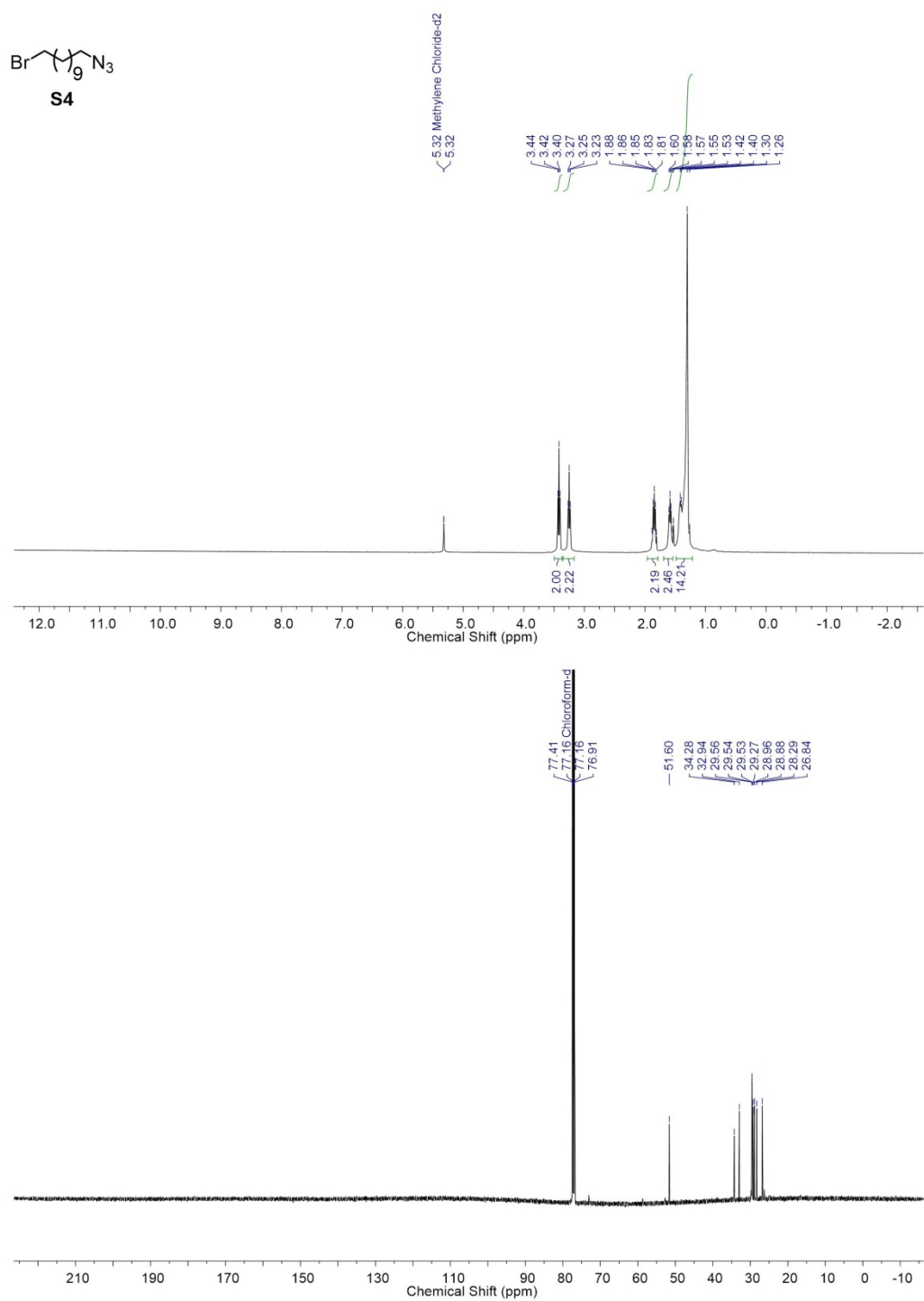
Figure 56 1H NMR and 13C NMR spectra of **S4**
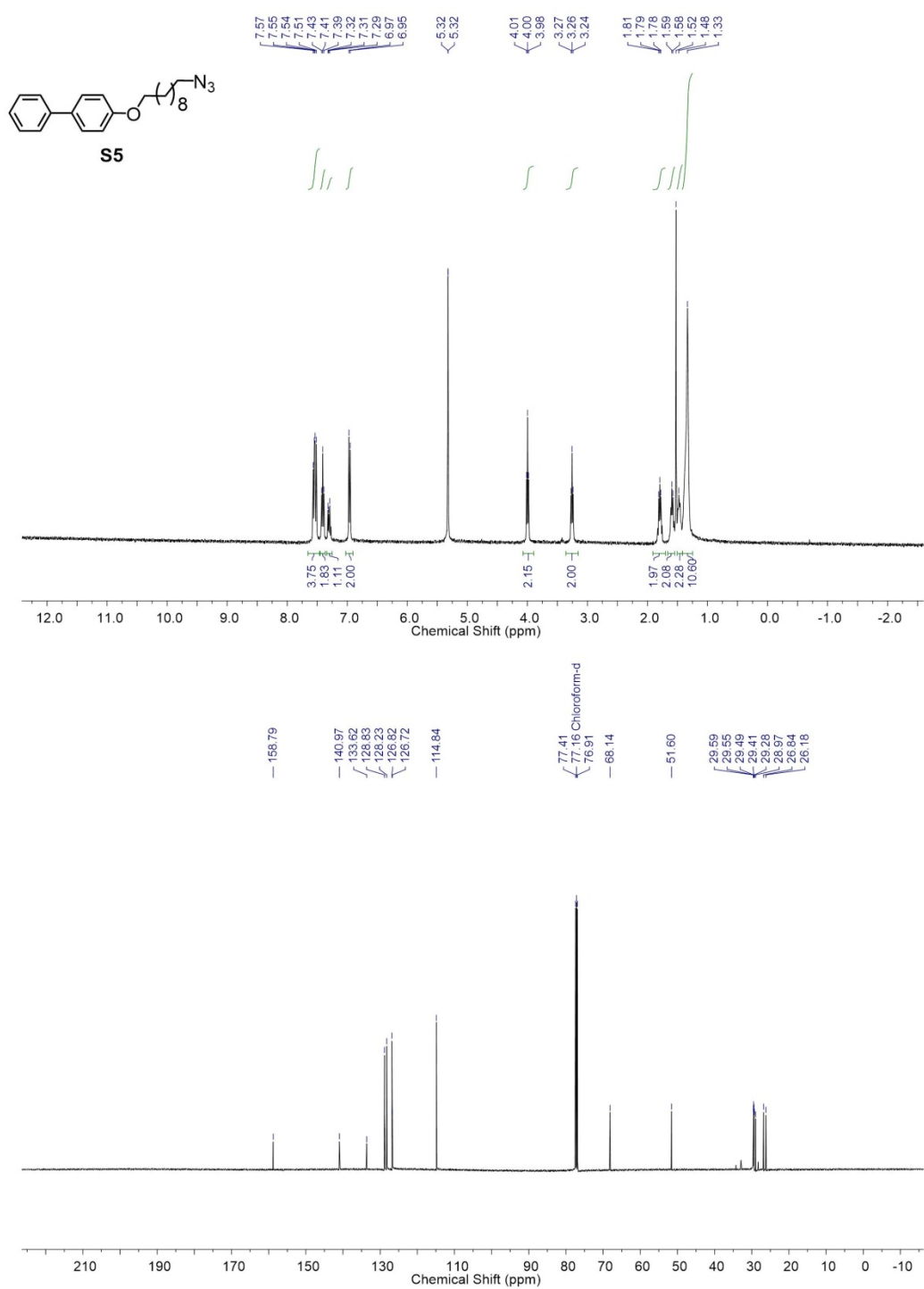
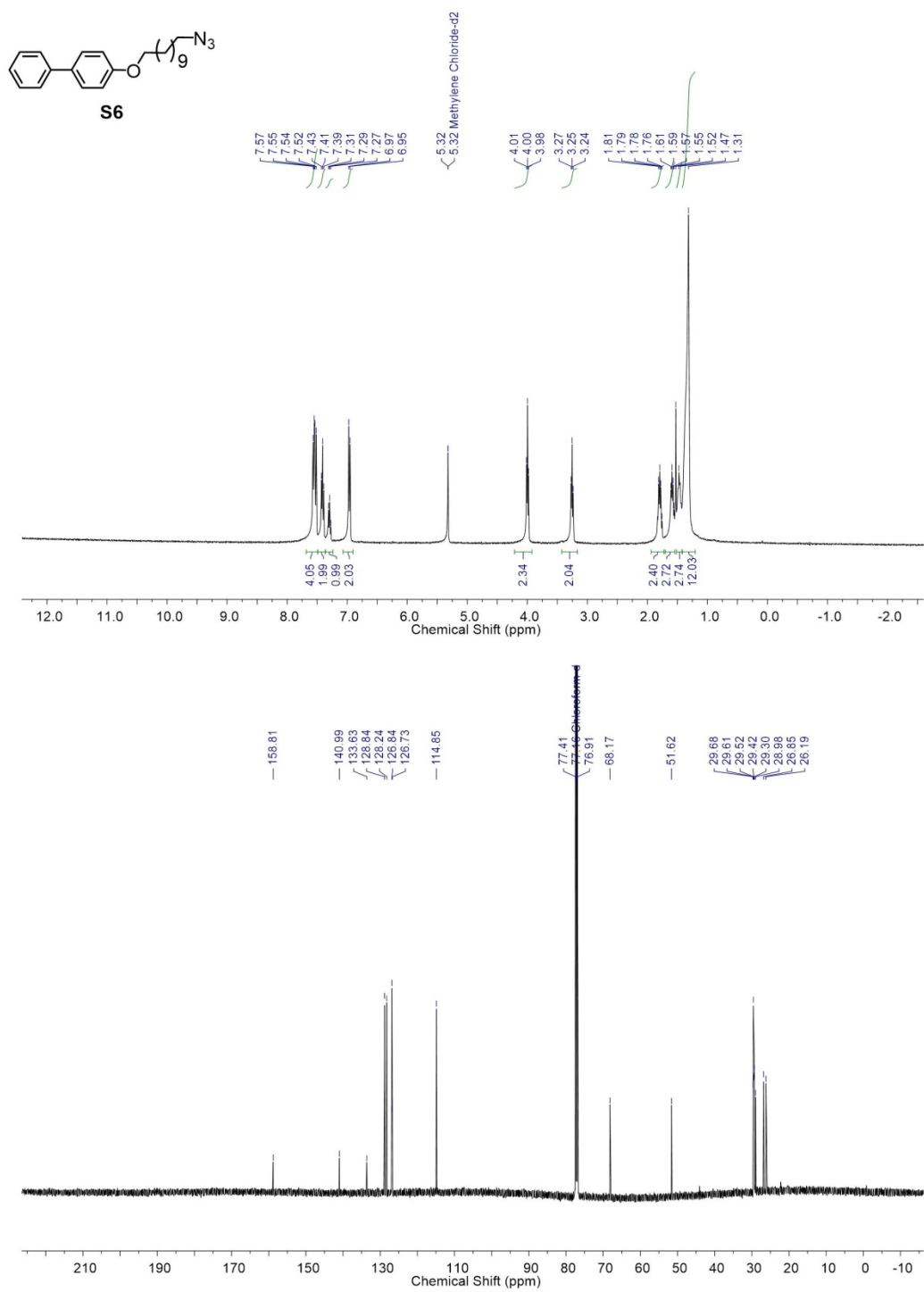**Figure 57** 1H NMR and 13C NMR spectra of **S5**

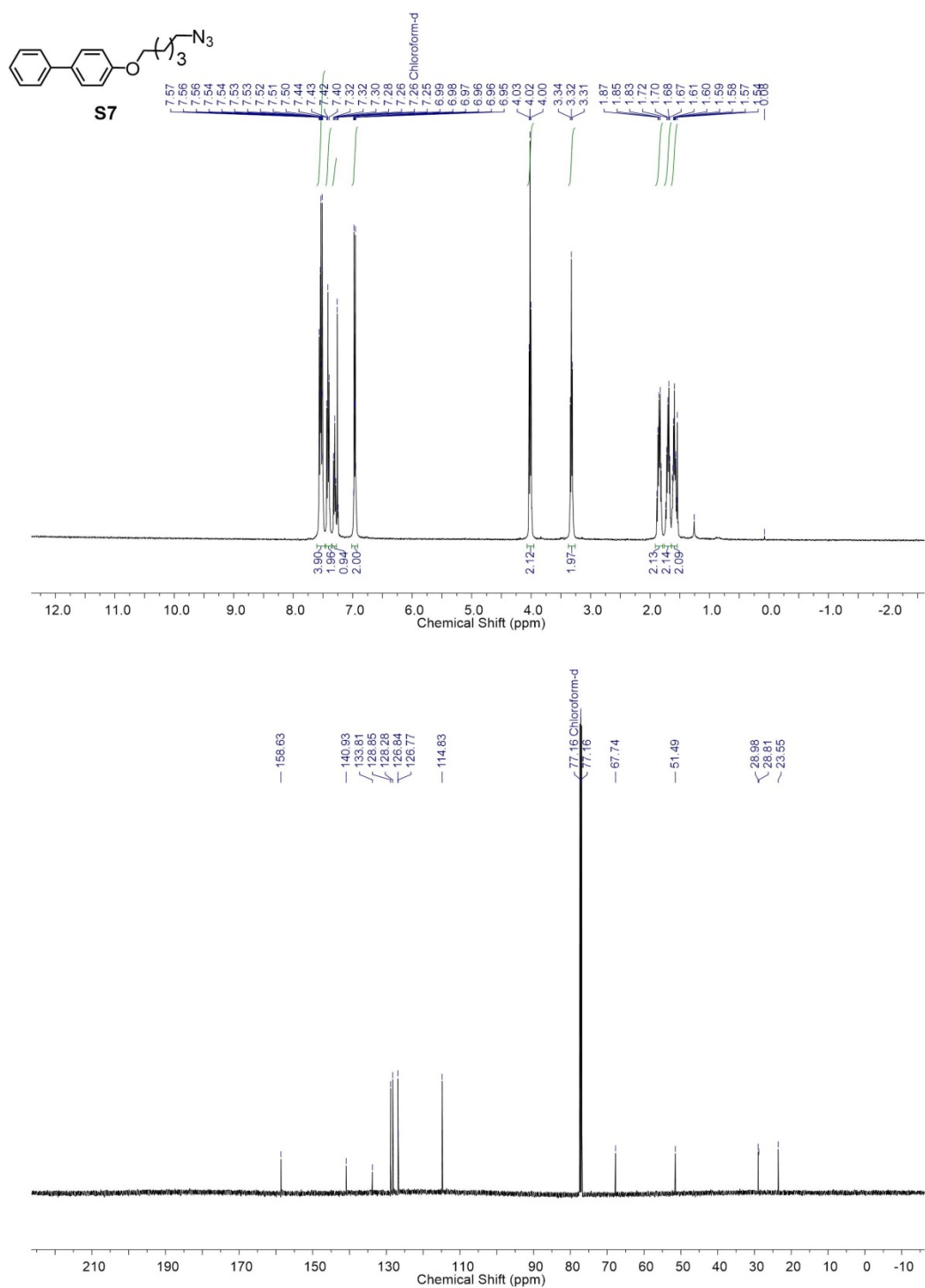**Figure 58** 1H NMR and 13C NMR spectra of **S6**

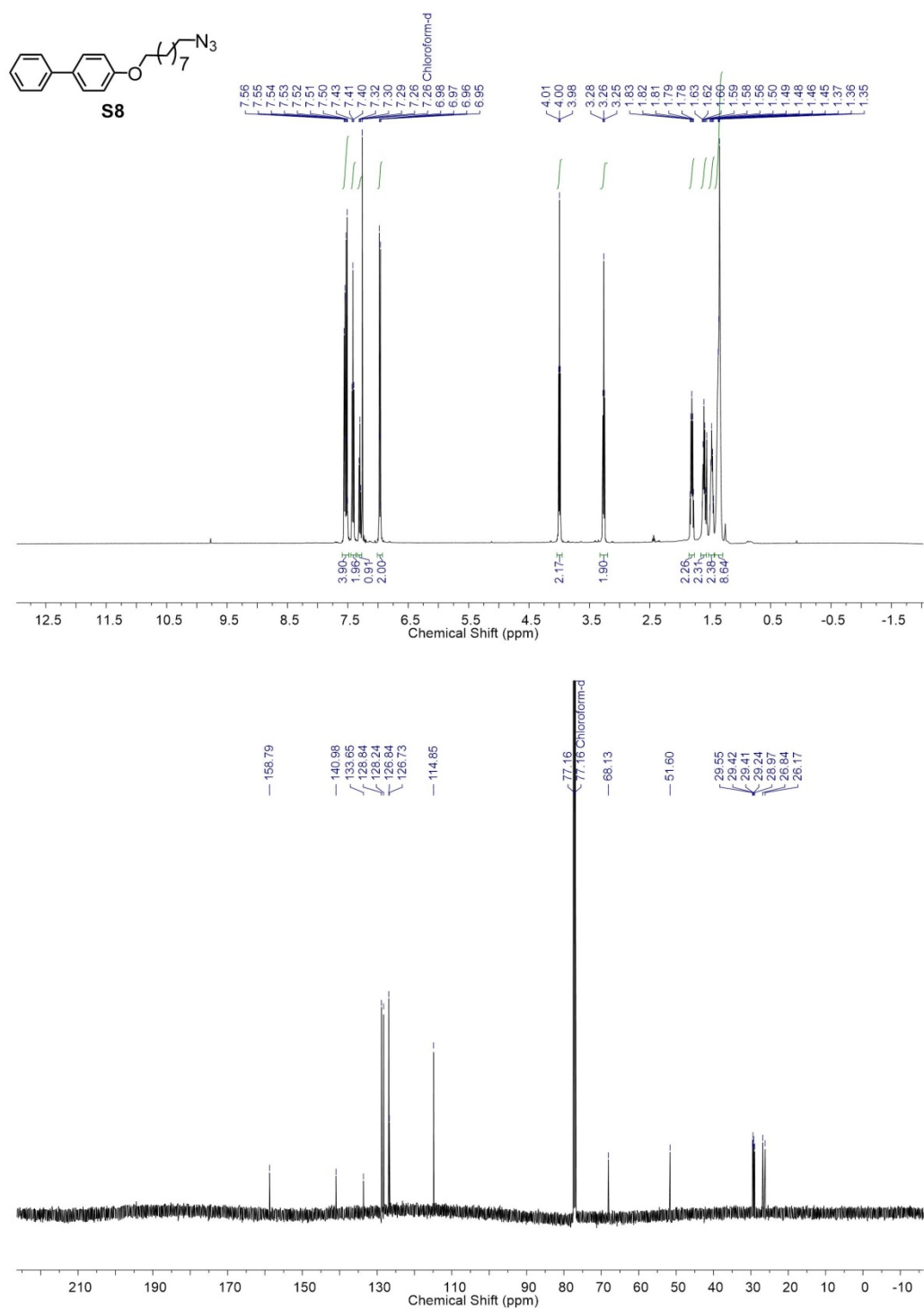**Figure 59** 1H NMR and 13C NMR spectra of **S7**

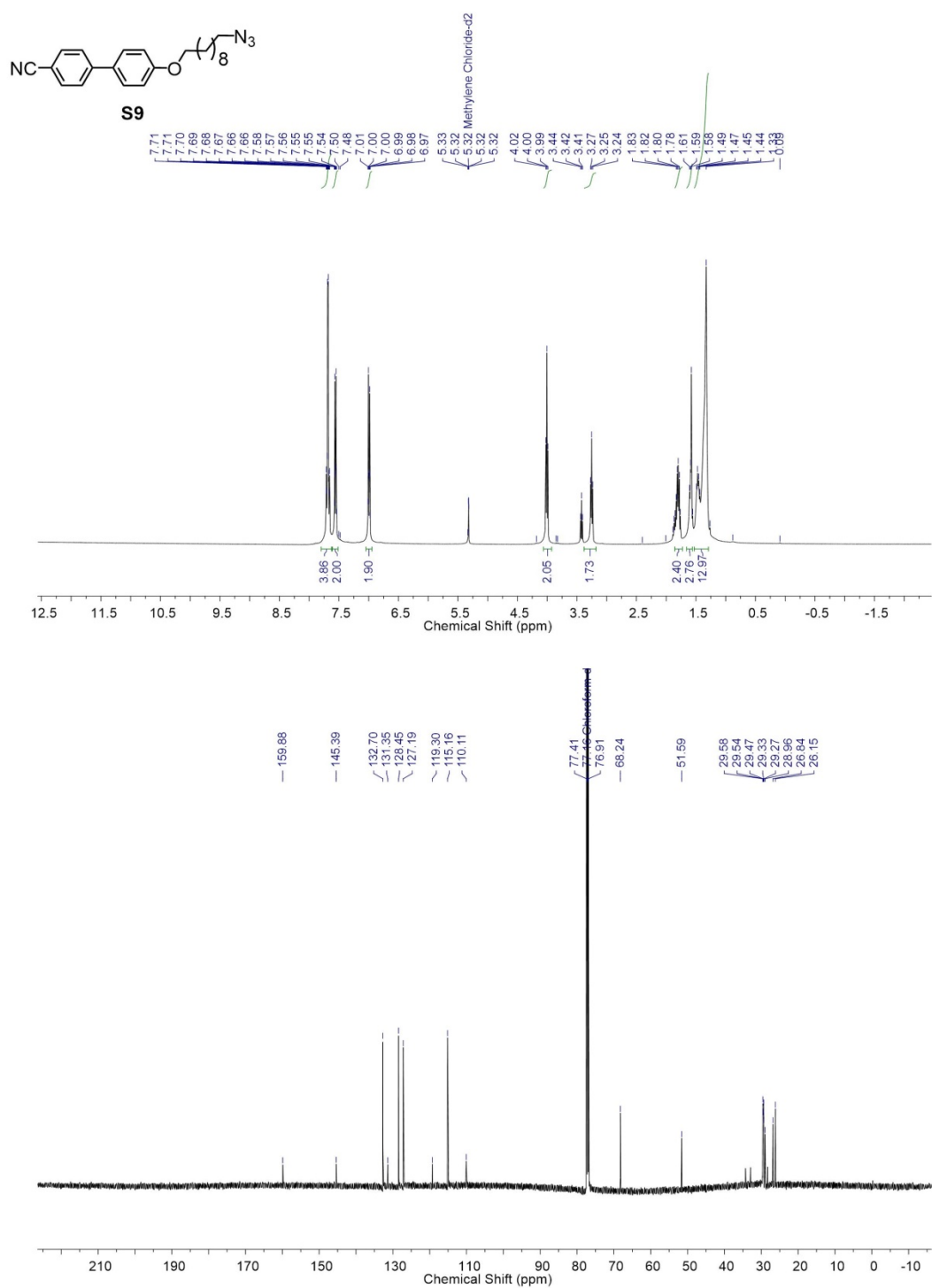**Figure 60** 1H NMR and 13C NMR spectra of **S8**

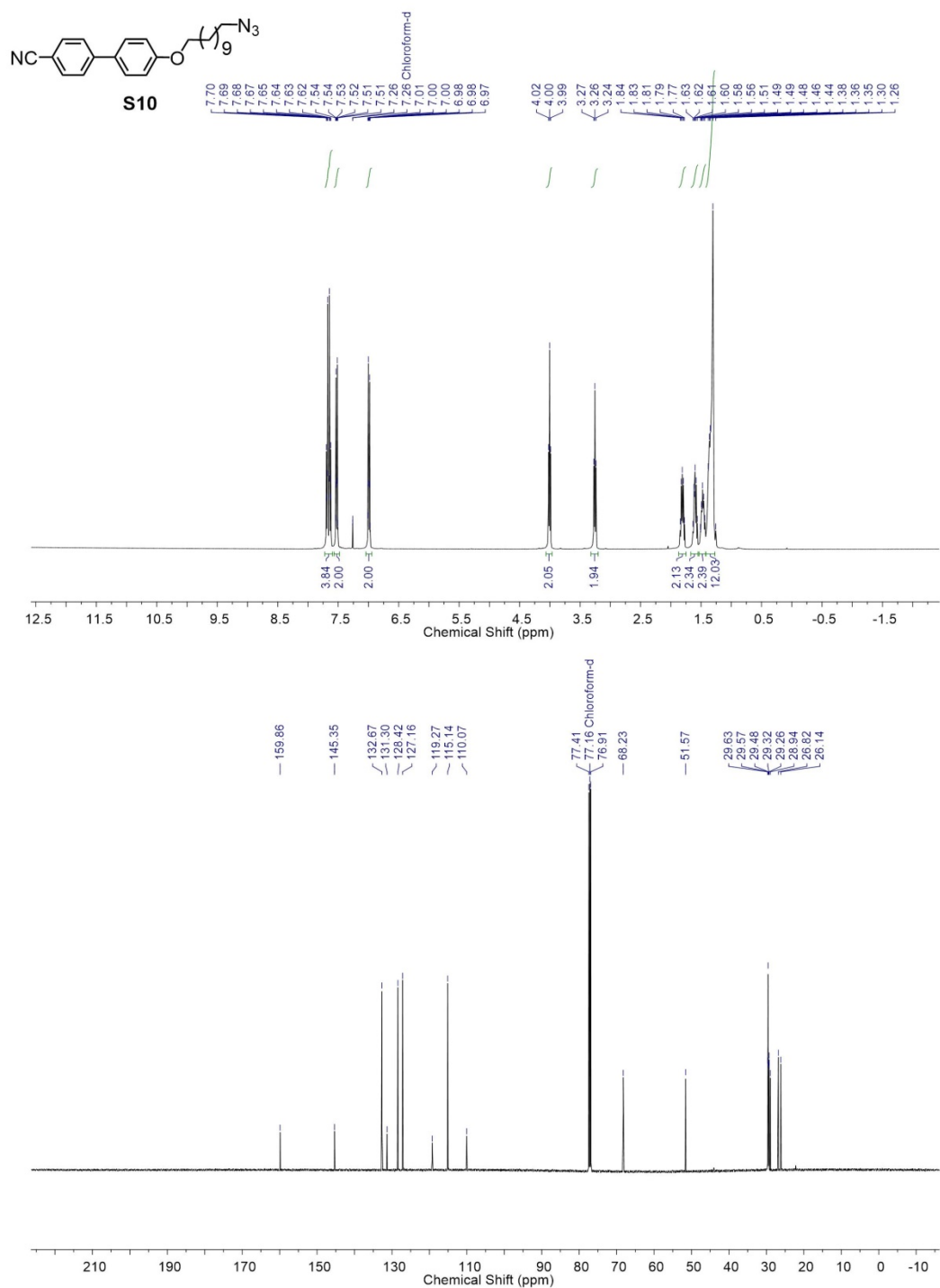**Figure 61** 1H NMR and 13C NMR spectra of **S9**

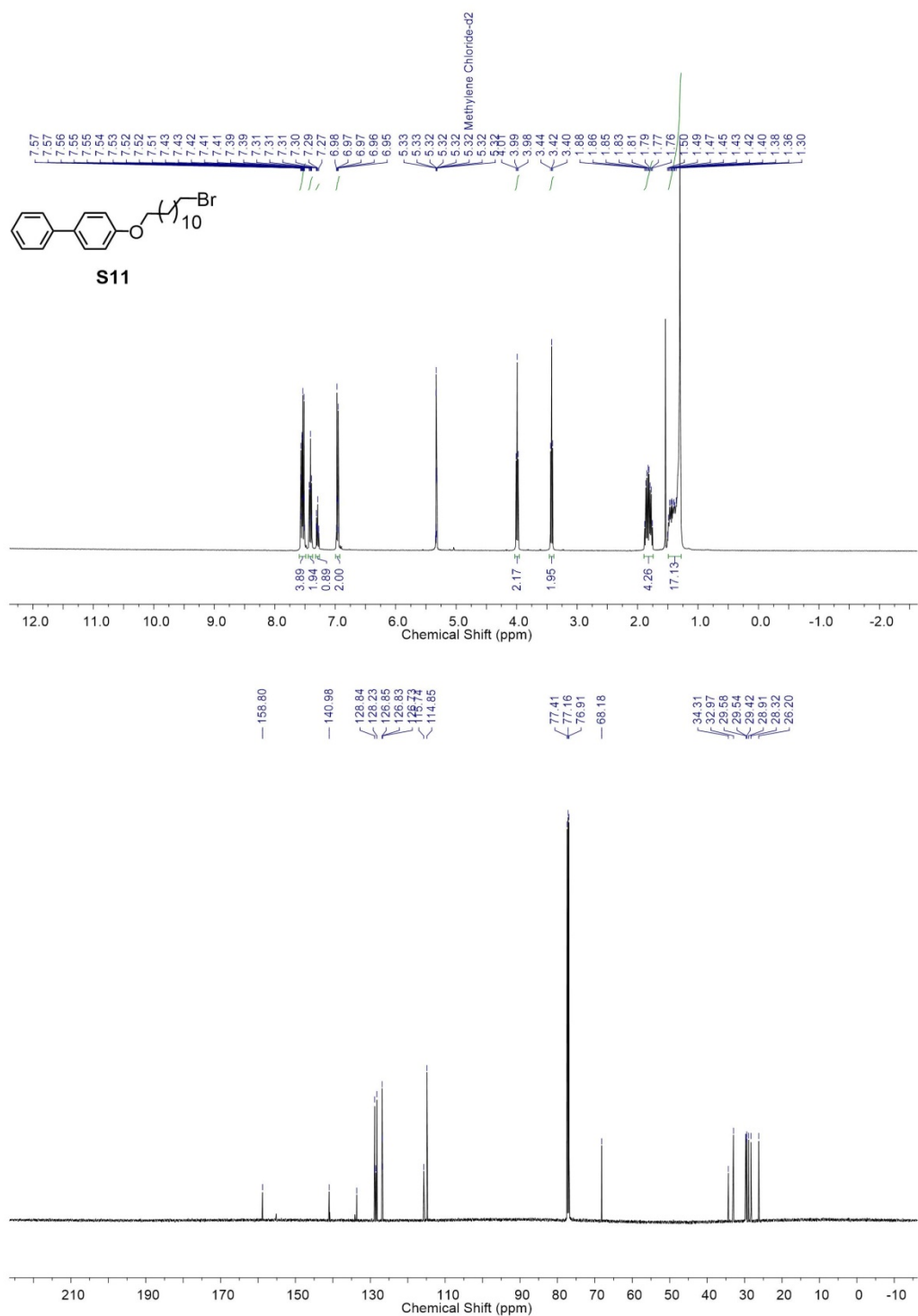**Figure 62** 1H NMR and 13C NMR spectra of **S10**

Figure 63 1H NMR and 13C NMR spectra of **S11**
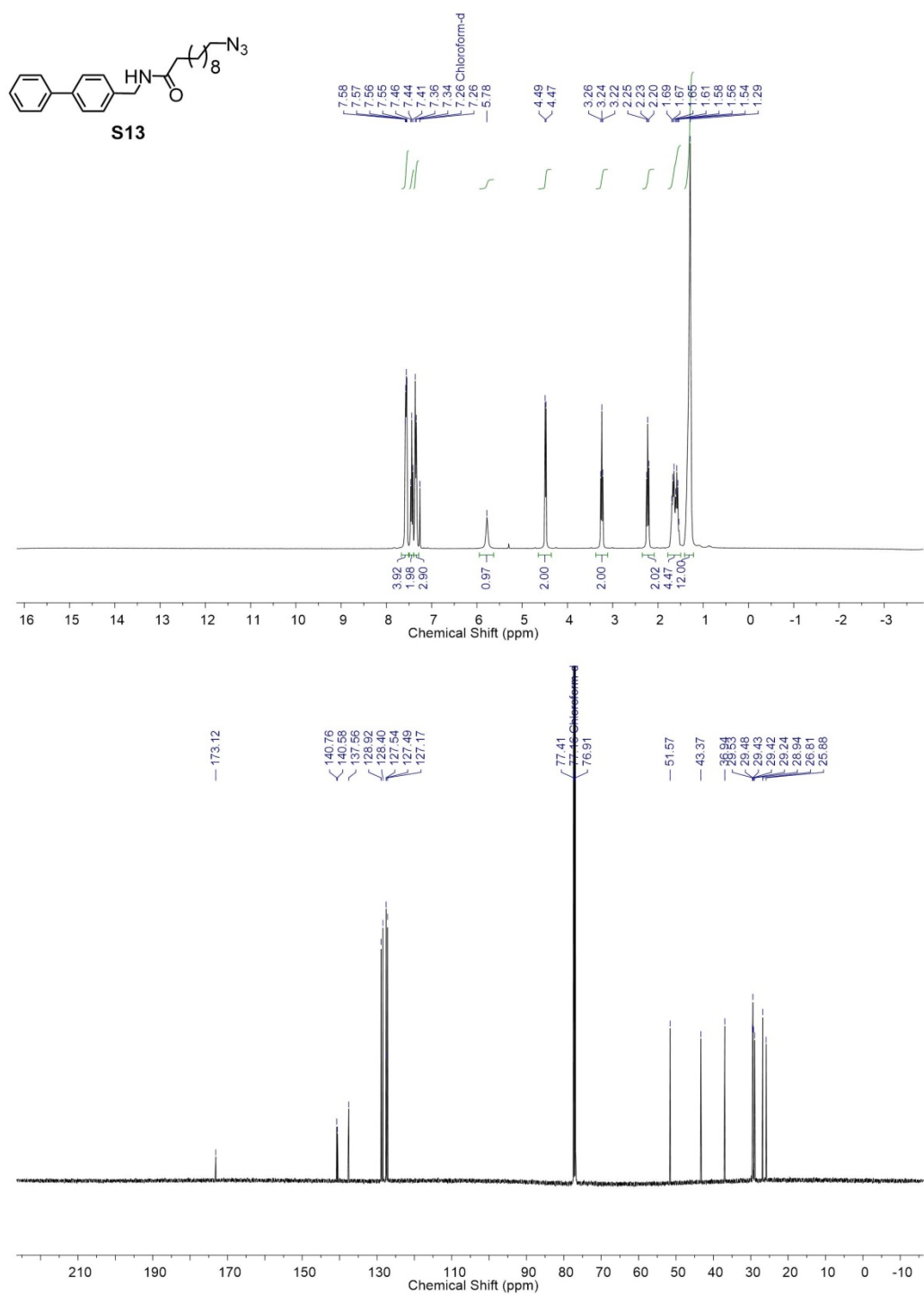
Figure 64 1H NMR and 13C NMR spectra of **S13**

1.1 *References*

1.   Khan, W. Synthesis and micellization of a novel diblock copolymer of poly(N-isopropylacrylamide)-b-SGLCP and its application in stability of 5CB droplets in aqueous medium. *Soft Matter* **7,** 780–787 (2011).

2.   Kinsinger, M. I., Sun, B., Abbott, N. L. & Lynn, D. M. Reversible Control of Ordering Transitions at Aqueous/Liquid Crystal Interfaces Using Functional Amphiphilic Polymers. *Adv. Mater.* **19,** 4208–4212 (2007).

3.   Khan, W. Configuration change of liquid crystal microdroplets coated with a novel polyacrylic acid block liquid crystalline polymer by protein adsorption. *Lab Chip* **12,** 4553 (2012).

4.   Lee, D.-Y. pH-responsive aqueous/LC interfaces using SGLCP-b-polyacrylic acid block copolymers. *Soft Matter* **6,** 1964 (2010).

5.   Kinsinger, M. I., Buck, M. E., Campos, F., Lynn, D. M. & Abbott, N. L. Dynamic Ordering Transitions of Liquid Crystals Driven by Interfacial Complexes Formed between Polyanions and Amphiphilic Polyamines. *Langmuir* **24,** 13231–13236 (2008).

6.   Ma, C. D. Liquid Crystal Interfaces Programmed with Enzyme-Responsive Polymers and Surfactants. *Small* **11,** 5747–5751 (2015).

7.   Kinsinger, M. I., Buck, M. E., Abbott, N. L. & Lynn, D. M. Immobilization of Polymer-Decorated Liquid Crystal Droplets on Chemically Tailored Surfaces. *Langmuir* **26,** 10234–10242 (2010).

8.   Khan, W. Microfluidic formation of pH responsive 5CB droplets decorated with PAA-b-LCP. *Lab Chip* **11,** 3493 (2011).

9.   Collings, P. J. & Hird, M. *Introduction to liquid crystals chemistry and physics*. (Taylor & Francis, 1997).

10.   Sanford, M. S., Love, J. A. & Grubbs, R. H. A Versatile Precursor for the Synthesis of New Ruthenium Olefin Metathesis Catalysts. *Organometallics* **20,** 5314–5318 (2001).

11.   Carlton, R. J. Chemical and biological sensing using liquid crystals. *Liq. Cryst. Rev.* **1,** 29–51 (2013).

12.   Bukusoglu, E., Bedolla Pantoja, M., Mushenheim, P. C., Wang, X. & Abbott, N. L. Design of Responsive and Active (Soft) Materials Using Liquid Crystals. *Annu. Rev. Chem. Biomol. Eng.* **7,** 163–196 (2016).

13.   Lowe, A. M. & Abbott, N. L. Liquid Crystalline Materials for Biological Applications. *Chem. Mater.* **24,** 746–758 (2012).

14.   Jeffrey M. Brake. Effect of Surfactant Structure on the Orientation of Liquid Crystals at Aqueous−Liquid Crystal Interfaces. *Langmuir* **19,** 6436–6442 (2003).

15.   and, A. M. G. da S., Filipe, E. J. M., and, J. M. R. d'Oliveira† & Martinho, J. M. G. Interfacial Behavior of Poly(styrene)−Poly(ethylene oxide) Diblock Copolymer Monolayers at the Air−Water Interface. Hydrophilic Block Chain Length and Temperature Influence. (1996). doi:10.1021/LA960604+

16.   Patel, P. R. Synthesis and Cell Adhesive Properties of Linear and Cyclic RGD Functionalized Polynorbornene Thin Films. *Biomacromolecules* **13,** 2546–2553 (2012).

17.   Caldarelli, S. A. New Bis-thiazolium Analogues as Potential Antimalarial Agents: Design, Synthesis, and Biological Evaluation. *J. Med. Chem.* **56,** 496–509 (2013).

18.   Decroocq, C. The Multivalent Effect in Glycosidase Inhibition: Probing the Influence of Architectural Parameters with Cyclodextrin-based Iminosugar Click Clusters. *Chem. - A Eur. J.* **17,** 13825–13831 (2011).

19.   Neumann, L. N. Supramolecular polymers for organocatalysis in water. *Org. Biomol. Chem.* **13,** 7711–7719 (2015).

SECTION 3: Design of Amphiphiles for Stablization of Perfluorocarbon Droplets as Ultrasound Responsive Materials

With methods in hand for producing complex brush polymers, and having shown they can be utilized in the context of responsive LC systems, we endeavored to extend these materials to other media, including perfluorocarbons, which could have applications in ultrasound responsive materials.

The boiling points (bp) of PFCs vary widely depending on carbon content and branching, from -183.6 ^{o}C to +142 ^{o}C or higher. PFCs with boiling points below physiological temperatures (low-bp PFCs) can be vaporized at acoustic pressures accessible to clinical, diagnostic US machines, but their inherent instability at those temperatures limits their utility in clinical applications. For those PFCs with boiling points higher than physiological temperatures (high-bp PFCs), rarefactional pressures allowed by clinical US are not able to trigger their liquid-to-gas phase transition.
Various nanocarriers have been employed for PFC-based ultrasound contrast agents, including liposomes, polymeric nanoparticles, protein, and inorganic nanoparticles. These strategies generally involve building a functionalized shell around the PFC core to improve stability by reducing surface tension, to provide a diffusion barrier, and in some cases a functionalizable surface for targeting.

Considering the volatility of low-bp PFCs, we envisioned a simple, fast, robust strategy involving amphiphile assembly at the interface, followed by a fast, highly efficient crosslinking reaction capable of working at low temperatures for stabilizing the low-bp PFC microdroplets. We reasoned that UV-induced thiol-ene click chemistry had potential in this application given ease of implementation, high yield at low temperatures, and rapid reaction rates. To enhance the stability of low-bp PFC droplets, we designed a triblock copolymer system synthesized by ring opening metathesis polymerization (ROMP),

consisting of a fluorinated block for emulsification of PFCs, an alkene-modified block for secondary thiol-ene crosslinking under UV radiation, and an oligoethylene glycol hydrophilic block (Figure 1). The strategy was to stabilize a low-bp PFC emulsion at physiological temperatures following UV-induced thiol-ene crosslinking, while allowing a liquid-to-gas phase transition using standard US systems.
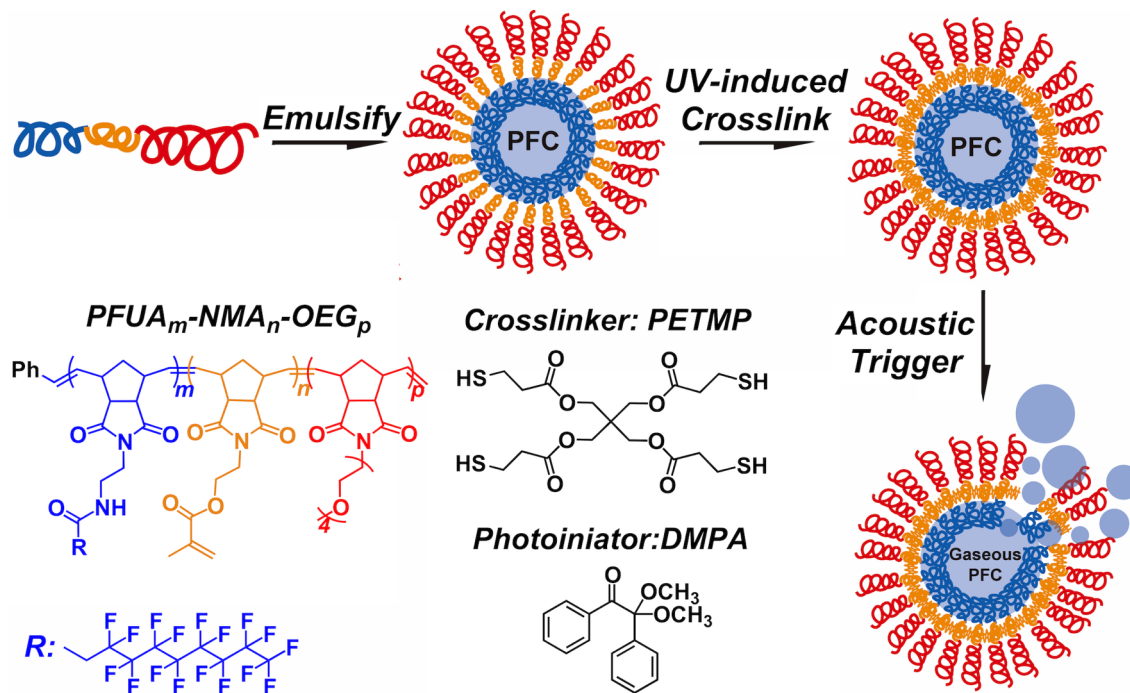

Figure 1. Preparation and acoustic droplet vaporization (ADV) of low-bp PFC emulsions stabilized by thiol-ene crosslinked ROMP block copolymers (PFUA$_m$-NMA$_n$-OEG$_p$) generated from monomers with sidechains: perfluorundecanoic acid (blue, PFUA), methacrylic acid (yellow, NMA) and amino-modified oligoethylene glycol (red, OEG).

Huang, Y.; Vezeridis, A.; Wang, J.; Wang, Z.; Thompson, M.; Mattrey, R.; Gianneschi, N. C. Polymer-Stabilized Perfluorobutane Nanodroplets for Ultrasound Imaging Agents. *J. Am. Chem. Soc.* **2017**, *139*, 15-18.

Supported Personnel

Nathan Gianneschi (PI)
Lisa Adamiak (graduate student)
Carrie James (graduate student)
Yuran Huang (graduate student)

Interactions/Transitions

Nick Abbott and team (Wisconsin)
-Interfacing peptide programmed polymers with liquid crystals as an way of propagating stimuli through materials to generate truly responsive systems on the macroscale.